Kazan Federal University
Zavoiskii Physical-Technical Institute
Russian Academy of Sciences
Bruker Ltd (Moscow)
"Dynasty" Foundation
Russian Foundation for Basic Reserch

ACTUAL PROBLEMS OF MAGNETIC RESONANCE AND ITS APPLICATION

XVI International Youth Scientific School

ACTUAL PROBLEMS OF MAGNETIC RESONANCE AND ITS APPLICATION
KAZAN

Program
Lecture Notes
Proceedings

Kazan
21 - 25 October 2013

Kazan Federal University
Program of KFU development
Zavoisky Physical-Technical Institute
Russian Academy of Sciences
Bruker Ltd (Moscow)
“Dynasty” Foundation
Russian Foundation for Basic Reserch

ACTUAL PROBLEMS OF MAGNETIC RESONANCE AND ITS APPLICATION

XVI International Youth Scientific School

Program
Lecture Notes
Proceedings

Kazan
21 – 25 October 2013

KAZAN UNIVERSITY
2013

УДК 537
ББК 22.334
А 19

The administration of School

Professor M.S. Tagirov (KFU, Kazan) — rector
Professor V.A. Zhikharev (KSTU, Kazan) — vice-rector
V.K. Voronkova (KFTI RAS, Kazan) — scientific secretary
I.P. Volodina (KFU, Kazan) — secretary

The program committee

The chairman
Professor V.A. Atsarkin (IREE, Moscow)

Committee members

Professor A.V. Aganov (KFU, Kazan)
Professor B.I. Kochelaev (KFU, Kazan)
Professor I.V. Ovchinnikov (KFTI RAS, Kazan)
Professor K.M. Salikhov (KFTI RAS, Kazan)

The organizing committee

M.S. Tagirov, V.A. Zhikharev, I.P. Volodina, I.G. Motygullin, A.V. Klochkov, E.M. Alakshin, I.V. Romanova, O.N. Chibisova, M.P. Rodionova, R.R. Gazizulin, A.M. Gazizulina, E.I. Kondratyeva, T.R. Safin, R.R. Safiullin, M.Yu. Zakharov

Actual problems of magnetic resonance and its application: program lecture notes proceedings of the XVI International Youth Scientific School (Kazan, 21 – 25 October 2013) / edited by M.S. Tagirov (Kazan Federal University), V.A. Zhikharev (Kazan State Technological University). – Kazan: Kazan University, 2013. – 122 p.

ISBN 978-5-00019-018-0

The reports of young scientists submitted on XVI International Youth Scientific School “Actual problems of magnetic resonance and its application” carry out by Kazan Federal (Volga Region) University and Zavoisky Physical-Technical Institute are included in the present collection.

ISBN 978-5-00019-018-0

XVI International Youth Scientists School
"Actual problems of magnetic resonance and its application"
Kazan, 21 – 25 October, 2013

Program

Monday, October 21

Institute of Physics

9:00 **Registration**

14:00 Master-classes

Tuesday, October 22

Auditorium 210. Institute of Physics.

10:00 – 10:20 **Opening Ceremony of School-2013**

Lectures

Auditorium 210. Institute of Physics.

Chairman – **M.S. Tagirov**

10:20 – 11:20 **Yu.M. Bunkov** (Institut Neel, CNRS, Grenoble, France; Kazan Federal University, Kazan, Russia), "Direct observation of a Majorana quasiparticle heat capacity in ^{3}He"

Conference Hall of hotel "Ibis".

Chairman – **M.S. Tagirov**

12:00 – 12:50 **I.R. Mukhamedshin** (Kazan Federal University, Kazan, Russia), "^{59}Co NMR study of the Na_xCoO_2 compound"

13:00 – 13:50 **Lunch**

Oral Session

Conference Hall of hotel "Ibis".

Chairman – **E.B. Fel'dman**

13:50 – 14:05 **I.A. Khodov,** "Preferred conformation of ibuprofen in chloroform by 2D NOESY"

14:05 – 14:20 **V.Y. Kudryashov,** "Spin dynamics and magnetic phase transitions in monoclinic honeycomb-layered antimonates $A_3Ni_2SbO_6$ (A=Li, Na)"

14:20 – 14:35 **O.A. Babanova,** "NMR studies of reorientational motion of complex $[B_{12}H_{12}]^{2-}$ anions in $A_2B_{12}H_{12}$ (A = K, Rb, Cs)"

14:35 – 14:50 **A.S. Ermolov,** "Static and dynamic magnetic properties of new layered antimonate of lithium and cobalt"

14:50 – 15:05 **N.G. Pavlov,** "Nuclear magnetic resonance in noncollinear antiferromagnet $Mn_3Al_2Ge_3O_{12}$"
15:05 – 15:20 **A.M. Vasiliev,** "ESR of the quasi-two-dimensional antiferromagnet$CuCrO_2$ with a triangular lattice"
15:20 – 15:35 **A.G. Smolnikov,** "^{17}O NMR study of the triangular lattice antiferromagnet $CuCrO_2$"
15:35 – 15:50 **A.V. Tkachev,** "BaV_3O_8: a possible Majumdar-Ghosh system with S = ½"

15:50 – 16:10 **Coffee break**

Chairman – **V.A. Zhikharev**

16:10 – 16:25 **S.G. Vasil'ev,** "Dynamic and decay of NMR quantum coherences in quasi-one-dimensional systems"
16:25 – 16:40 **S.O. Rabdano,** "Hydration shells of functional groups of organic molecules studied by NMR-relaxation and quantum chemical calculations"
16:40 – 16:55 **R.B. Zaripov,** "ENDOR studies of a Cu(II)-bis(oxamato) complex"
16:55 – 17:10 **N.A. Tukmakova,** "Monitoring of the paramagnetic reduced forms of the complex $Cr(III)(bpy)_3$"
17:10 – 17:25 **T.M. Salikhov,** "NMR of adsorbed polarity fluid in the zeolite"
17:25 – 17:40 **N.A. Krylatykh,** "Detection of liquids using low-field magnetic resonance imaging and spectroscopy"
17:40 – 17:55 **V.E. Vorobeva,** "Peculiarities of spin crossover magnetic behavior of dendrimeric iron(III) complex"
17:55 – 18:10 **M.F. Iakovleva,** "Spin glass in the kagome compound $YBaCo_3AlO_7$"

18:20 **Welcome Party**

Wednesday, October 23

Lectures

Conference Hall of hotel "Ibis".

Chairman – **V.A. Atsarkin**

9:00 – 9:50 **R.M. Eremina** (Zavoisky Kazan Physical-Technical Institute of RAS, Kazan, Russia), "Anisotropic exchange and effective crystal field parameters for some low dimensional spin systems, ESR data"
9:50 – 10:40 **E.B. Fel'dman** (Institute of Problems of Chemical Physics of RAS, Chernogolovka, Moscow region, Russia), "Investigations of quantum and classical correlations by NMR methods"

10:40 – 11:10 **Coffee break**

Coherent Optics and Nanophotonics section. The joint providing with International Youth Scientific School "Coherent Optics and Optic Spectroscopy"

Conference Hall of hotel "Ibis".

Chairman – **M.Kh. Salakhov**

11:10 – 12:00 **K.I. Gerasimov** (Zavoisky Kazan Physical-Technical Institute of RAS, Kazan, Russia), "Introduction to magneto-optical spectroscopy and its modern applications"

12:00 – 12:50 **V.A. Atsarkin** (Kotel'nikov Institute of Radio Engineering and Electronics of RAS), "Negative refraction index: a new hot area in physics and engineering"

13:00 – 13:50 **Lunch**

Oral Session

Conference Hall of hotel "Ibis".

Chairman – **K.I. Gerasimov**

13:50 – 14:05 **N.F. Rakhimov,** "Optical properties of fluorite crystals CaF_2: Ce^{3+}, Yb^{3+}, Lu^{3+}"
14:05 – 14:20 **V.V. Pavlov,** "Transient responses of the dielectric permittivity of $LiLuF_4$ crystals doped by Ce^{3+} and Yb^{3+} ions"
14:20 – 14:35 **I.V. Romanova,** "Impact of multipole interactions between Tm^{3+} ions on spectral and magnetic properties of $LiTmF_4$ single crystals"
14:35 – 14:50 **M.A. Volodin,** "High-frequency EPR study of crude oils"
14:50 – 15:05 **J.V. Mamedov,** "Features of the EPR of the ZrO_2-Y_2O_3 system"
15:05 – 15:20 **A.M. Gazizulina,** "Continuous wave electron paramagnetic resonance of Gd^{3+} in LaF_3 nano- and micro-sized particles"
15:20 – 15:35 **T.B. Biktagirov,** "Nitrogen-containing species in the structure of hydroxyapatite nanocrystals: a combined multifrequency EPR/ENDOR and DFT study"
15:35 – 15:50 **V.O. Sakhin,** "EPR study of magnetic anomalies in the $La_{2-x}Sr_xCuO_4$ single crystals above the critical temperature"

15:50 – 16:10 **Coffee break**

Chairman – **F.S. Dzheparov**

16:10 – 16:25 **K.B. Konov,** "Glycerol penetration profile in phospholipid bilayers measured by ESEEM of spin-labeled lipids"
16:25 – 16:40 **A.A. Gabitov,** "Attempt to detect charge density waves in $YBa_2Cu_3O_{6.5}$ using copper NQR"
16:40 – 16:55 **B.V. Yavkin,** "ODMR study of NV centers in HPHT diamond"
16:55 – 17:10 **A.A. Sukhanov,** "Time-resolved and pulse EPR study of photo-induced spin polarization of zinc porphyrin trimer and zinc porphyrin-copper ion dimmer"
17:10 – 17:25 **Yu.S. Kutin,** "High-frequency EPR/ENDOR study of charge-compensated Fe^{3+} centers in ZnO single crystals"
17:25 – 17:40 **E.M. Gataullin,** "ESR in the laves phase alloy $YbNi_2$"
17:40 – 17:55 **E.I. Kondratyeva,** "Application of EPR for controlling wood properties during processing"
17:55 – 18:10 **T.R. Safin,** "Long-lived free induction decay signal in $CsMnF_3$ single crystal"
18:10 – 18:25 **M.Y. Zakharov,** "The spin kinetics of ^3He in contact with nanosized crystalline powders LaF_3"

Thursday, October 24

Lectures

Conference Hall of hotel "Ibis".

Chairman – **S.B. Orlinskii**

9:00 – 9:50 **E.L. Vavilova** (Zavoisky Kazan Physical-Technical Institute of RAS, Kazan, Russia), "Frustration phenomena in the intrinsic two-component magnetoelectric material Li_2ZrCuO_4"

9:50 – 10:40 **F.S. Dzheparov** (Institute for Theoretical and Experimental Physics, Moscow, Russia), "Phase relaxation in magnetically diluted crystals"

10:40 – 11:10 **Coffee break**

Chairman – **E.L. Vavilova**

11:10 – 12:00 **A.A. Katanin** (Institute of Metal Physics, Ural Div. of RAS, Ekaterinburg, Russia), "Intercommunication of electronic and magnetic properties of iron and iron pnictides"

12:00 – 12:50 **S.B. Orlinskii** (Kazan Federal University, Kazan, Russia), "Optimization of functionalized nanodiamond platforms for gene delivery to area of peripheral nerve trauma by HF EPR"

13:00 – 14:00 **Lunch**

14:30 **Excursion to Planetarium (V.P. Engel'gardt Astronomical Observatory)**

Friday, October 25

Lectures

Conference Hall of hotel "Ibis".

Chairman – **M.S. Tagirov**

9:00 – 9:50 **E.I. Baibekov** (Kazan Federal University, Kazan, Russia), "Spin dynamics and relaxation in the presence of microwaves"

9:50 – 10:40 **V.M. Murzakaev,** (TNG-Group Ltd, Bugulma, Tatarstan, Russia) "NMR at the solution of geological tasks of well logging"

10:40 – 11:10 **Coffee break**

11:10 **Closing Ceremony of School-2013**

13:00 – 14:00 **Lunch**

Assembly Hall of Kazan Federal University

15:00 **Zavoisky Award for Youth Scientists**

^{59}Co NMR study of the Na_xCoO_2 compound

I. R. Mukhamedshin

Institute of Physics, Kazan Federal University, 420008 Kazan, Russia

e-mail: Irek.Mukhamedshin@kpfu.ru

Since the discovery of high thermoelectric power [1] and superconductivity [2] in layered cobaltates Na_xCoO_2, extended efforts have been made in order to understand the importance of electronic correlations in their metallic and magnetic properties. They are somewhat similar to the HTSC cuprates in as much as the charge doping of the CoO_2 layers is controlled on a large range by variation of the Na content. One significant difference with the cuprates is that the Co of the CoO_2 plane are ordered on a triangular lattice and not on a square lattice as for the CuO_2 plane of the cuprates.

While many experiments and theoretical calculations have considered that the Co magnetism is uniform, it has been evidenced by NMR that Na displays an atomic ordering associated with Co charge disproportionation in the planes [3, 4].

In this lecture I'll represent a complete set of ^{59}Co NMR data taken on the $x = 2/3$ phase of sodium cobaltates Na_xCoO_2, for which we have formerly established the in plane Na ordering and its 3D stacking [5]. Also a method of analysis of NMR spectra which allowed us to resolve the parameters of the Zeeman and quadrupolar Hamiltonians for all four cobalt sites in the unit cell and the temperature dependencies of the NMR shift data for these sites will be reported. The moderately complicated atomic structure resumes then in a very simple electronic structure in which the electrons delocalize on the kagomé sublattice of the triangular lattice of Co sites. We evidence that they display a strong in plane electronic anisotropy initially unexpected but which accords perfectly with an orbital ordering along the kagomé sublattice organization [6].

Also I'll report ^{59}Co NMR data taken on the phase with $x \approx 0.77(1)$ which exhibits an antiferromagnetic order at a Néel temperature $T_N = 22$ K. The comparison of data for two phases allowed us to establish reliably the relation between the local Na order, the actual Na content, and the local magnetic properties of the studied phases. The incidence of the structural order on the charge disproportionation and on the physical properties of sodium cobaltates will also be discussed.

This work was partially supported by the Ministry of Education and Science of the Russian Federation (Budget Theme No. 12-24).

References

[1] I.Terasaki *et al.*, Phys. Rev. B **56**, R12685 (1997).

[2] K.Takada *et al.*, Nature (London) **422**, 53 (2003).

[3] H.Alloul *et al.*, EPL **82**, 17002 (2008).

[4] G. Lang *et al.*, Phys.Rev.B **72**, 094404 (2005).

[5] T.A.Platova *et al.*, Phys. Rev. B **80**, 224106 (2009).

[6] I.R.Mukhamedshin and H.Alloul, Phys. Rev. B **84**, 155112 (2011).

Anisotropic exchange and effective crystal field parameters for some low dimensional spin systems, ESR data

R.M. Eremina

Kazan Physical-Technical Institute, Kazan, Sibirskii trakt 10/7 Russia

e-mail: REremina@yandex.ru

Electron-spin resonance (ESR) is a convenient method to probe anisotropic spin-spin interactions of low dimensional spin systems. Due to strong fluctuation they are in the paramagnetic phase up to low temperatures, although the isotropic exchange interaction between magnetic ions in them is quite strong. The ESR linewidth displays the average amplitude of the fluctuating field on the magnetic ion, which can be directly related to the parameters of the anisotropic spin-spin interactions. The ESR signal of this system consists of a single exchange-narrowed resonance line. Here we focus mainly on the problem how to extract the spin-Hamiltonian parameters from the angular and temperature dependencies of the EPR frequencies and the linewidth. In particular, measuring EPR linewidth in three mutually orthogonal planes (ab), (ac) and (bc) one is able to obtain a information about the anisotropic exchange parameters. Few examples of such kind of studies will be shortly described.

The theory of the ESR linewidth based on momentum method, as a rule. It has been shown that in the case of sufficiently strong exchange interaction the ESR spectrum is narrowed into a single Lorentz line. Assuming that the EPR line is Lorentzian, the linewidth ΔH is given by [1]:

$$\Delta H_L = \sqrt{\frac{\pi}{3}}\left[\frac{M_2^3}{M_4}\right]^{1/2}, \tag{1}$$

where M_2 and M_4 — the second and fourth moments of line, respectively. Both moments can be expressed in terms of the microscopic parameters of the Hamiltonian of the spin system as:

$$\begin{aligned} M_2 &= \frac{<\left[H_{an}, S^+\right]\left[S^-, H_{an}\right]>}{\hbar^2 < S^+S^- >}, \\ M_4 &= \frac{<\left[H_{ex}, \left[H_{an}, S^+\right]\left[S^-, H_{an}\right], H_{ex}\right]>}{\hbar^4 < S^+S^- >}. \end{aligned} \tag{2}$$

Here, H_{an} contains anisotropic exchange interaction, crystal field, dipole-dipole and anisotropic Zeeman term, H_{ex} is the isotropic Heisenberg exchange $H_{ex}^{ij} = JS_iS_j$ between neighboring spins $\mathbf{S}_i$ and $\mathbf{S}_j$. In a high-temperature approximation ($kT >> J$) the calculations of the second and the fourth moments are described in Ref. [1]. There is a wide temperature range in the paramagnetic state where antiferromagnetic correlations have to be taken into account.

The exchange interactions of the spin in the chain are not necessarily inversely symmetric, i.e. interactions to the left and to the right neighbours in a chain may not be identical [2] (see fig.1). In what follows, we use the spin Hamiltonian:

$$H = J_{1a}\cdot\left(\bar{S}_1\cdot\bar{S}_a\right)+\sum_{\alpha,\beta=x,y,z} J_{1a}{}^{\alpha\beta}\cdot S_1^{\alpha}\cdot S_a^{\beta}+J_{1b}\cdot\left(\bar{S}_1\cdot\bar{S}_b\right)+ \\ +\sum_{\alpha,\beta=x,y,z} J_{1b}{}^{\alpha\beta}\cdot S_1^{\alpha}\cdot S_b^{\beta}+\sum_{\substack{\alpha,\beta=x,y,z\\ \gamma=1,3}} g_{\gamma}{}^{\alpha\beta}\cdot\mu_B\cdot H_{\gamma}^{\alpha}\cdot S_{\gamma}^{\beta}. \tag{3}$$

Here J_{1a}, $J_{1a}^{\alpha\beta}$ are the parameters of the isotropic and anisotropic exchange interactions with the left nearest neighbour copper ion, and J_{1b}, $J_{1b}^{\alpha\beta}$ are the parameters of the isotropic and

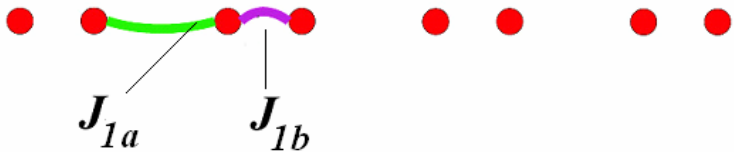

Fig.1. The quasi-one dimensional spin-system with alternating isotropic exchange interaction.

anisotropic exchange interactions with right nearest neighbor copper ion, respectively. The last term denotes the interaction of spins with an external magnetic field. In a coordinate system with the z axis directed along the external magnetic field, the second and fourth moments of the EPR line are given by:

$$M_2(J)=\frac{S(S+1)}{3}\cdot\left(B(J_{1a})+B(J_{1b})\right), \tag{4}$$

$$M_4=\frac{a(6a-7)}{30}\cdot\left(J_{1a}{}^2\cdot B(J_{1a})+J_{1b}{}^2\cdot B(J_{1b})\right)+\frac{a^2}{9}\cdot\left(J_{1b}{}^2\cdot B(J_{1a})+J_{1a}{}^2\cdot B(J_{1b})\right)+ \\ +\frac{a^2\cdot J_{1a}\cdot J_{1b}}{9}\cdot\begin{pmatrix}\left(2J_{1a}^{zz}-J_{1a}^{xx}-J_{1a}^{yy}\right)\cdot\left(2J_{1b}^{zz}-J_{1b}^{xx}-J_{1b}^{yy}\right)+\\ +\left(J_{1a}^{xx}-J_{1a}^{yy}\right)\cdot\left(J_{1b}^{xx}-J_{1b}^{yy}\right)+\\ +10\cdot J_{1a}^{xz}\cdot J_{1b}^{xz}+10\cdot J_{1a}^{yz}\cdot J_{1b}^{yz}+4\cdot J_{1a}^{xy}\cdot J_{1b}^{xy}\end{pmatrix}, \tag{5}$$

where

$$a=S(S+1), \\ B(J_{1a})=\left(2J_{1a}^{zz}-J_{1a}^{xx}-J_{1a}^{yy}\right)^2+\left(J_{1a}^{xx}-J_{1a}^{yy}\right)^2+10\left(J_{1a}^{xz}\right)^2+10\left(J_{1a}^{yz}\right)^2+4\left(J_{1a}^{xy}\right)^2. \tag{6}$$

The quantities $J_{1\gamma}^{\alpha\beta}$ (where $\alpha,\beta=x,y,z$; and $\gamma=a,b$) are determined in a local coordinate system with z-axis being parallel to the external magnetic field. However, it is important to bear in mind that the number of independent parameters of the anisotropic symmetric exchange is less if one works in the crystallographic coordinate system. Therefore, it is useful to express the relevant combinations of quantities $J_{1\gamma}^{\alpha\beta}$ via its values in crystallographic coordinate system (*a, b, c*). Performing the necessary rotation, the following relation can be derived:

$$\left(J_{1a}^{xx}-J_{1a}^{yy}\right)^2+4\left(J_{1a}^{xy}\right)^2=4\begin{bmatrix}\left(J_{bb}-J_{aa}\right)\cos\beta\sin\alpha\cos\alpha+\\ J_{ab}\cos\beta\cos2\alpha+J_{ac}\sin\beta\sin\alpha-J_{bc}\sin\beta\cos\alpha\end{bmatrix}^2+$$
$$+\begin{bmatrix}J_{aa}\left(\cos^2\beta\cos^2\alpha-\sin^2\alpha\right)+J_{bb}\left(\cos^2\beta\sin^2\alpha-\cos^2\alpha\right)+J_{cc}\sin^2\beta+\\ +J_{ab}\sin2\alpha\left(\cos^2\beta+1\right)-J_{ac}\cos2\beta\cos\alpha-J_{bc}\cos2\beta\sin\alpha\end{bmatrix}^2 \tag{7}$$

$$\left(2J_{1a}^{zz}-J_{1a}^{xx}-J_{1a}^{yy}\right)^2=\begin{bmatrix}J_{cc}\left(3\cos^2\beta-1\right)+J_{aa}\left(3\sin^2\beta\cos^2\alpha-1\right)+\\ +J_{bb}\left(3\sin^2\beta\sin^2\alpha-1\right)+\\ +3J_{ab}\sin^2\beta\sin2\alpha+3J_{ac}\sin2\beta\cos\alpha+3J_{bc}\sin2\beta\sin\alpha\end{bmatrix}^2 \tag{8}$$

$$\left(J_{1a}^{xz}\right)^2+\left(J_{1a}^{yz}\right)^2=\begin{bmatrix}\left(J_{aa}\cos^2\alpha+J_{bb}\sin^2\alpha-J_{cc}+J_{ab}\sin2\alpha\right)\cos\beta\sin\beta+\\ +J_{ac}\cos\alpha\cos2\beta+J_{bc}\sin\alpha\cos2\beta\end{bmatrix}^2+$$
$$+\left[\left(J_{bb}-J_{aa}\right)\sin\beta\cos\alpha\sin\alpha+J_{ab}\sin\beta\cos2\alpha-J_{ac}\cos\beta\sin\alpha+J_{bc}\cos\beta\cos\alpha\right]^2 \tag{9}$$

where

$$\cos\alpha=\frac{A}{\sqrt{A^2+B^2}},\qquad \cos\beta=\frac{C}{\sqrt{A^2+B^2+C^2}} \tag{10}$$

$$\begin{aligned}g&=\sqrt{A^2+B^2+C^2}\\ A&=g_{aa}\sin\vartheta\cos\varphi+g_{ab}\sin\vartheta\cos\varphi+g_{ac}\cos\vartheta\\ B&=g_{ba}\sin\vartheta\cos\varphi+g_{bb}\sin\vartheta\cos\varphi+g_{bc}\cos\vartheta\\ C&=g_{ca}\sin\vartheta\cos\varphi+g_{cb}\sin\vartheta\cos\varphi+g_{cc}\cos\vartheta\end{aligned} \tag{11}$$

The angles ϑ and φ are the magnetic field orientation with respect to the crystallographic axes. The quantities $J_{\eta\xi}$, $g_{\eta\xi}$ $(\eta,\xi=a,b,c)$ are parameters of anisotropic exchange interaction and *g*-tensor in crystallographic coordinate system, respectively. It is assumed, that in the coordinate system (*x', y', z'*), with axis *z'* along the chain, the symmetric intrachain anisotropic exchange interaction between two neighbouring spins S_i and S_j can be written as

$$H_{AEX}=J_{x'x'}S_i^{x'}S_j^{x'}+J_{y'y'}S_i^{y'}S_j^{y'}+J_{z'z'}S_i^{z'}S_j^{z'}, \tag{12}$$

where $J_{x'x'}+J_{y'y'}+J_{z'z'}=0$. Also the g tensor in the crystallographic coordinates is obtained from its counterpart in local coordinates (*x'', y'', z''*), where *g*-tensor have only diagonal components $\begin{pmatrix}g_{xx}^{''} & 0 & 0\\ 0 & g_{yy}^{''} & 0\\ 0 & 0 & g_{zz}^{''}\end{pmatrix}$, by means of a rotation.

For example, shortly, it is presented ESR studies of a $CuTe_2O_5$ single crystal. At temperatures of 25 to 300 K, the EPR spectrum of copper ions consists of one Lorentzian-shaped line with $g\sim2$. The angular dependences of the EPR linewidth of $CuTe_2O_5$ calculated theoretically and measured at frequencies of 9.4 and 160 GHz at T = 200 K are presented in fig.2. The detailed calculation and values of g- tensor and exchange interaction are presented in [2].

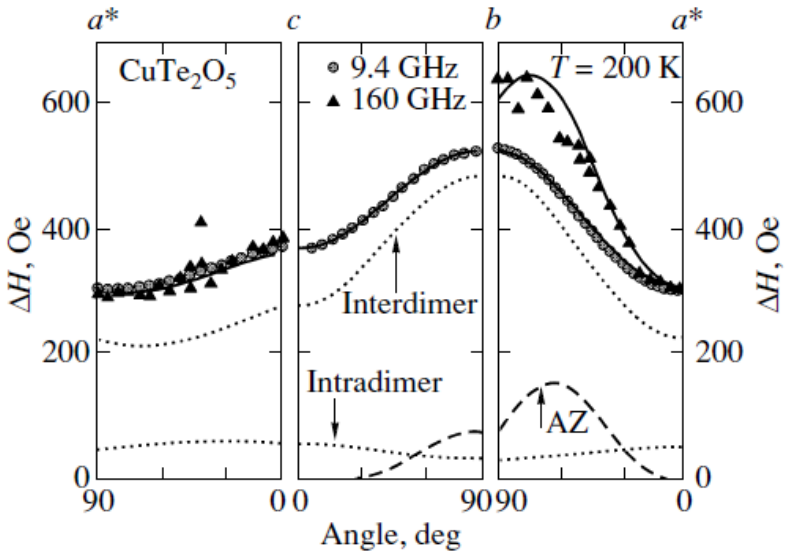

Fig.2. Angular dependences of the EPR linewidth in CuTe2O5 at frequencies of 9.4 GHz (circles) and 160 GHz (triangles) in three crystallographic planes measured at $T = 200$ K. The dotted lines show the contribution to the EPR linewidth from the spin–spin interactions between copper ions in a dimer and between copper ions belonging to neighboring dimers. The dashed line corresponds to the contribution from the anisotropic Zeeman effect at 160 GHz. The solid lines show the sum of all the contributions (for each frequency).

If the EPR linewidth along one axis at a different frequency is greater than its value in the X band, i.e. it depends on the field as H^2, it is logical to assume that this effect originates from the difference between the individual g factors of interacting spins (anisotropic Zeeman effect). As a rule it is can be seen from the analysis of the structural data, where one finds that the unit cell contains two magnetically nonequivalent ligands surrounding the paramagnetic ions producing an EPR signal. Since the EPR spectrum exhibits only one line, its effective g factor is the average of the g factors of two magnetic centers located at the nonequivalent positions. The frequency-dependent contribution to the EPR linewidth due to the difference between the g factors is given by [3]

$$\Delta H_{AZ} = \left(\frac{\Delta g}{g}\right)^2 \frac{g\mu_B H_{res}^2}{J_{1c}} \tag{13}$$

where Δg is the difference between the g factors of the nonequivalent paramagnetic centers. The resonance frequency is related to the resonance magnetic field by the relation $g\beta H_{res} = h\nu$. Using values of Δg and ΔH_{AZ} as determined from the experimental data, we can find J_{1c} exchange integral between magnetic nonequivalent paramagnetic ions.

As noted in fig.2, the EPR linewidth along the b axis at a frequency of 160 GHz is greater than its value in the X band in $CuTe_2O_5$. Indeed, from analyzing the structural data (see fig.3), it follows that the unit cell contains two magnetically nonequivalent octahedral of oxygen ions that surround the paramagnetic copper ions producing an EPR signal. The frequency-dependent contribution to the EPR linewidth due to the difference between the g factors is given by (13). The angular dependence of the EPR linewidth measured at 160 GHz shows that the difference between the g factors of the two nonequivalent octahedra is maximum along the b axis of the crystal and is minimum along the other directions. Since the geometric sizes of the two magnetically nonequivalent octahedra are equal, the principal values of the g tensors in a local coordinate system of the octahedra also have to be equal.

When fitting the experimental values of the EPR linewidth obtained at 160 GHz, we took into account that the contribution from the anisotropic symmetric interactions is the same as that in the *X* band. The isotropic exchange interaction between the spins of the copper ions belonging to neighboring magnetically nonequivalent octahedra as estimated is J_{1c} = 0.5 K.

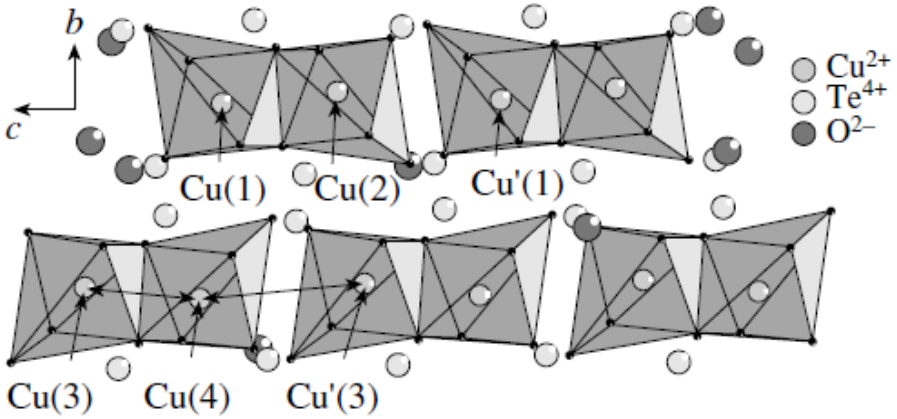

Fig.3. Quasi-one-dimensional chain formed by copper ions Cu(1)–Cu(2)–Cu'(1) and Cu(3)–Cu(4)–Cu'(3) in the *bc* plane.

The expressions for M_2 and M_4 in case of antisymmetric Dzyalozhinsky-Moriya interaction were obtained previously in Ref. [15]. Note that in Ref. [15] a three-dimensional cmpound of $LaMnO_3$ was considered. The components D_x, D_y, and D_z refer to the pair within the *ab* plane, whereas $D_{x'}$ and $D_{z'}$ refer to the Mn ions along *c*-axis. J_{ac} and J_b are the parameters of the isotropic exchange interaction between the spins of magnetic ions in the (*ac*) plane and along the b axis, respectively.

We use the spin Hamiltonian for antisymmetric Dzyaloshinsky-Moriya interaction with the z-axis parallel to the applied magnetic field H:

$$H = \sum_{i,i+1} D_\alpha \left[S_i \times S_j \right] + g\mu_B H S_Z \tag{14}$$

where D_α ($\alpha = x, y, z$) are parameters of antisymmetric Dzyaloshinsky-Moriya interaction in the coordinate system with the *z*-axis parallel to the applied magnetic field. The transformation between the crystallographic system (a, b, c) and the coordinate system (x, y, z) are determinated by expressions:

$$\begin{aligned} D_x &= D_a \cos\beta \cos\alpha + D_b \cos\beta \sin\alpha - D_c \sin\beta; \\ D_y &= D_b \cos\alpha - D_a \sin\alpha; \\ D_z &= D_a \sin\beta \cos\alpha + D_b \sin\beta \sin\alpha + D_c \cos\beta; \end{aligned} \tag{15}$$

The second and fourth moments are expressed as

$$\begin{aligned} M_2 &= (2/3) S (S+1) \left[D_x^2 + D_y^2 + 2D_z^2 \right], \\ M_4 &= (4/9) S^2 (S+1)^2 \left(S(S+1) - 1 \right) J^2 \left[D_x^2 + D_y^2 + 2D_z^2 \right] \end{aligned} \tag{16}$$

In the local coordinate system the spin Hamiltonian of the crystal field is taken, as a rule, in the following form:

$$H_{cf} = D S_{z'}^2 + E \left(S_{x'}^2 - S_{y'}^2 \right) \tag{17}$$

In the coordinate system with the z axis directed along the external magnetic field, the Hamiltonian (17) may be expressed as [4]:

$$\begin{aligned} &H_{cf} = \lambda_{xx}S_x^2 + \lambda_{yy}S_y^2 + \lambda_{zz}S_z^2 + \lambda_{xy}\left(S_xS_y + S_yS_x\right) + \lambda_{xz}\left(S_xS_z + S_zS_x\right) + \lambda_{yz}\left(S_yS_z + S_zS_y\right) \\ &\lambda_{\xi\zeta} = EA_{x'\xi}A_{x'\zeta} - EA_{y'\xi}A_{y'\zeta} + DA_{z'\xi}A_{z'\zeta} \\ &\xi,\ \zeta = x, y, z \end{aligned} \tag{18}$$

The expression for the second moment of the linewidth is known in the coordinate system where the z axis is parallel to the external magnetic field [4]

$$M_2 = \frac{1}{20h^2}(4a-3)\left[(\lambda_{xx}-\lambda_{yy})^2 + 4\lambda_{xy}^2 + (\lambda_{xx}+\lambda_{yy}-2\lambda_{zz})^2 + 10(\lambda_{xz}^2+\lambda_{yz}^2)\right] \tag{19}$$

$a = S(S + 1)$, and h is Planck's constant. The expression for the fourth moment taking into account the isotropic exchange interaction and crystal field is [4]:

$$M_4 = (4J_{ac}^2 + 2J_b^2)\frac{a}{10h^4}(4a-3)\left[(\lambda_{xx}-\lambda_{yy})^2 + 4\lambda_{xy}^2 + (\lambda_{xx}+\lambda_{yy}-2\lambda_{zz})^2 + 10(\lambda_{xz}^2+\lambda_{yz}^2)\right] \tag{20}$$

where J_{ac} — isotropic exchange interaction in plane; J_b — isotropic exchange interaction between plane.

The crystal field (CF) and antisymmetric Dzyalozhinsky-Moriya interaction (DM) are important for description angular dependencies of ESR linewidth in $La_{0.95}Sr_{0.05}MnO_3$ [5]. In three orthogonal planes in $La_{0.95}Sr_{0.05}MnO_3$, one observes a broad, exchange-narrowed resonance line. The contributions of CF and DM interaction consist of the superposition of the four nonequivalent Mn ions in the orthorhombic unit cell. The crystal-field parameters for all Mn positions and the Dzyaloshinsky-Moriya interaction for nearest-neighbor Mn ions along the b axis as well as in the *ac* plane were successfully extracted [5] from angular dependencies of ESR linewidth.

References

[1] S. A. Altshuler and B. M. Kozyrev, Electron Paramagnetic Resonance in Compounds of Transition Elements (Wiley, New York, 1974; Nauka, Moscow, 1972).

[2] R. M. Eremina, T. P. Gavrilova, N.-A. Krug von Nidda, A. Pimenov, J. Deisenhofer, and A. Loidl, Physics of the Solid State, **50**, 283-289 (2008).

[3] B. Pilawa, J.Phys.:Condens.Matter **9,** 3779-3792 (1997).

[4] I. V. Yatsyk, R. M. Eremina, M. M. Shakirzyanov, Ya. M. Mukovskii, H.-A. Krug von Nidda, and A. Loidl, JETP Letters, **87**, p. 447-451, (2008).

[5] J. Deisenhofer, M. V. Eremin, D. V. Zakharov, V. A. Ivanshin, R. M. Eremina, H.-A. Krug von Nidda, A. A. Mukhin, A. M. Balbashov, and A. Loidl, ArXiv: cond-mat / 0108515 (2001)

Investigations of quantum and classical correlations by NMR methods

E.B. Fel'dman

Institute of Problems of Chemical Physics of Russian Academy of Sciences, Chernogolovka, 142432, Moscow Region, Russia

e-mail: efeldman@icp.ac.ru

We consider methods of liquid-state NMR and solid-state NMR for quantum computing and solving different problems of quantum information theory. We discuss pseudo-pure states which are very important for quantum computation with liquid-state NMR. The realization of the main logic operations in liquid-state NMR is considered in details. Entanglement and quantum discord are introduced as measures of quantum correlations. A scheme of a solid state quantum computer is given. Possibilities of multiple quantum (MQ) NMR for problems of quantum information theory are discussed. In particular, we discuss investigations of entanglement and quantum discord by MQ NMR methods. As an example of investigations of quantum correlations, discord and entanglement of a spin pair in a nano-cavity in an external magnetic field are studied.

The work is supported by the Russian Foundation for Basic Research (grant 13-03-00017).

Introduction to magneto-optical spectroscopy and its modern applications

K.I. Gerasimov

E.K. Zavoisky Kazan Physical-Technical Institute of the RAS, 420029, Sibirsky Trakt 10/7, Kazan, Russia

Kazan Federal University, 420008, Kremlevskaya 18, Kazan, Russia

e-mail: gerasimov@kfti.knc.ru

Since the discovery of the Zeeman effect the magneto-optical spectroscopy was evolving as an additional method of optical spectroscopy and magnetic resonances. Today this is a powerful and full-featured instrument which is applied in a wide area of physical and chemical experiments. Investigations of the magneto-optical activity of compounds (magnetic linear and circular dichroism of optical transitions, Faraday rotation, Cotton-Mouton effect, etc.) based on the Zeeman splitting of energy levels give more information in comparison with optical spectroscopy techniques. More detailed and often unique information about the properties of matter can be obtained in experiments, in which the combination of two or three resonances is implemented (optical detection of magnetic resonance and its variations). This is one of the main reasons of using these complicated combined techniques and the origin of the progress of magneto-optical spectroscopy on the whole.

The lecture has an educational character and is addressed to young scientists. The lecture includes information about the principles of magneto-optical effects and also is an overview of classical and modern magneto-optical spectroscopy methods and of their applications to the research in various fields of physics.

Negative refraction index: a new hot area in physics and engineering

V.A. Atsarkin

Kotel'nikov Institute of Radio Engineering and Electronics of RAS, 125009 Moscow, Mokhovaya 11

e-mail: atsarkin@mail.cplire.ru

In the past few years, a new class of artificial metamaterials has been arisen, which possess both negative dielectric permittivity and negative magnetic permeability. Such materials were shown to have negative refraction index (n<0), thus leading to a number of exotic phenomena in microwave and optical ranges. In this report, a review is given on fundamental concepts and design features of the negative refractive index ("left-handed") materials, starting from the pioneer theoretical work by V.G. Veselago [1] and remarkable practical ideas by J.B. Pendry and his co-workers [2]. Interplay with magnetic resonance is emphasized, including the use of FMR for producing negative permeability. Attention is given to physical grounds and experimental realizations of such striking effects as abnormal refraction, far-field imaging beyond the diffraction limit ("perfect lenses" and "hyperlenses"), the invisibility cloak, etc. Current state and further prospects in this field are discussed.

References

[1] V.G. Veselago, *Usp. Fiz. Nauk* **92**, 517 (1967)

[2] J.B. Pendry et al., 1996 *Phys. Rev. Lett.* **76,** 4773 (1996); *IEEE Trans.MTT* **47**, 2075 (1999); *Phys. Rev. Lett.* **85**, 3966 (2000)

Frustration phenomena in the intrinsic two-component magnetoelectric material Li_2ZrCuO_4

E.L.Vavilova

Zavoisky Physical-Technical Institute, Kazan Scientific Center of Russian Academy of Sciences, 420029 Sibirskii Trakt 10/7, Kazan, Russia

e-mail: Jenia.vavilova@gmail.com

Frustrated magnetism now is an extremely active field of research in condensed matter physics. An important field is to discover and understand the new phases of matter that often emerge at low temperatures in the frustrated materials. These phases provide examples of non-trivial phenomena, arising from the interaction of large numbers of spins. In the lecture we are going to consider the different types of frustrations and various states induced by effects of frustration. The chain compound γ-Li_2ZrCuO_4 will be presented as an example of a frustrated magnet. There are interpenetrating sublattices of frustrated quasi-one-dimensional $s = 1/2$ quantum Heisenberg magnetic Cu^{2+} chains and quantum Ising electric sublattice of Li ions in this oxide material. This compound can be treated as a promising model material for investigations of fundamental interactions between magnetic and electric degrees of freedom in complex transition metal oxides.

Phase relaxation in magnetically diluted crystals

F.S. Dzheparov[1,2,3], D.V. Lvov[1,2], M.A.Veretennikov[4]

[1]Institute for Theoretical and Experimental Physics, 117218, Moscow, Russia

[2]National Research Nuclear University "MEPhI", 115409, Moscow, Russia

[3]Moscow Institute of Physics and Technology, 141700, Dolgoprudny, Moscow Region, Russia

[4]Institute of Radio Engineering and Electronics of RAS, 125009, Moscow, Russia

e-mail: dzheparov@itep.ru

New method for construction of main correlation functions of nuclear paramagnets is developed. The method combines projection techniques (convolution master equations) and cumulant expansions (convolutionless master equations) and produces satisfactory description for free induction decay (FID) and resonance line form function (LFF) in magnetically concentrated crystals. Transfer of polarization in magnetically diluted crystals is taken into account for the first time. It produces substantial slowing down of the FID if time is larger then phase relaxation time T_2. FID in magnetically diluted systems remains positive contrary to its oscillating behavior in magnetically concentrated crystals. Comparison with existing experimental results is fulfilled.

Resonance line form function (LFF) $G(\omega)$ and free induction decay (FID) $F(t)$ belong to main measurable values in nuclear magnetic resonance (NMR) [1]. They are measured carefully now in magnetically concentrated crystals (MCC) both for matrix (^{19}F in CaF_2 [2] for example) and impurity (^{8}Li in LiF [3]) spins, and corresponding theoretical description is constructed, see for example [1, 3-6] and reference therein. But reliable experimental information about magnetically diluted crystalline systems (MDC), like ^{29}Si in silicon or ^{13}C in diamond, is absent. Recently a unification of the theory of phase relaxation in MCC and MDC was constructed [7-9]. The lecture is devoted to discussion of main properties of the new theory and to its correspondence with existing measurements [10-14].

The theory combines projection operator technique of Nakajima-Zwanzig with Anderson-Weiss-Kubo (AWK) stochastic local field approach. Both methods are famous and have many names. Projection operator technique is frequently referred to as memory function method or convolution master equations. Other names of Anderson-Weiss-Kubo approach are cumulant expansions or convolutionless master equations. There exists extensive literature, where the methods are compared and their merits and demerits are revealed. We combined both approaches because memory function method is more flexible, but very important for our aims problem of one-spin phase relaxation in one-dimensional continuous stochastic field has exact solution in AWK model. Moreover, when interaction of the spin with this stochastic field is small, and we can expect, that the process can be described by memory function method within expansion in powers of the field, the perturbation solution has unphysical behavior near the top of corresponding one-spin LFF, contrary to exact solution [15]. Another contradiction consists in the fact that AWK approach gives reliable description of LFF of impurity nuclei [3, 6], but it can not reproduce oscillating FID for matrix spins, for example, in CaF_2.

Basis of the new theory is formed by connection between memory kernel $M(\tau)$ of master equation

$$\frac{\partial}{\partial t}F(t) = -\int_0^t d\tau M(\tau)F(t-\tau)$$
$$F(t) = \frac{\langle I_- I_+(t)\rangle_0}{\langle I_- I_+\rangle_0}, \quad I_+ = I_x + iI_y = \sum_{j=1}^N I_j^+, \quad I_- = (I_+)^+, \quad \langle\cdots\rangle_0 = \mathrm{Tr}(\cdots)/\mathrm{Tr}(1), \tag{1}$$

for FID $F(t)$ of matrix spins, and auxiliary memory kernel $M_I(\tau)$ of master equation

$$\frac{\partial}{\partial t}F_I(t) = -\int_0^t d\tau M_I(\tau)F_I(t-\tau), \qquad F_I(t) = \frac{\langle I_0^- I_0^+(t)\rangle_0}{\langle I_0^- I_0^+\rangle_0}, \tag{2}$$

for one-spin FID $F_I(t)$ in auxiliary system, where flip-flop interactions of the spin "0" are omitted, and other interactions and spins are the same, as in main system. Auxiliary FID $F_I(t)$ can be calculated independently, basing on the version of AWK theory, developed in [3, 6], then equation (2) defines auxiliary kernel $M_I(\tau)$. The connection between $M(\tau)$ and $M_I(\tau)$ defines $M(\tau)$, and Eq. (1) produces required FID $F(t)$ of matrix spins.

The program can be realized directly for magnetically concentrated systems (for the crystal CaF_2 for example) basing on exact values of first terms of expansions of main and auxiliary FIDs in powers of time (on knowledge of so called moments $M_{2n} = (-1)^n \frac{d^{2n}}{dt^{2n}}F(t=0)$ for main and auxiliary systems), and on general understanding of memory kernels evolution. Using representations

$$M(\tau) = M_2\chi(\tau), \qquad M_I(\tau) = M_{2I}\chi_I(\tau), \tag{3}$$

where M_{2I} is second moment for auxiliary system, we can expect, that the relation $\chi(\tau) = \chi_I(\tau)$ will be fulfilled with an accuracy of order of $1/z_e$. Here z_e is effective number of nearest neighbors. As a result we receive

$$G(\omega) = \int_{-\infty}^{\infty}\frac{dt}{2\pi}e^{i\omega t}F(t) = \frac{36}{25\pi}\cdot\frac{g_c(\omega)}{(\omega g_s(\omega) - 9/5)^2 + (\omega g_c(\omega))^2} \tag{4}$$

Here $M_2 = \frac{16}{9}M_{2I}$, and real functions $g_c(\omega)$ and $g_s(\omega)$ are defined as

$$\int_0^\infty dt e^{i\omega t}F_I(t) = g_c(\omega) + ig_s(\omega) \tag{5}$$

Auxiliary FID is

$$F_I(t) = \exp\left(-M_{2I}\int_0^t d\tau\,(t-\tau)\,\kappa(\tau)\right). \tag{6}$$

The result for magnetically concentrated system is shown on fig.1.

Application of the theory to magnetically diluted systems requires substantial modifications, because in main (continuum media) approximation FID $F(t)$ is not an analytical function of time, and in leading orders in spin concentration c [17]

$$F(t) = 1 - D_A|t| + \frac{5}{9}(D_A t)^2 + O\left(|D_A t|^3\right), \qquad D_A = \frac{2\pi^2}{3\sqrt{3}}\gamma^2 n\hbar \tag{7}$$

Here $n = c/\Omega$ is density of nuclei, γ is gyromagnetic ratio and Ω is a volume per one crystal site. Therefore we will use below the concentration expansion instead of time Taylor

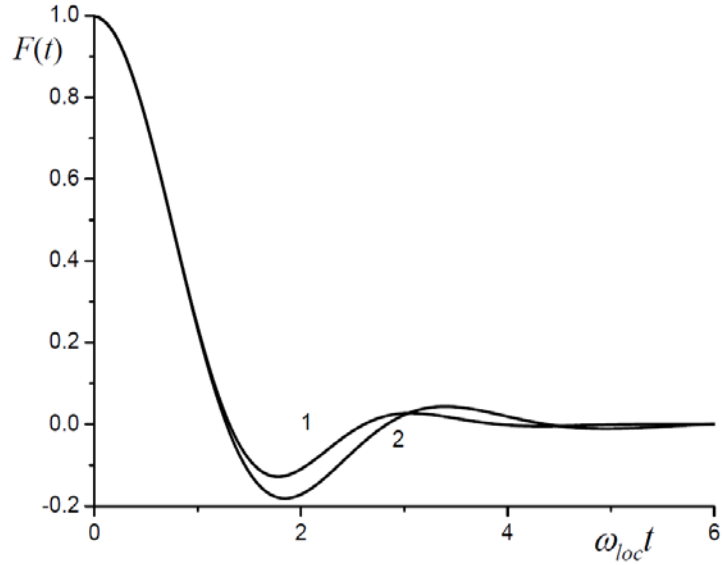

Fig.1. Free induction decay according to Eq. (4) (line 2) *vs* fitting [2] relation (line 1) $F(t) = a\sin(bt)/(b\mathrm{sh}(at))$. A relation $M_4 = 19/9 \cdot M_2^2$ is used as simple approximation for cubic crystals (see details in [16]). Three model approximations $\kappa(t) = \exp(-(\omega_{loc}t)^2/4)$, $\kappa(t) = 1/\cosh(\omega_{loc}t/\sqrt{2})$, $\kappa(t) = 1/(1+(\omega_{loc}t)^2/3)^{3/4}$, where $\omega_{loc} = M_2^{1/2}$, produce lines, coinciding within the thickness.

series, used above. Instead of the relation (6) we apply

$$F_I(t) = \exp\left(-\left(2B^2\int_0^t d\tau\left(t-\tau\right)\exp\left(-\alpha B\tau\right)\right)^{1/2}\right) \tag{8}$$

with $B = \frac{2}{3}D_A$, and value of $\alpha = 1/2$ will be obtained by comparison of calculated $F(t)$ with (7). The function $\kappa(\tau) = \exp\left(-\alpha B\tau\right)$ here has the same sense as $\kappa(\tau) = \exp(-M_2 t^2/4)$ in Eq. (6). It is simplest function, which represents influence of flip-flop transitions in surrounding spins and is compatible with analytical structure of the expansion (7). The radical in (8) represents static fluctuations of interactions due to random distribution of positions of spins. If $\alpha = 0$, then (8) coincides with exact solution, obtained by Anderson and Abragam [18] for MDC in absence of flip-flop transitions. Other argumentation for relation (8) can be found in Ref. [9]. To introduce the connection between the main and auxiliary kernels we use Laplace representation

$$M(\lambda) = \int_0^\infty dt\exp(-\lambda t)M(t) = m(\lambda)\sigma(\lambda), \quad M_I(\lambda) = \int_0^\infty dt\exp(-\lambda t)M_I(t) = m_I(\lambda)\sigma_I(\lambda). \tag{9}$$

Here the functions $m(\lambda)$ and $m_I(\lambda)$ contain terms of order c^1 only, correspondingly $\sigma(\lambda, c\to 0) = 1$, and $\sigma_I(\lambda, c\to 0) = 1$. A difference between $\sigma(\lambda)$ and $\sigma_I(\lambda)$ is expected of order $1/z_e$, where effective number of neighbors $z_e = 6.6$ [9]. As a result, continuum media approximation produces $M(\lambda) = 3/2\cdot M_I(\lambda)$, $\alpha = 1/2$ and

$$G(\omega) = \frac{6}{\pi}\cdot\frac{g_c\left(\omega\right)}{\left(\omega g_s\left(\omega\right)-3\right)^2 + \left(\omega g_c\left(\omega\right)\right)^2} \tag{10}$$

Numerical and analytical analysis indicate [9] that in main time domain, where $F_I(t) > 0.01$, with a satisfactory accuracy

$$F(t) \approx \Phi(t) = \frac{2}{5} F_I(t) \left(1 + \frac{3}{2} F_I^{5/6}(t) - \frac{5}{12} \left(1 - F_I(t) \right)^2 \right). \tag{11}$$

Dependence on crystal structure is restored by a substitution

$$|t| \to t_e(t) = \frac{c}{D_A} \sum\nolimits_{\mathbf{r} \neq 0} \left(1 - \cos\left(\frac{3}{2} b_{0\mathbf{r}} t \right) \right), \qquad b_{0\mathbf{r}} = \frac{\gamma^2}{2r^3} \left(1 - 3\cos^2 \vartheta_{0\mathbf{r}} \right). \tag{12}$$

Here $b_{0\mathbf{r}}$ is standard coefficient of dipole-dipole interaction. Equality $|t| = t_e(t)$ is fulfilled, if the sum is substituted by the integral $\sum_{\mathbf{r} \neq 0} \to \int \frac{d^3 r}{\Omega}$. This action has took place when the relation (7) for D_A has been obtained. Correspondingly, LFF for the crystal is

$$G(\Delta) = \int_{-\infty}^{\infty} \frac{dt}{2\pi} e^{i\Delta t} \Phi\left(t_e(t) \right). \tag{13}$$

Results for FID $F(t)$ in magnetically diluted systems are shown on fig.2. It should be noted that both new result and preceding one are based on the same concentration expansion (7), therefore they coincide at small time. It is clearly seen, that oscillations on the scale $T_2 = \int_0^{\infty} dt F(t)$ are absent, while they exist in magnetically concentrated systems on fig.1.

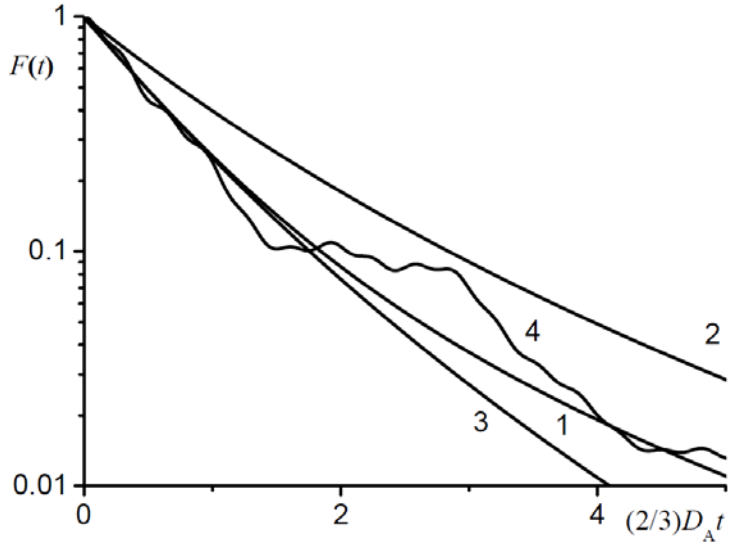

Fig.2. Free induction decay $F(t)$ for magnetically diluted system (line 1) obtained from Eq. (11). Other lines: 2 — auxiliary FID $F_I(t)$, 3 — FID from [17], where relation, similar to (8) was applied to $F(t)$ directly, 4 — FID for silicon crystal when $c = 0.0467$ and external field $\mathbf{H}_0 \parallel [111]$.

Experimental data for direct comparison with our theory in 3-dimentional systems are absent now, because broadening by additional interactions was substantial in all known measurements. Nevertheless we marked out Refs. [10-14], where comparison can be fulfilled with minimal additional assumptions. These studies were carried out using nuclei ^{29}Si in silicon crystals. Fig.3 in Ref. [10, 11] presents a FID for silicon powder, measured using Hahn spin echo method. The result is in satisfactory agreement with the relation

$$F(t) = F_0(t) = \left\langle \exp\left(-c \sum\nolimits_{\mathbf{r} \neq 0} \left(1 - \cos\left(b_{0\mathbf{r}} t \right) \right) \right) \right\rangle_p, \tag{14}$$

where $\langle \cdots \rangle_p$ indicates averaging on crystallites orientations. The relation (14) corresponds to absence of flip-flop interactions for all spins in the sample (see for example [19]). It was unknown for authors and they used direct numerical simulation. The result indicates that the samples were worthless for studies of pure dipole dynamics. Indeed, it has been shown in [20], that the doping level, used in [11], produces large inhomogeneous broadening due to inhomogeneous Knight shift. Estimations indicate, that difference of the Knight shifts for nuclei ^{29}Si, placed at mean distance $r_c = (\Omega / c)^{1/3}$, is much larger, than expected dipole line width $D_A(c = 0.0467) = 42.1$ Hz. Therefore flip-flop interactions are non secular and should be omitted, that gives the relation (14).

Line form function $G(\Delta)$ was measured in [12] on single crystals with concentration $c = 0.012$, 0.0467 and 0.103 at $\mathbf{H}_0 \parallel [111]$. Authors tried to separate pure dipole part in the HWHM $\Delta_{1/2}$ and in $G(\omega = 0)$. They supposed that additional broadening is the same for all samples, revealed that these parameters have linear dependence on *c*, and considered as dipole the parts, proportional to *c*. We fulfilled more extensive analysis using calculated (without fitting parameters) LFF and broadening by Voigt function. It was the same for all samples and has $D_L = 2\pi \cdot 7.6(4)$ Hz and $D_G = 2\pi \cdot 22.6(6)$ Hz for Lorenz and Gauss components respectively. It is seen from the fig.3, fig.4 and fig.5 that central parts of the lines are in

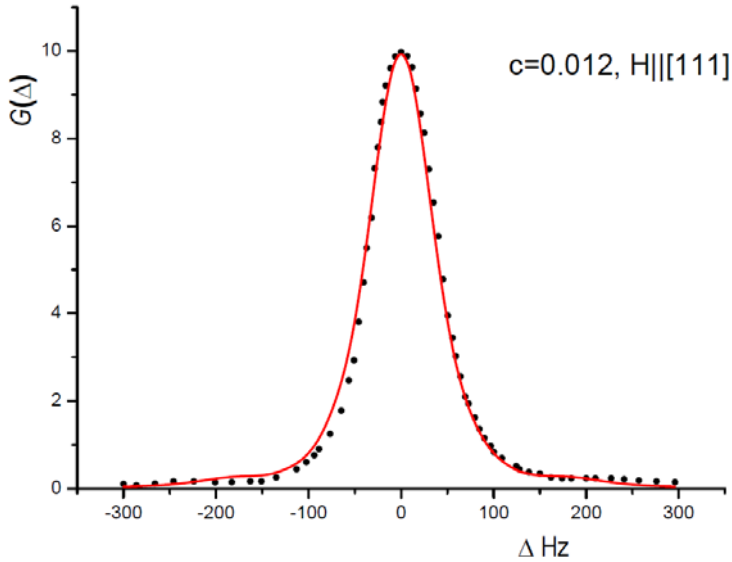

Fig.3. Comparison of experimental data [12] (points) with theoretical line (13) (containing no fitting parameters), broadened by the Voigt function (see the text).

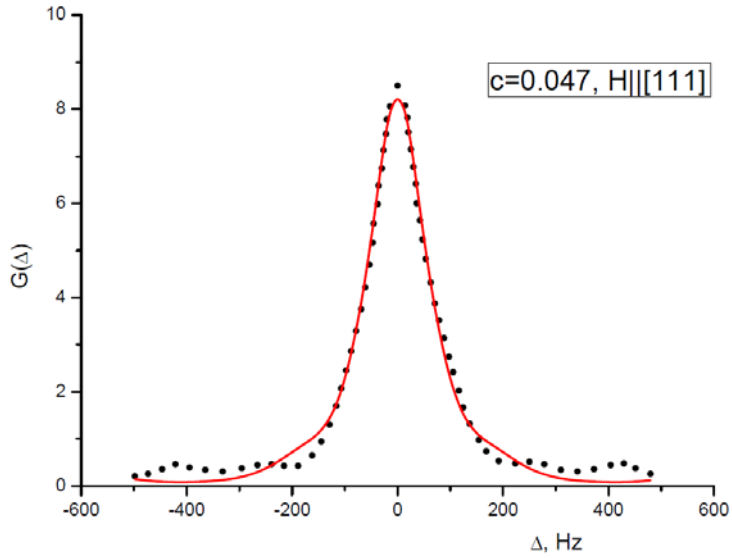

Fig.4. Comparison of experimental data [12] (points) with theoretical line (13) (containing no fitting parameters), broadened by the Voigt function (see the text).

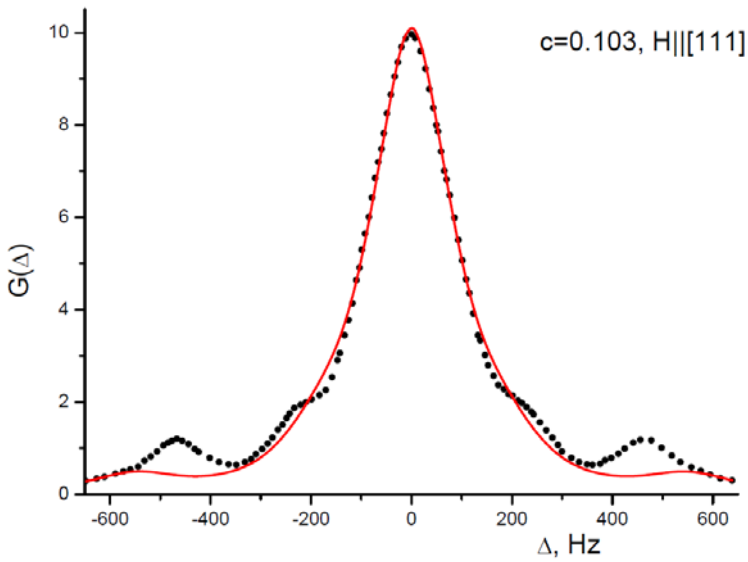

Fig.5. Comparison of experimental data [12] (points) with theoretical line (13) (containing no fitting parameters), broadened by the Voigt function (see the text).

satisfactory agreement with the theory, but description of positions and magnitudes of satellites is not good. The satellites are produced by spins, placed at distance, comparable with minimal spacing between nuclei in the crystal.

Therefore we fulfilled similar treatment of line form functions, measured in single crystals with c=0.0467 for three orientations of the external field [13, 14]. Authors of these works gave special attention to satellites, and declared good agreement of measurements with theoretical estimations. Our results are shown on fig.6, fig.7 and fig.8.

Coincidence of our theory and measurements [13, 14] in central parts of the lines is satisfactory as well, and agreement in satellites is much better, then on fig.3, fig.4 and fig.5, but the broadening is larger: $D_L = 2\pi \cdot 16(2)$ Hz and $D_G = 2\pi \cdot 41(2)$ Hz, that suppress the differences.

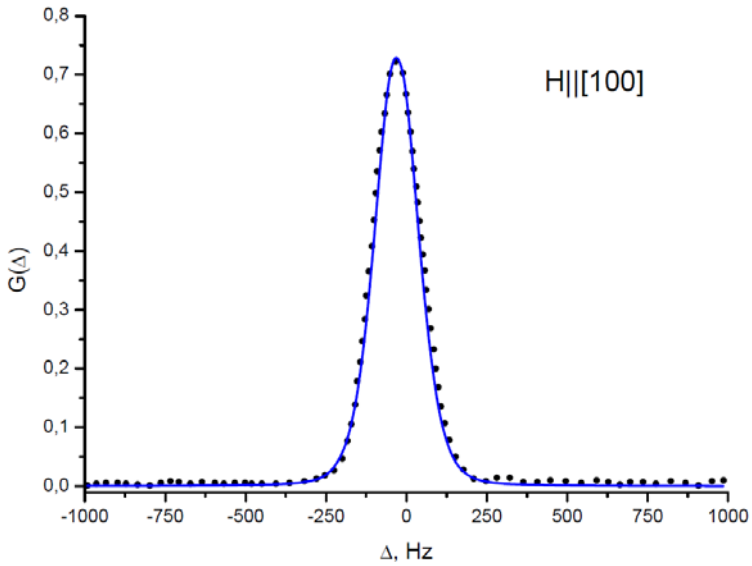

Fig.6. Comparison of experimental data [13, 14] (points) with theoretical line (13) (containing no fitting parameters), broadened by the Voigt function (see the text).

Theoretical arguments of Refs. [13, 14] on satellites magnitudes and positions are two-particle in essence, and they are reproduced in our relation (13) automatically. Therefore we compared additionally our results with numerical modeling, fulfilled on 6-spin system, which is presented at Fig. 17 of Ref. [10], and we received practical agreement for positions and magnitudes of satellites. The result indicates, that prescription (12) as accurate enough, and difference of the theory with experiment [12] remains unclarified.

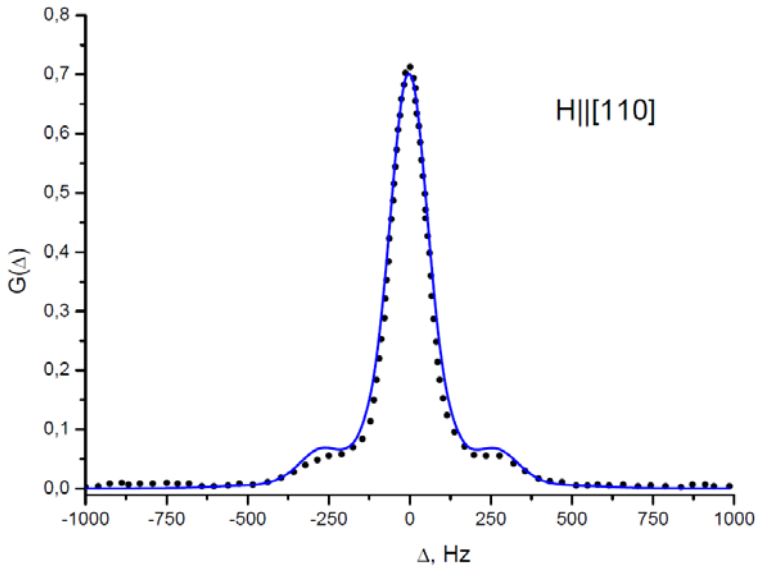

Fig.7. Comparison of experimental data [13, 14] (points) with theoretical line (13) (containing no fitting parameters), broadened by the Voigt function (see the text)

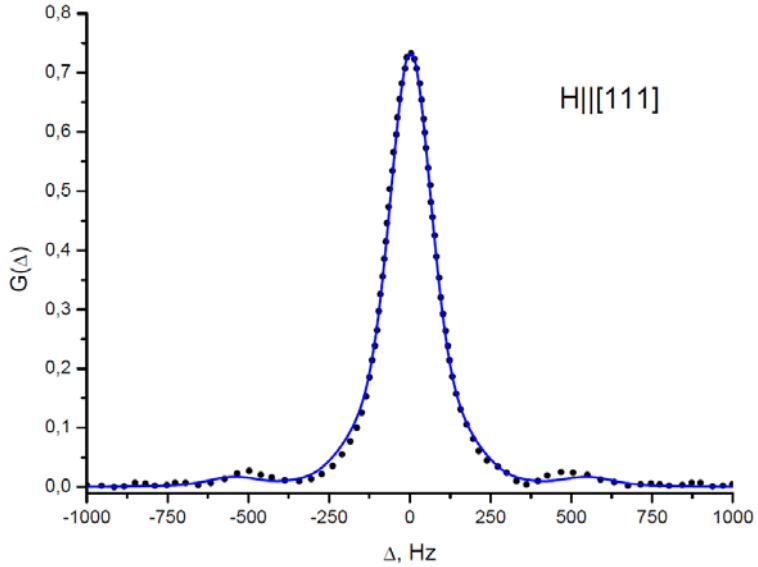

Fig.8. Comparison of experimental data [13, 14] (points) with theoretical line (13) (containing no fitting parameters), broadened by the Voigt function (see the text).

New measurements are necessary.

The work was supported by RFBR, project № 11-02-00880a.

References

[1] A. Abragam, M. Goldman. Nuclear magnetism: Order & disorder. Clarendon press, Oxford 1982.

[2] M. Engelsberg, I.J. Lowe. Phys. Rev. **B10**, 822, 1974.

[3] M.I. Bulgakov, A.D. Gulko, F.S. Dzheparov, S.V. Stepanov, S.S. Trostin. Pis'ma v ZhETF **58**, 614, 1993.

[4] V.E. Zobov, M.A. Popov. ZhETF **127**, 877, 2005.

[5] V.L. Bodneva, A.A. Lundin. ZhETF **135**, 1142, 2009.

[6] Yu.G. Abov, A.D. Gulko, F.S. Dzheparov, S.V. Stepanov, S.S. Trostin. Phys. Part. Nucl. **26**, 692, 1995.

[7] F.S. Dzheparov. Combining of projection operator technique of Nakajima-Zwanzig with Anderson-Weiss-Kubo stochastic local field approach for calculation of correlation functions in spin dynamics. Pp. 11-18 in "Actual Problems of Magnetic Resonance and

Its Application. XIII Intern. Youth Scientific School. Program, Lecture Notes, Proceedings." Kazan State University 2010.

[8] F.S. Dzheparov. J. of Phys.: Conf. Ser. **324**, 012004, 2011.

[9] F.S. Dzheparov, D.V. Lvov, M.A.Veretennikov. Pis'ma v ZhETF **98**, 543, 2013.

[10] D. Li, Y. Dong, R.G. Ramos, J.D. Murray, K. MacLean, A.E. Dementyev, S.E. Barrett. Phys. Rev. **B77**, 214306, 2008.

[11] D. Li, Y. Dong, R.G. Ramos, J.D. Murray, K. MacLean, A.E. Dementyev, S.E. Barrett. arXiv: 0704.3620v [cond-mat.mes-hall].

[12] H. Hayashi, K.M. Itoh, L.S. Vlasenko. Phys. Rev. B **78**, 153201, 2008.

[13] A.S. Verhulst, D. Maryenko, Y. Yamamoto, K.M. Itoh. Phys. Rev. B **68**, 054105, 2003.

[14] A.S. Verhulst. Optical pumping experiments to increase the polarization in nuclear-spin based quantum computers. Thesis. Stanford University 2004.

[15] F.S. Dzheparov. Some modern problems in beta-NMR-spectroscopy. Pp. 58-65 in "VI Int. School on Neutron Physics, Lectures", v.2, Dubna 1991.

[16] T. Charpentier, D. Sakellariou, J. Virlet, F.S. Dzheparov, J.-F. Jacquinot. J. of Chem. Phys. **127**, 224506, 2007.

[17] F.S. Dzheparov, I.V. Kaganov. JETP Lett. **75**, 259, 2002.

[18] A. Abragam. The Principles of Nuclear Magnetism. Oxford 1961.

[19] F.S. Dzheparov. J. of Superconductivity and Novel Magnetism, **20**, 161, 2007

[20] M.J. Hirsch, D.F. Holcomb. Phys. Rev. B **33**, 2520, 1986.

Intercommunication of electronic and magnetic properties of iron and iron pnictides

A.A. Katanin, P.A. Igoshev, A.V. Efremov, A.I. Poteryaev, V.I. Anisimov

Institute of Metal Physics Ural Div. RAS, Ekaterinburg

e-mail: katanin@mail.ru

Investigations of ferromagnetism of iron attract a lot of attention in spite of both, theoretical and practical interest to this substance. To explain physical properties of iron it is important whether local moments exist in this material and whether (some) electronic states are incoherent. We consider this problem within the ab initio LDA+DMFT approach, considering in particular orbitally-resolved contributions to one- and two-particle properties [1-3].

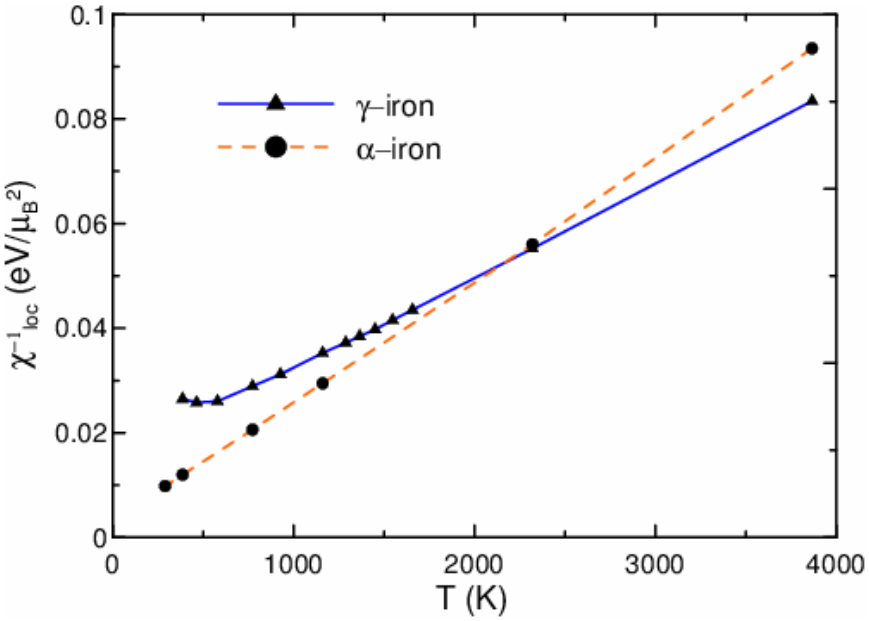

Fig.1.

Fig.1 shows the temperature dependence of the obtained inverse local spin susceptibility. For α-iron it is almost linear with temperature, while for γ-iron the linearity is observed for T > 1000 K only. The local dynamic spin susceptibility (fig.2) has for α -iron has a peak at ω = 0, which width (height) scales (inversely) proportional to the temperature. For γ- (fcc) iron the width of the peaks of dynamic susceptibility remains sufficiently small, while its height and frequency dependence does not follow the same scaling form, as in α-iron. These features are attributed to the existence of local moments (for γ-iron above 1000 K) in these materials, which appear due to flat parts of electronic dispersion (extended van Hove singularity) and Hund exchange interaction. The obtained size of the effective moments is $\mu = 3.3\ \mu_B$ for α-iron and $\mu = 3.8\ \mu_B$ for γ-iron.

The temperature dependence of the instantaneous average $\langle S_Z^2 \rangle$ is shown on fig.3. One can see that at not too low temperatures $T > 1500$ K, $\langle S_Z^2 \rangle$ for γ-iron shows even weaker temperature dependence, than for α-iron, and its value is closer to the local moment value $\mu_{loc}^2 / 3\mu_B^2$, extracted from the temperature dependence of the local susceptibility. Therefore,

one can expect that at intermediate and high temperatures magnetic properties of γ-iron can be to a good accuracy described within the pure local-moment picture.

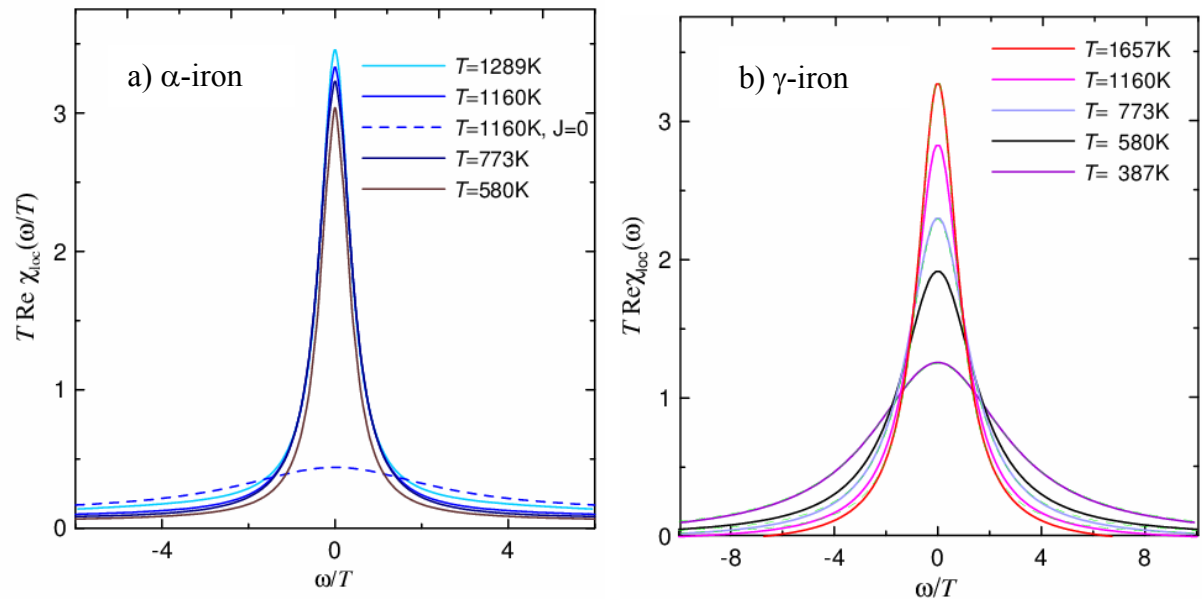

Fig.2.

At low temperatures γ-iron (when stabilized in precipitates) is better described within itinerant picture, in particular its antiferromagnetism is naturally explained by nesting features between different sheets of the Fermi surface.

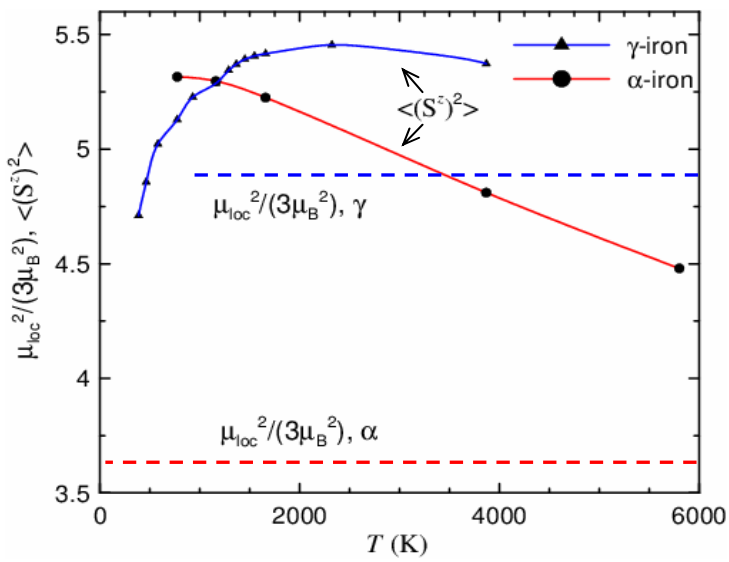

Fig.3.

References

[1] A. A. Katanin, A. I. Poteryaev et al., Phys. Rev. B **81**, 045117 (2010)

[2] S.L. Skornyakov, A.A. Katanin, and V.I. Anisimov, Phys. Rev. Lett. **106**, 047007 (2011).

[3] P. A. Igoshev, A. I. Efremov, etal., ArXiv 1210.2188; Phys. Rev. B, in press(2013).

Optimization of functionalized nanodiamond platforms for gene delivery to area of peripheral nerve trauma by HF EPR

T. Biktagirov[1], B. Yavkin[1], G. Mamin[1], S. Orlinskii[1], I.I. Salafutdinov[2], A.A. Rizvanov[2], Yu.A. Chelyshev[1,3], S.I. Nikolaev[3], Y.O. Muhamedshina[3], O.A. Shenderova[4]

[1]Kazan Federal University, Institute of Physics, Kremlevskaya str. 18, 420008 Kazan, Russia

[2]Kazan Federal University, Institute of Fundamental Medicine and Biology , Kremlevskaya str. 18, 420008 Kazan, Russian

[3]Kazan State Medical University, Russia, 420012, Kazan, Butlerov Str., 49

[4]International Technology Center, 8100 Brownleigh Dr., Raleigh, NC 27617, USA

e-mail: Sergei.Orlinskii@kpfu.ru

The attractive properties of nanodiamonds (NDs) will be exploited for the development of therapeutic agents for diagnostic probes, gene therapy and novel medical devices. Today it is important to develop methods for control nanosystems [1, 2, 3].

Herein, we present the first results of observation of EPR spectra of functionalized nanodiamond platforms for gene delivery (ND-NH_2-pDNA). Quality and number of ND we control by EPR spectra of N^0 center. This paramagnetic defect is associated with single substitutional nitrogen atom in a zero-charge state.

The remaining contributions to the spectra can be described by two overlapped Voigtian lines with isotropic g-values of 2.0030 (the narrow line, denoted as SC1) and 2.0024 (the broad line, denoted as SC2) as presented on fig.1.

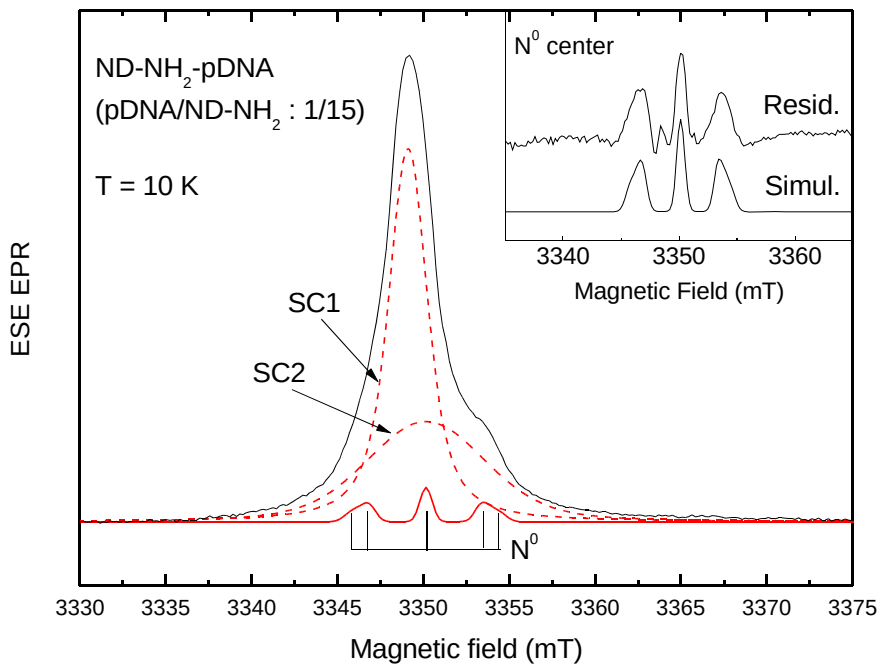

Fig.1. EPR spectrum of ND-NH2-pDNA complex prepared with relative pDNA content of 1/15. Simulated spectra of the surface centers (SC1 and SC2) and N^0. Experimental spectrum was measured in W-band mode at 10 K. Inset: The result of subtraction of SC1 and SC1 from the experimental spectrum (top) compared to simulated spectrum of N^0 (bottom).

We found that the width of the EPR line (SC2**)** correlates with the amount of pDNA bound to ND-NH_2. At the same time, complex ND-NH_2 (EPR SC1) are located closer to the surface of nanocrystal.

To summarize, we propose that the spectral and dynamical parameters of the surface paramagnetic defects can be used to control the properties of the nanosized complexes based on functionalized ND.

References

[1] Soltamova, A. A., Ilyin, I. V., Baranov, P. G., Vul, A. Y., Kidalov, S. V., Shakhov, F. M., G.V. Mamin, S.B.Orlinskii, N.I.Silkin, Salakhov, M. K. (2009). Detection and identification of nitrogen defects in nanodiamond as studied by EPR. Physica B: Condensed Matter, 404(23), 4518-4521.

[2] Baranov, P.G. Enormously High Concentrations of Fluorescent Nitrogen-Vacancy Centers Fabricated by Sintering of Detonation Nanodiamonds. / P.G. Baranov, A.A. Soltamova , D.O. Tolmachev, N.G. Romanov, R.A. Babunts, F.M. Shakhov, S.V. Kidalov, A.Y. Vul', G.V. Mamin, S.B. Orlinskii, N.I. Silkin// Small. -2011. –V.7. N.11. -P. 1533-1537.

[3] S. B. Orlinskii, R. S. Bogomolov, A. M. Kiyamova, B. V. Yavkin, G. M. Mamin, S. Turner, G. Van Tendeloo, A. Shiryaev, I. I. Vlasov, and O. Shenderova, Identification of Substitutional Nitrogen and SurfaceParamagnetic Centers in Nanodiamond of Dynamic Synthesis by Electron Paramagnetic Resonance. Nanoscience and Nanotechnology Letters Vol. 3, 1–5, 2011

Spin dynamics and relaxation in the presence of microwaves

E.I. Baibekov

Kazan Federal University, 420008, Kremlevskaya 18, Kazan, Russian Federation

e-mail: edbaibek@gmail.ru

Solids containing ensembles of electron spins are considered as promising materials in quantum information processing because of relatively long coherence times and potential for scalability [1]. Coherent spin manipulations that are necessary for quantum computation can be achieved with proper adjustment of the strength and duration of pulsed microwave field. However, suppressing the decoherence in the spin ensemble driven by microwaves still represents a challenging problem. We analyze possible mechanisms of such "driven decoherence", some of those have no direct analogues in the microwave-free regime. They are best described in terms of fluctuating magnetic fields produced at the position of a given spin. The sources of these fields can be

- internal, such as dipole interactions between the spins of the ensemble,
- external (interactions with the neighboring nuclear spins),
- or come directly from the interaction with the microwave field.

The role of dipole interactions between the electron spins is analyzed in the framework of Anderson's statistical theory modified for the rotation reference frame. The corresponding coherence times obtained in the continuum approximation are found to be inversely proportional to the spin concentration and depend on the microwave field strength [2]. The interaction of the electron spins with the nuclear spin bath represents the case when the coupled spins have completely different resonance frequencies, and relatively long coherence times are expected. However, Hartmann-Hahn polarization transfer boosts the relaxation when the electron spin nutation frequency comes close to the nuclear spin precession frequency [3]. Finally, the coupling of the electron spin ensemble with the resonant mode of a microwave cavity will be discussed. At low temperature, the whole system is known to be in a coherent spin-photon state that manifests itself by the splitting of the cavity mode frequency (vacuum Rabi splitting [4]). This coherence is lost with the increase of temperature as the splitting is gradually reduced and the split lines of the cavity emission spectrum are broadened.

This work was supported by RFBR (grant no. 12-02-31336) and by Dynasty Foundation.

References

[1] D. Loss, D. P. Di Vincenzo, Phys. Rev. A **57**, 120 (1998).

[2] E. I. Baibekov, JETP Lett. **93**, 292 (2011).

[3] J.H. Shim, S. Bertaina, S. Gambarelli, T. Mitra, A. Müller, E. I. Baibekov, B. Z. Malkin, B. Tsukerblat, B. Barbara, Phys. Rev. Lett. **109**, 050401 (2012).

[4] J.J. Sanchez-Mondragon, N.B. Narozhny, J.H. Eberly, Phys. Rev. Lett. **51**, 550 (1983).

Preferred conformation of ibuprofen in chloroform by 2D NOESY

I.A. Khodov[1], S.V. Efimov[2], V.V. Klochkov[2], L.A.E. Batista de Carvalho[3]

[1]G.A. Krestov Institute of Solution Chemistry of the Russian Academy of Sciences, 153045, ul. Akademicheskaya 1, Ivanovo, Russia

[2]Kazan Federal University, 420008, ul. Kremlevskaya 18, Kazan, Russia

[3]University of Coimbra, P 3004-535, Rua Larga, Coimbra, Portugal

e-mail: ilya.khodov@gmail.com

Determination of spatial structure and conformational state of biologically active molecules attracts an increasing interest today [1–3]. Polymorphism of drug compounds is known to affect their biological activity, and thus it plays an important role in the production of pharmaceuticals. In turn, properties of a polymorph depend on the structure of the molecules and their ability to exist in different conformations in a solvent from which recrystallization is conducted. For this reason, seeking for new polymorphic forms of drugs is closely related to investigations of conformational state of biologically active molecules in saturated solvents.

In this work, we determined the preferred conformation among known structures A–H (fig. 1) and parameters of conformational equilibrium of ibuprofen in chloroform by two independent methods: nuclear Overhauser effect spectroscopy (NOESY) and comparison of ^{13}C NMR data with quantum chemical calculations [1–3]. Observed 13C NMR chemical shifts were in qualitative agreement with conformers G and H dominating in solution. The

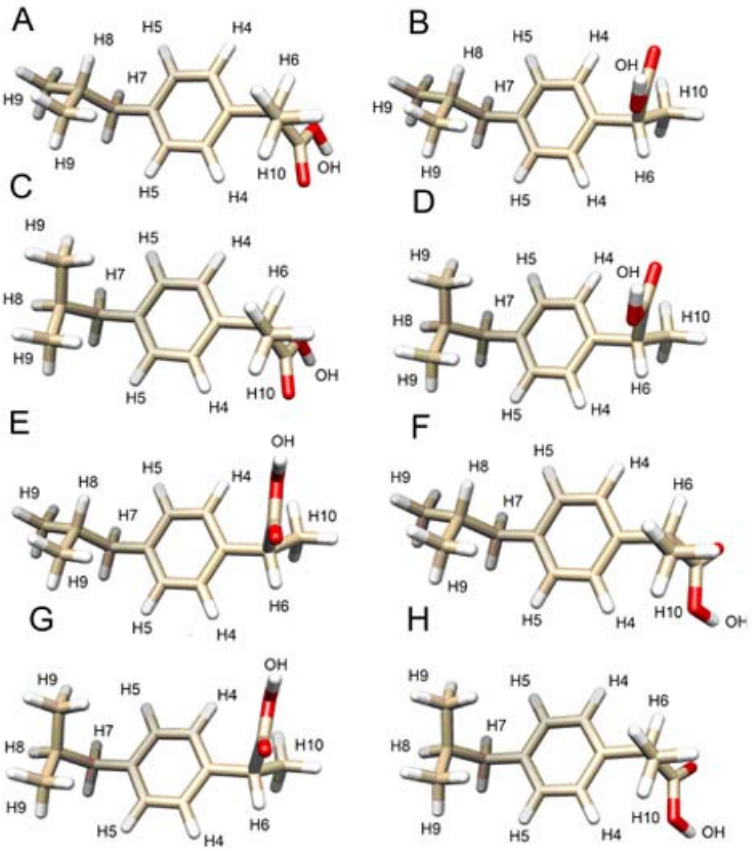

Fig.1. Main possible conformation of (*R*)-ibuprofen, according to the quantum chemical calculations [4].

choice of solvent was justified by high solubility of ibuprofen in $CHCl_3$ and practical significance of this solvent in the recrystallization process. Information on the distribution of conformers at maximal solution saturation may be used in studying processes of crystal nucleation from the solvent. Results of our experiments were also analyzed in the light of literature data, obtained by other methods.

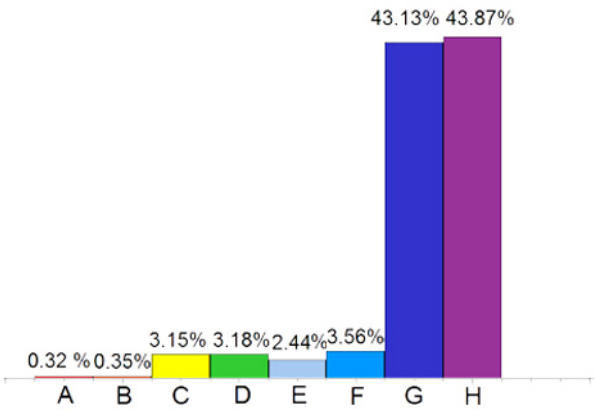

Fig.2. Distribution of ibuprofen conformers in the saturated solution by 2D NOESY analysis.

We proposed an approach to establish conformational state (preferred conformers) of small molecules in solutions, close to saturation, using the ibuprofen–chloroform system as an example. It was revealed by two independent methods that conformers G and H dominate in the saturated solution (fig. 2).

More accurate quantitative data on the distribution of conformers were obtained with the aid of the advanced analysis approach (ridge-regression analysis). An inversion-like change in the distribution was found upon transition from an unsaturated solution to the saturated one (fig. 3). Comparison of results of NOESY and X-ray data was used to demonstrate the importance of knowledge of preferred conformers in solutions: two different polymorph modifications are close to the structures which turn to dominate under different conditions in solution. On the present stage, however, we cannot determine relations between

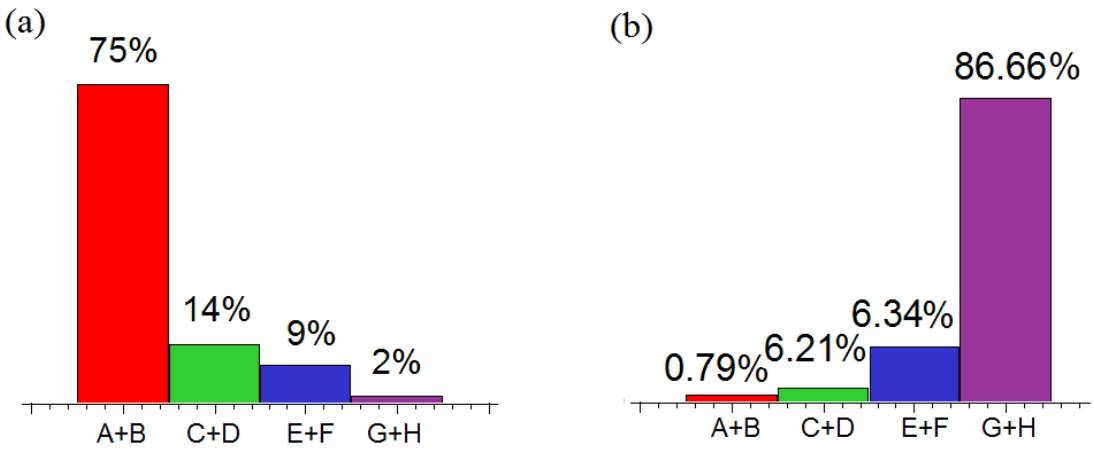

Fig.3. Distribution of ibuprofen conformers obtained from (a) quantum chemical calculations [4] and (b) analysis of 2D NOESY spectra in saturated $CDCl_3$ solution.

conformational state in solution and molecular structure in a given crystalline polymorph, since more detailed analysis of screening and X-ray data [5] for a crystal grown from chloroform are needed. (Literature data used here refer to a crystal grown from another solvent.) We hope that our general approach may help to shed light on fundamental laws regulating nucleation of crystalline polymorphs of other compounds.

Acknowledgements.

This work was performed under the auspices of the Marie Curie International Research Staff Exchange Scheme PIRSES-GA-2009-247500. Financial support was from the Russian Foundation for Basic Research, projects no. 13-03-97041 r_povolzh'e_a and no. 12-03-00775 a.

References

[1] Spatial structure of felodipine dissolved in DMSO by 1D NOE and 2D NOESY NMR spectroscopy / I.A. Khodov, M.Yu. Nikiforov, G.A. Alper et al. // Journal of Molecular Structure. – 2013. – Vol. 1035. – P. 358–362.

[2] Spatial structure of cyclosporin A and insight into its flexibility / S.V. Efimov, F.Kh. Karataeva, A.V. Aganov et al. / Journal of Molecular Structure. – 2013. – Vol. 1036. – P. 298–304.

[3] Spatial structure of heptapeptide Glu-Ile-Leu-Asn-His-Met-Lys, a fragment of the HIV enhancer prostatic acid phosphatase, in aqueous and SDS micelle solutions / D.S. Blochin, O.V. Aganova, A.R. Yulmetov et al. // Journal of Molecular Structure. – 2013. – Vol. 1033. – P. 59–66.

[4] Vueba, M.L. Conformational Stability of Ibuprofen: Assessed by DFT Calculations and Optical Vibrational Spectroscopy / M.L. Vueba, M.E. Pina, L.A.E.B. de Carvalho // Journal of Pharmaceutical Sciences. – 2008. – Vol. 97. – P. 845–859.

[5] Derollez, P. Ab initio structure determination of phase II of racemic ibuprofen by X-ray powder diffraction / P. Derollez, E. Dudognon // Acta Crystallographica Section B. – 2010. – Vol. 66. – P. 76–80.

Spin dynamics and magnetic phase transitions in monoclinic honeycomb-layered antimonates $A_3Ni_2SbO_6$ (A=Li, Na)

V.Y. Kudryashov[1], E.A. Zvereva[1], O.A. Savelieva[1], V.B. Nalbandyan[2], M. Evstigneeva[2], A.N. Vasiliev[1], B. Buechner[3]

[1]Faculty of Physics, Moscow State University, Leniskie Gory, 119991, Moscow, Russia
[2]Chemistry Faculty, South Federal University, Zorge 7, 344090, Rostov-na-Donu, Russia
[3]Leibniz Institute for Solid State and Materials Research IFW Dresden, D-01069, Germany
e-mail: nickkick@mail.ru

Introduction

The progress in synthesis of new layered oxides of alkaline and transition metals, which are potentially very interesting as solid electrolites and electrode materials in modern ionics [1,2], thermoelectric materials [3,4] and even superconductors [5] stimulates intensive studies of their physical properties, first of all, their magnetism as a fundamental property of any species possessing unpaired electrons. A great interest of scientists attracts recently a new generation of layered complex metal oxides with honeycomb-based crystal structure such as $A_3M_2XO_6$ and $A_2M_2YO_6$ (A=Li, Na; M = TM; X=Bi, Sb; Y=Te) phases. Here, we report on the static and dynamic magnetic properties of two new quasi-2D honeycomb oxides $Li_3Ni_2SbO_6$ and $Na_3Ni_2SbO_6$, which are characterized by above mentioned structural type (fig.1).

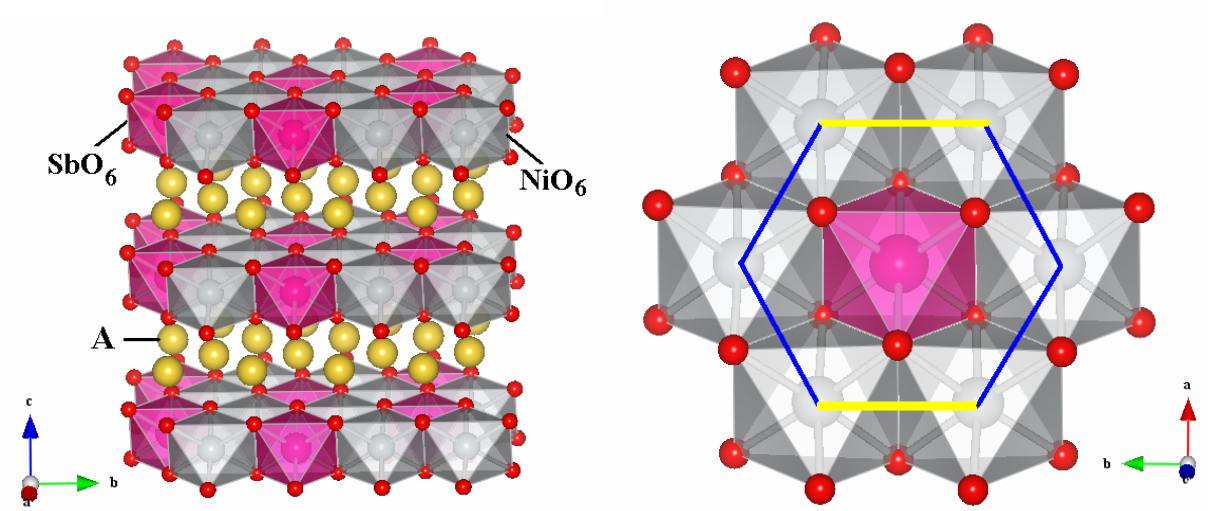

Fig.1. (left) Polyhedral view of a layered C2/m crystal structure of $A_3Ni_2SbO_6$ (A=Li, Na): SbO_6 are shown in pink, NiO_6 are in gray, A ions are yellow spheres, and oxygen are small red spheres. The octahedra around A ions are omitted for simplicity. (right) A fragment of the the C2/m structure in *ab*-plane (the magneto-active layers).

Experimental

New layered compounds $A_3Ni_2SbO_6$ (A=Li, Na) were prepared by conventional solid-state synthesis at 1150ºC. The magnetic measurements were performed using a Quantum Design MPMS-7 SQUID magnetometer. The temperature dependence of magnetic susceptibility was measured under variation of the magnetic field $B \leq 7$ T in the temperature range 1.8÷300 K. Electron spin resonance (ESR) studies were carried out using an X-band ESR spectrometer CMS 8400 (ADANI) (f≈9.4 GHz, B≤0.7 T) equipped by a low temperature

mount, operating in the range T=6-470 K. The effective g-factors of our samples have been calculated with respect to an external reference for the resonance field. We used BDPA (*a,g* -bisdiphenyline-*b*-phenylallyl), g_{et}=2.00359, as a reference material.

Results

It was found that both compounds $A_3Ni_2SbO_6$ (A=Li, Na) order antiferromagnetically with the Néel temperature ~ 15 and 17 K respectively. At high temperatures, the magnetic susceptibility follows the Curie-Weiss law the positive values of Weiss temperature ~ 8 K for Li sample and ~15 K for Na sample indicating predominance of ferromagnetic interactions. The effective magnetic moment is 4.3 μ_B/f.u. and agrees satisfactorily with theoretical estimations using determined in our work effective g-value ~2.15 and assuming high-spin configuration of Ni^{2+} (S=1). In applied magnetic fields the position of the Néel temperature is shifted to low temperature side. At the same time the magnetization curves demonstrate an upward curvature suggesting the possible presence of a magnetic field induced spin-flop transition at around 3 T at 2 K. The position of this anomaly shifts towards lower fields upon increasing the temperature and eventually disappears above the Néel temperature.

Electron spin resonance spectra in paramagnetic phase show a broad single Lorenzian shape line with isotropic temperature independent effective g-factor attributed to Ni^{2+}ion in octahedral coordination. Upon approaching the AFM ordering transition from above, both the g-value and the linewidth demonstrate sharp anomalies. The ESR linewidth, which is a measure of spin relaxation rate, anomalously increases when the temperature decreases up to T_N. The magnetic exchange pathways have been rationalized in accordance with the Goodenough-Kanamori rules. An analysis of the layered honeycomb crystal structure of $A_3Ni_2SbO_6$ has shown that the dominant superexchange interaction within mixed-cation layers of Ni and Sb appears to be ferromagnetic, while the coupling between magnetically-active layers is obviously antiferromagnetic providing the antiferromagnetic ground state of this compound. In consistence with the results obtained, the magnetic phase diagrams for new layered antimonates were proposed (fig.2).

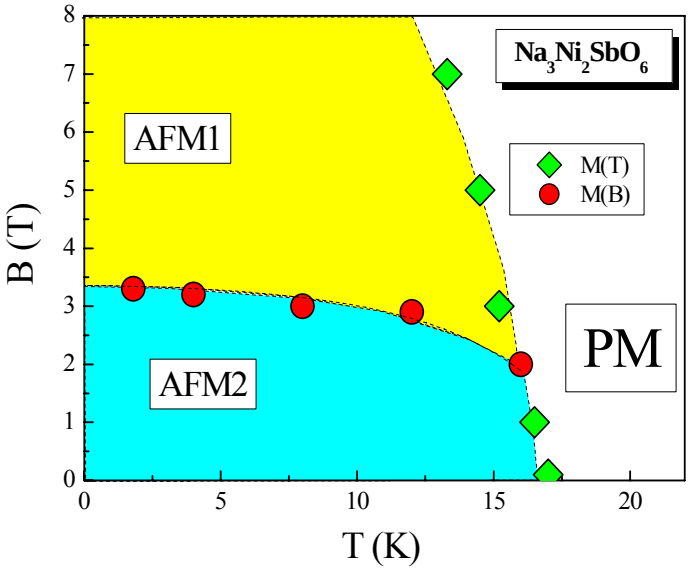

Fig.2. Magnetic phase diagram for quasi-2D honeycomb oxide $Na_3Ni_2SbO_6$.

References

[1] B. Xu, D. Qian, Z. Wang, Y.S. *Meng. Mater. Sci. Eng. R* **73**, 51–65 (2012).

[2] J.B. Goodenough, *J. Solid State Electrochem.* **16**, 2019–2029 (2012).

[3] I. Terasaki Y. Sasago, K. Uchinokura, *Phys. Rev. B* **56**, R12685 (1997).

[4] Y.Y. Wang, N.S. Rogado, R.J. Cava, N.P. Ong, *Nature* **423**, 425 (2003).

[5] K. Takada H. Sakurai, E. Takayama-Muromachi, F. Izumi, R.A. Dilanian, T. Sasaki, *Nature* **422**, 53 (2003).

NMR studies of reorientational motion of complex $[B_{12}H_{12}]^{2-}$ anions in $A_2B_{12}H_{12}$ (A = K, Rb, Cs)

O.A. Babanova[1], A.V. Soloninin[1], A.V. Skripov[1], V. Stavila[2], N. Verdal[3,4], T.J. Udovic[3], J.J. Rush[3,4]

[1]Institute of Metal Physics, Urals Branch of the Russian Academy of Sciences, 620990, S. Kovalevskoi 18, Ekaterinburg, Russia

[2]Sandia National Laboratories, 7011 East Avenue, Livermore, CA 94551-0969, USA

[3]NIST Center for Neutron Research, National Institute of Standards and Technology, 100 Bureau Dr., MS6102, Gaithersburg, MD 20899-6102, USA

[4]Department of Materials Science and Engineering, University of Maryland, College Park, MD 20742, USA

e-mail: babanova@imp.uran.ru

Introduction

Alkali-metal dodecahydro-*closo*-dodecaborates $A_2B_{12}H_{12}$ have received recent attention in hydrogen storage research, since they appear to be intermediate compounds in the decomposition of the corresponding tetraborohydrides ABH_4 [1]. The high stability of these compounds is believed to be partly responsible for the poor hydrogen cycling performance of the borohydrides. Therefore, information on atomic motion of the $B_{12}H_{12}$ groups in $B_{12}H_{12}$-based compounds may contribute to understanding the role of these intermediates in the processes of hydrogen desorption in borohydrides.

Alkali-metal dodecahydro-*closo*-dodecaborates are ionically bounded salts consisting of metal cations A^+ and icosahedral complex anions $[B_{12}H_{12}]^{2-}$. X-ray diffraction studies of alkali-metal compounds $A_2B_{12}H_{12}$ (A = K, Rb, and Cs) have revealed that they all have the cubic *Fm*-3 structure at room temperature [2]. The schematic view of the coordination environment of $B_{12}H_{12}$ groups in these compounds is shown in fig.1.

The aim of the present work is to study the reorientation motion of $B_{12}H_{12}$ groups in *closo*-dodecaborates $A_2B_{12}H_{12}$ (A = K, Rb, and Cs) using ^1H and ^{11}B NMR measurements of the spectra and spin-lattice relaxation rates. NMR appears to be especially effective for studies of atomic motion in ionic compounds like *closo*-dodecaborates $A_2B_{12}H_{12}$ systems or borohydrides [3] because nuclear spin-lattice relaxation rates in these compounds do not contain any significant contributions not related to atomic motion (such as the conduction-electron contribution in metallic systems). This allows us to trace the atomic jump rates in $A_2B_{12}H_{12}$ systems over the range of five orders of magnitude ($10^5 – 10^{10}$ s^{-1}).

Experimental methods

^1H and ^{11}B NMR measurements were performed on a modernized Bruker SXP pulse spectrometer with quadrature phase detection at the frequencies $\omega/2\pi$ = 14 and 23.8 MHz for ^1H, 14 and 28 MHz for ^{11}B. The magnetic field was provided by a 2.1 T iron-core Bruker magnet. A home-built multinuclear continuous-wave NMR magnetometer working in the range 0.32 – 2.15 T was used for field stabilization. Before the measurements, samples were annealed in vacuum at 200 ^oC to remove residual water and flame-sealed in glass tubes. For NMR measurements at $T \leq 470$ K, a probehead with the sample was placed into an Oxford Instruments CF1200 continuous-flow cryostat using N_2 as a cooling agent. The sample temperature, monitored by a chromel-(Au-Fe) thermocouple, was stable to ± 0.1 K.

Measurements in the temperature range 470 – 570 K were performed using a furnace probe head; for this setup, the sample temperature, monitored by a copper-constantan thermocouple, was stable to ± 0.5 K. The nuclear spin-lattice relaxation rates were measured using the saturation – recovery method. NMR spectra were recorded by Fourier transforming the spin echo signals.

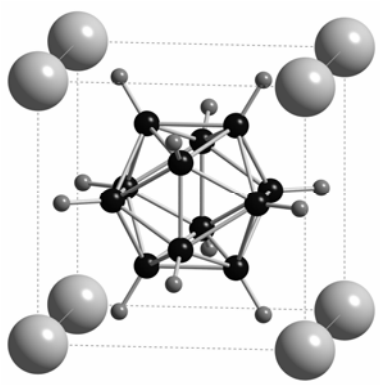

Fig.1. Schematic view of the coordination environment of $B_{12}H_{12}$ groups in alkali-metal dodecahydro-*closo*-dodecaborates $A_2B_{12}H_{12}$ (A = K, Rb, and Cs).
Large spheres: A atoms (A = K, Rb, and Cs), black spheres: boron atoms, and small grey spheres: hydrogen atoms.

Results and discussion

The results of NMR measurements of the proton spin-lattice relaxation rates R_1^H for dodecahydro-*closo*-dodecaborates $K_2B_{12}H_{12}$, $Rb_2B_{12}H_{12}$ and $Cs_2B_{12}H_{12}$ at two resonance frequencies $\omega/2\pi$ are shown in fig.2. The general features of the observed behavior of R_1^H for studied systems are typical of the relaxation mechanism due to nuclear dipole-dipole interaction modulated by thermally activated reorientational motion [4]. The proton relaxation rate exhibits the frequency-dependent peak at the temperature at which the reorientation jump rate τ^{-1} becomes nearly equal to ω. In the limit of slow motion ($\omega\tau >> 1$), R_1^H is proportional to $\omega^{-2}\tau^{-1}$, and in the limit of fast motion ($\omega\tau << 1$), R_1^H is proportional to τ being frequency-independent. If the temperature dependence of τ follows the Arrhenius law $\tau = \tau_0\exp(E_a/k_BT)$ with the activation energy E_a, a plot of log R_1^H vs. T^{-1} is expected to be linear in the limits of both slow and fast motion with the slopes of $-E_a/k_B$ and E_a/k_B, respectively. Thus, the activation energy E_a for the reorientational motion of $B_{12}H_{12}$ groups can be obtained directly from these slopes. In order to evaluate the motional parameters for $A_2B_{12}H_{12}$, we have used

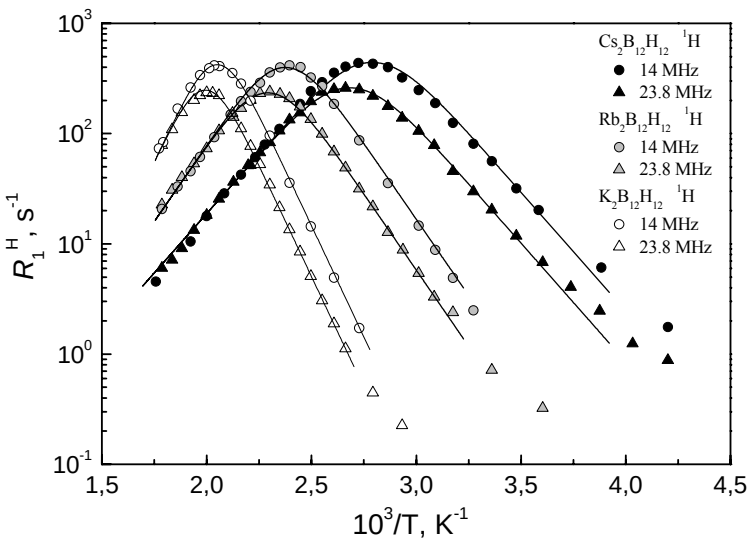

Fig.2. Proton spin-lattice relaxation rates measured at 14 and 23.8 MHz for $K_2B_{12}H_{12}$ $Rb_2B_{12}H_{12}$ and $Cs_2B_{12}H_{12}$ as functions of the inverse temperature. The solid lines show the simultaneous fit of the standard theory to the data.

the standard theory [4] relating R_1^H and τ and taking into account the $^1H - ^{11}B$ and $^1H - ^1H$ dipole-dipole interactions, as well as the Arrhenius law relating τ and T. The parameters of the model are the pre-exponential factor τ_0^{-1}, the activation energy E_a of the reorientations, and the fluctuating parts ΔM_{HB} and ΔM_{HH} of the dipolar second moment due to the H – B and H – H interactions. These parameters are varied to find the best fit to the $R_1^H(T)$ data at the two resonance frequencies *simultaneously*. The motional parameters resulting from the fit are shown in table 1.

Table 1. Motional parameters (activation energies E_a and pre-exponential factors τ_0 from the Arrhenius law) for reorientations of $B_{12}H_{12}$ groups in $A_2B_{12}H_{12}$ (A = K, Rb, and Cs).

	E_a, meV	τ_0, s	T-range, K
$K_2B_{12}H_{12}$	800 ± 8	$(6.0 \pm 0.5) \times 10^{-17}$	366 – 564
$Rb_2B_{12}H_{12}$	549 ± 5	$(3.1 \pm 0.7) \times 10^{-15}$	315 – 560
$Cs_2B_{12}H_{12}$	427 ± 4	$(1.1 \pm 0.4) \times 10^{-14}$	260 – 570

For all the studied *closo*-dodecaborates $A_2B_{12}H_{12}$ (A = K, Rb, and Cs), ^{11}B NMR measurements were performed. The temperature dependences of the ^{11}B spin-lattice relaxation rates R_1^B measured at two resonance frequencies for $Rb_2B_{12}H_{12}$ and $Cs_2B_{12}H_{12}$ are shown in fig.3. Comparison of fig.1 and fig.2 indicates that the general features of the behavior of the ^{11}B relaxation rates are similar to those of the proton relaxation rates. The dominant contribution to R_1^B originates from the $^{11}B - ^1H$ quadruple interaction. We performed simultaneous fits of the experimental data by the standard theory taking into account the $^{11}B - ^1H$ quadruple interaction to the $R_1^B(T)$ data at two resonance frequencies. It should be noted, that for all studied compounds, the motional parameters derived from the ^{11}B relaxation data are close to those obtained from the ^1H relaxation data.

The full width at half-maximum (FWHM) of the ^1H NMR line for $K_2B_{12}H_{12}$, $Rb_2B_{12}H_{12}$ and $Cs_2B_{12}H_{12}$ is shown on fig.4. For all the studied compounds, the proton NMR line narrowing is observed. This narrowing indicates the excitation of hydrogen jump motion on

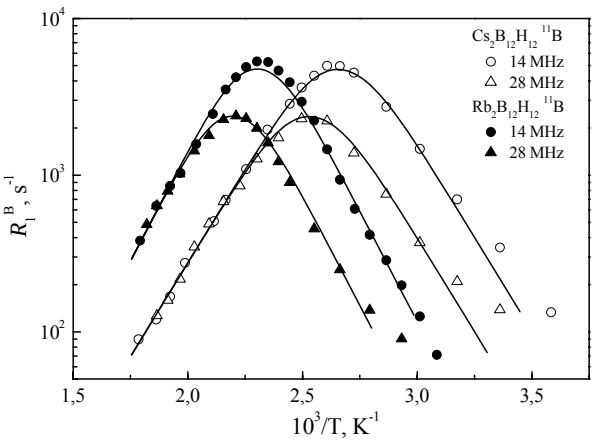

Fig.3. ^{11}B spin-lattice relaxation rates measured at 14 and 28 MHz for $Rb_2B_{12}H_{12}$ and $Cs_2B_{12}H_{12}$ as functions of the inverse temperature. The solid lines show the simultaneous fit of the standard theory to the data.

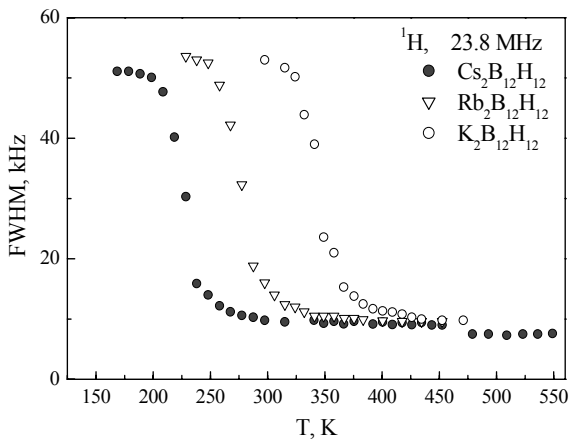

Fig.4. Temperature dependences of the width (full width at half-maximum) of the proton NMR spectra measured at 23.8 MHz for $K_2B_{12}H_{12}$, $Rb_2B_{12}H_{12}$ and $Cs_2B_{12}H_{12}$.

the frequency scale of the order of 10^5 s^{-1}. The FWHM of the ^1H NMR line in the range 300 – 550 K (for $Cs_2B_{12}H_{12}$), 330 – 450 K (for $Rb_2B_{12}H_{12}$), and 390 – 470 K (for $K_2B_{12}H_{12}$) is about 9 – 10 kHz, being nearly temperature-independent up to the highest temperature of our measurements. Such a plateau value of the line width indicates that the motion responsible for the observed line narrowing is indeed localized, since such a motion leads to only partial averaging of the dipole-dipole interactions between nuclear spins. This motion corresponds to thermally activated reorientations of $B_{12}H_{12}$ groups. It should be noted that for $Cs_2B_{12}H_{12}$ the drop of the proton line width occurs at the lowest temperature among all the *closo*-dodecaborates studied so far; this corresponds to the fastest reorientational motion of $B_{12}H_{12}$ groups. Previous ^{11}B NMR and quasielastic neutron scattering studies of the cubic alkali-metal dodecahydro-*closo*-dodecaborates ($A_2B_{12}H_{12}$, A = Cs, Rb, and K) [2, 5] have confirmed that the $[B_{12}H_{12}]^{2-}$ anions undergo rapid reorientational jumps with the motional jump rate at a given temperature increasing with increasing cation radius and the unit-cell dimension.

Conclusions

The measured temperature dependences of the ^1H and ^{11}B spin-lattice relaxation rates for alkali-metal dodecahydro-*closo*-dodecaborates $A_2B_{12}H_{12}$ (A = K, Rb, and Cs) at different resonance frequencies are consistent with thermally-activated reorientations of the $[B_{12}H_{12}]^{2-}$ anions. The analysis of the experimental data has revealed the parameters of reorientational motion of $B_{12}H_{12}$ groups in these compounds.

As can be seen from Table 1, the values of the activation energies for the reorientational motion of $B_{12}H_{12}$ groups in the isomorphous cubic $A_2B_{12}H_{12}$ (A = K, Rb, Cs) compounds decrease with increasing cation radius. This result is in qualitative agreement with previous NMR and QENS data [2, 5]. However, our analysis is expected to yield more accurate values of the activation energies, since our data are analyzed over much broader temperature ranges and dynamic ranges of jump rates.

References

[1] S.-J. Hwang, R. C. Bowman Jr., J. W. Reiter, J. Rijssenbeek, G. L. Soloveichik, J.-C. Zhao, H. Kabbour, C. C. Ahn, *J. Phys. Chem. C.* **2008,** 112, 3164 – 3169.

[2] I. Tiritiris, T. Schleid, K. Muller, *Appl. Magn. Reson*. **2007**, 32, 459 – 481.

[3] O. A. Babanova, A. V. Soloninin, A. P. Stepanov, A. V. Skripov, Y. Filinchuk, *J. Phys. Chem. C* **2010**, 114, 3712 – 3718.

[4] A. Abragam. *The Principles of Nuclear Magnetism*, Clarendon Press: Oxford, 1961.

[5] N. Verdal, T. J. Udovic, J. J. Rush, R. L. Cappelletti, W. Zhou, *J. Phys. Chem. A.* **2011**, 115, 2933 – 2938.

Static and dynamic magnetic properties of new layered antimonate of lithium and cobalt

A.S. Ermolov[1], E.A. Zvereva[1], M.I. Stratan[1], V.B. Nalbandyan[2], M. Evstigneeva[2], A.N. Vasiliev[1]

[1]Faculty of Physics, Moscow State University, Leninskie Gory, 119991, Moscow, Russia
[2]Chemistry Faculty, South Federal University, Zorge 7, 344090, Rostov-na-Donu, Russia
e-mail: antonermolov@yandex.ru

Introduction

The problem of conservation and transfer of the energy is one of the most important and challenging tasks of the modern physics and chemistry of solids, and the central place herein is occupied by the compounds with the movable alkali ions for a fabrication of either the electrode (cathode) or the electrolyte to produce the lithium-ion batteries [1,2]. The present work is devoted to the investigation of static and dynamic magnetic properties of quasi 2D honeycomb-lattice compound $Li_3Co_2SbO_6$. The crystal structure was determined as monoclinic (C2/m). Ordered mixed layers of magnetic cations Co^{2+} and antimony Sb^{5+} alternate with Li layers, providing conditions for lower dimensional magnetic interactions. At the same time in the magnetoactive layers the edge-sharing CoO_6 octahedra form the honeycomb cell, which is a variant of triangular geometry. In presence of antiferromagnetic (AFM) interactions the magnetic subsystem could be frustrated due to next nearest-neighbors interactions.

Experimental

New layered compound $Li_3Co_2SbO_6$ was prepared by conventional solid-state synthesis. The magnetic and specific heat measurements were performed using a Quantum Design PPMS-9 system. The temperature dependence of magnetic susceptibility was measured under variation of the magnetic field $B \leq 9$ T in the temperature range $1.8 \div 300$ K. Electron paramagnetic resonance (EPR) studies were carried out using an X-band EPR spectrometer CMS 8400 (ADANI) ($f \approx 9.4$ GHz, $B \leq 0.7$ T) equipped by a low temperature mount, operating in the range T=6-270 K. The effective g-factors of our samples have been calculated with respect to an external reference for the resonance field. We used BDPA (a,g - bisdiphenyline-b-phenylallyl), g_{et}=2.00359, as a reference material.

Results

It was found that new compound $Li_3Co_2SbO_6$ demonstrates antiferromagnetic behavior with the Néel temperature ~ 10 K (fig.1). At high temperatures, the magnetic susceptibility follows the Curie-Weiss law $\chi = \chi_0 + C/(T - \Theta)$ with the positive values of Weiss temperature ~ 15 K indicating predominance of ferromagnetic interactions. The effective magnetic moment is 6.6 μ_B/f.u. and agrees satisfactorily with theoretical estimations using determined in our work effective g-value ~2.3 and assuming high-spin configuration of Co^{2+} (S=3/2). The magnetization curves do not saturate up to 9 T even at lowest temperature (1.8 K) but demonstrate an upward curvature suggesting the possible presence of a magnetic field induced spin-flop transition at around 0.6 T at 2 K. The position of this anomaly shifts towards lower fields upon increasing the temperature and eventually disappears above the Néel temperature. Specific heat data are in agreement with static magnetic susceptibility revealing λ-type anomaly at about 10 K.

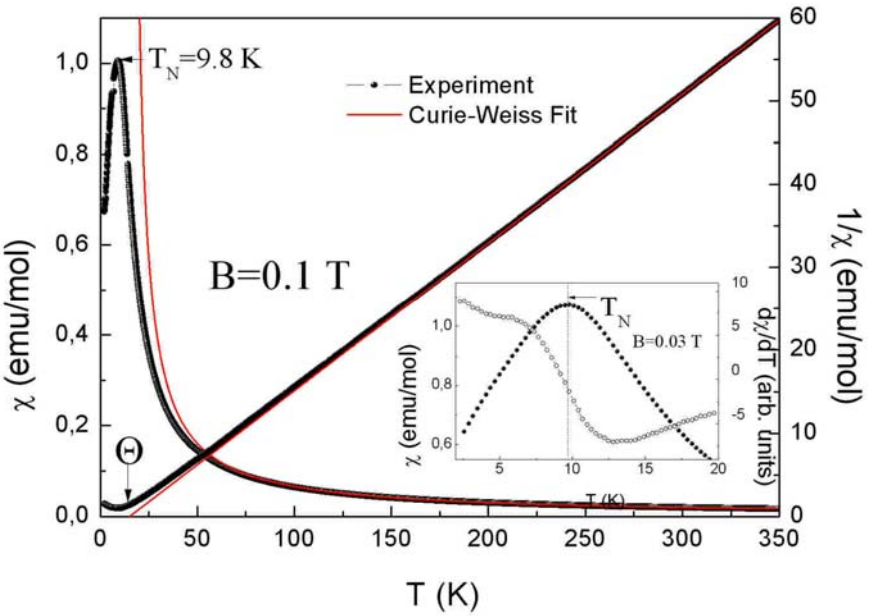

Fig.1. Temperature dependence of magnetic susceptibility for $Li_3Co_2SbO_6$.

Electron paramagnetic resonance spectra in paramagnetic phase show inhomogeneously

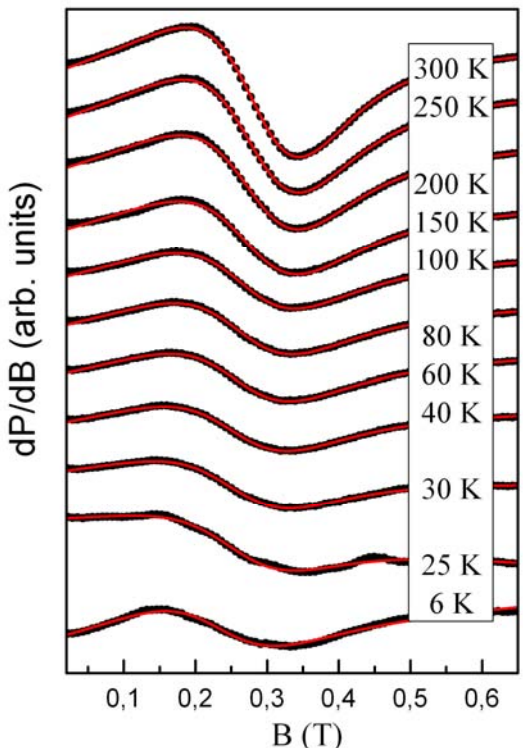

Fig.2. Evolution of EPR spectra for $Li_3Co_2SbO_6$ with temperature.

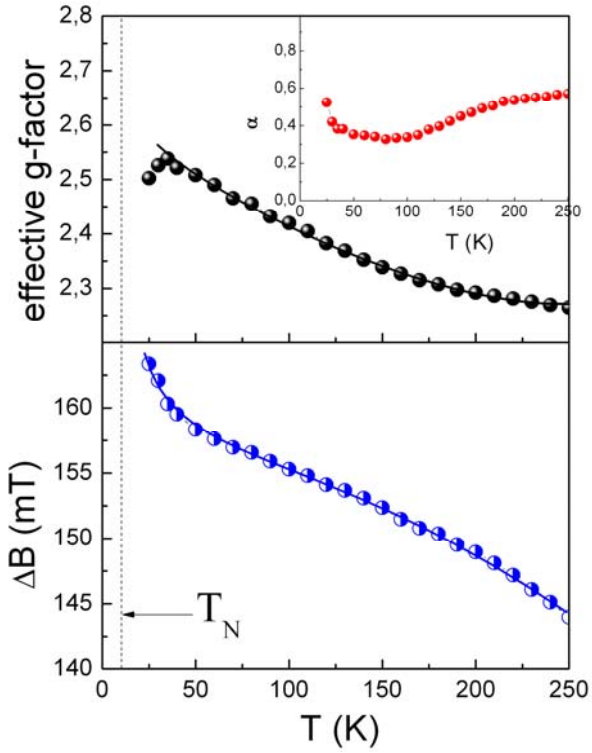

Fig.3. Temperature dependence of effective g-factor and EPR linewidth. Inset: the asymmetry parameter vs temperature.

broaden single Dysonian shape line (fig.2) with isotropic effective g-factor attributed to Co^{2+} ion in distorted octahedral coordination. Upon decreasing the temperature EPR signal broadens, weakens and shifts to lower field side. For quantitative analysis each spectrum has been fitted by Dysonian profile in accordance with formula:

$$\frac{dP}{dB} \propto \frac{d}{dB}\left[\frac{\Delta B + \alpha\left(B - B_r\right)}{\left(B - B_r\right)^2 + \Delta B^2} + \frac{\Delta B - \alpha\left(B + B_r\right)}{\left(B + B_r\right)^2 + \Delta B^2}\right]$$

The main EPR parameters are collected in fig.3. The absorption line significantly broadens when the temperature decreases probably due to critical line broadening as a result of slowing down of spins. The fact that the line width increases over the entire temperature range indicates a very important role short-range correlations at temperatures significantly above the Neel temperature, that is typical for system with low-dimensional magnetic interactions. The effective g-factor at room temperature has a value as high as g = 2.3±0.1, which is characteristic of Co^{2+} ions in the distorted octahedral oxygen coordination. With decreasing the temperature the effective g-factor is also markedly increased indicating the displacement of the resonance field due to the growth of the role of anisotropy effects and strong short-range correlations over the whole temperature range investigated.

References

[1] B. Xu, D. Qian, Z. Wang, Y.S. *Meng. Mater. Sci. Eng. R* **73**, 51–65 (2012).

[2] J.B. Goodenough, *J. Solid State Electrochem.* **16**, 2019–2029 (2012).

Nuclear magnetic resonance in noncollinear antiferromagnet $Mn_3Al_2Ge_3O_{12}$

A.M. Tikhonov[1], N.G. Pavlov[1,2], O.G. Udalov[3]

[1]Kapitza Institute for Physical Problems, RAS, 119334, Moscow, Russia

[2]Moscow Institute of Physics and Technology, 141700, Dolgoprudnyi , Moscow region, Russia

[3]Institute for Physics of Microstructures, RAS, 603950, Nizhni Novgorod, Russia

e-mail: pavlov@kapitza.ras.ru

In this work, the garnet magnetic structure is studied using the nuclear magnetic resonance (NMR) spectra of ^{55}Mn. Information about the relativistic distortions of the exchange spin structure of $Mn_3Al_2Ge_3O_{12}$ owing to the spin reduction anisotropy and weak antiferromagnetism is obtained from these spectra.

The triangular 12-sublattice antiferromagnetic ordering is implemented in manganese garnet $Mn_3Al_2Ge_3O_{12}$ at $T < 6.8$ K. According to the neutron diffraction studies, the magnetic moments of Mn^{2+} (the ground state $^6S_{5/2}$) in the magnetic ordered state of $Mn_3Al_2Ge_3O_{12}$ (crystallographic symmetry group O_h^{10}) lie in the (111) plane and are directed along or contrary to the [211], [121], and [112] axes (see fig.1) [1, 2]. When the external magnetic field H is applied along the [001] direction, the spin plane is rotated until the critical external field $H_c \approx 2.4$ T is achieved [3]. The spin plane is perpendicular to the external field if its magnitude is higher than H_c.

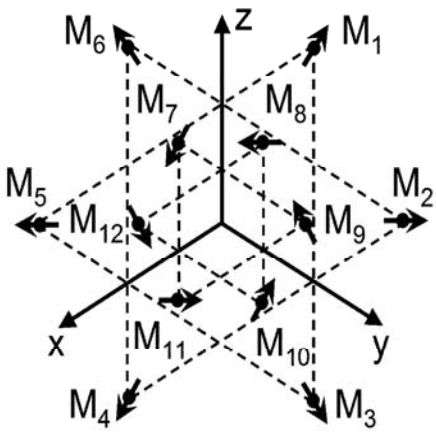

Fig.1. Magnetic structure of noncollinear $Mn_3Al_2Ge_3O_{12}$ antiferromagnet in the exchange approximation.

Three branches of the antiferromagnetic resonance were earlier observed in the study of $Mn_3Al_2Ge_3O_{12}$ at liquid helium temperatures in fields less than H_c [4]. The frequency of one of them decreases strongly at $H \parallel [001]$ when H_c is approached. The exchange approximation was used to describe the results obtained in [4]. Since the experimental study of the magnetic resonance was performed at frequencies higher than 20 GHz, the results of this study were interpreted disregarding the relativistic distortions of the exchange spin structure and the hyperfine interaction in the Mn^{2+} ion.

The effect of the relativistic interactions in the $Mn_3Al_2Ge_3O_{12}$ crystal including the hyperfine interaction on the low frequency part of the magnetic resonance spectrum was

theoretically considered in [5]. To determine the theoretical constants and to test the theoretical results, we studied the ^{55}Mn NMR spectrum (100% isotopic composition) in $Mn_3Al_2Ge_3O_{12}$ crystals using a broadband continuous wave NMR spectrometer, the functioning of which was described in [6].

The ^{55}Mn nuclear magnetic resonance spectrum of noncollinear 12-sublattice antiferromagnet $Mn_3Al_2Ge_3O_{12}$ has been studied in the frequency range of 200 – 640 MHz in the external magnetic field $H \parallel [001]$ at $T = 1.2$ K [7]. Three absorption lines have been observed in fields less than the field of the reorientation transition H_c at the polarization h || H of the rf field (see fig.2). Two lines have been observed at $H > H_c$ and $h \perp H$. The spectral parameters indicate that the magnetic structure of manganese garnet differs slightly from the exchange triangular 120-degree structure. The anisotropy of the spin reduction and (or) weak antiferromagnetism that are allowed by the crystal symmetry lead to the difference of ≈ 3% in the magnetization of sub lattices in the field $H < H_c$. When the spin plane rotates from the orientation perpendicular to the C_3 axis to the orientation perpendicular to the C_4 axis, all magnetic moments of the electronic subsystem decrease by ≈ 2% from the average value in the zero field.

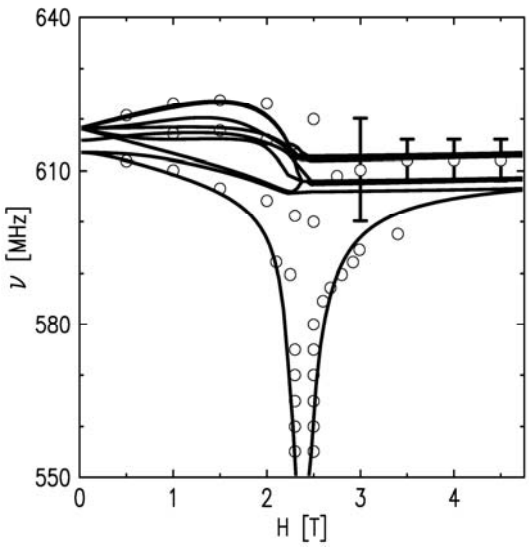

Fig.2. Nuclear magnetic resonance spectrum in $Mn_3Al_2Ge_3O_{12}$: circles are the positions of the absorption maxima in the experiment and lines are theoretical calculations [5].

References

[1] N. Prandl, Phys. Status Solidi B 55, K159 (1973).
[2] A. Gukasov, V. P. Plakhty, B. Dorner, et al., J. Phys.Condens. Matter 11, 2869 (1999).
[3] Z.A. Kazei, N.P. Kolmakova, M.V. Levanidov, et al., Sov. Phys. JETP 65, 1283 (1987).
[4] L.A. Prozorova, V.I. Marchenko, and Yu.V. Krasnyak, JETP Lett. 41, 637 (1985).
[5] O.G. Udalov, J. Exp. Theor. Phys. 113, 490 (2011).
[6] A.Yu. Semanin, G.D. Sokolov, and A.M. Tikhonov, Instrum. Exp. Tech. 54, 92 (2011).
[7] A.M. Tikhonov, N.G. Pavlov, O.G. Udalov, JETP Lett. 96, 568 (2012).

ESR of the quasi-two-dimensional antiferromagnet $CuCrO_2$ with a triangular lattice

V. Dziom[1], Anna Pimenov[1], A. Pimenov[1], L.A. Prozorova[2], A. Shuvaev[1], L.E. Svistov[2], V. Tsurkan[3], A.M. Vasiliev[2]

[1]Institute of Solid State Physics, Vienna University of Technology, A-1040 Vienna, Austria

[2]P. L. Kapitza Institute for Physical Problems RAS, Moscow, Russia

[3]Institute of Applied Physics, Academy of Sciences of Moldova, MD–2028 Chisinau, Republic of Moldova and Center for Electronic Correlations and Magnetism EKM, Experimentalphysik V, Universität Augsburg, Germany

e-mail: vasiliev@kapitza.ras.ru

For more than a decade, the study of frustrated antiferromagnets has been a fascinating subject of condensed-matter physics. Unconventional types of magnetic ordering and phases in frustrated quantum spin chains are attractive issues, because they appear under a fine balance of the exchange interactions and are sometimes caused by much weaker interactions or fluctuations.

$CuCrO_2$ compound is an example of the quasi-two dimensional antiferromagnet ($S = 3/2$) on a triangular lattice with easy axis anisotropy. At temperatures lower than transition temperatures (T_{N1} = 23.6 K and T_{N2} =24.2 K) the magnetic system of $CuCrO_2$ is long range ordered in the triangular planes and has short range correlations between planes. The planar spiral spin structure with the incommensurate vector (0.329; 0.329; 0) was recently detected in $CuCrO_2$ compound [1]. The small deviation from 120-degrees magnetic structure is probably caused by small distortion of triangular lattice, so that the exchange parameter along one side of the triangle differs from two others (fig.1).

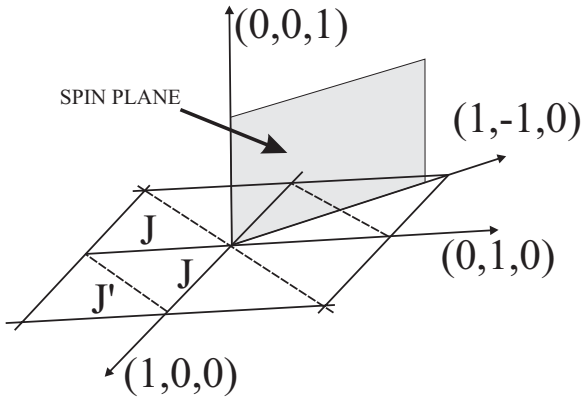

Fig.1.

Using the electron-spin-resonance technique we investigate the magnetic structure of CuCrO2, a quasi-two-dimensional antiferromagnet with a weakly distorted triangular lattice. Resonance frequencies and the excitation conditions in $CuCrO_2$ at low temperatures are well described in the frame of cycloidal spin structure, which is defined by two susceptibilities parallel and perpendicular to the spin plane ($\chi_{||}$ and $\chi_{\perp}$) and by biaxial crystal-field anisotropy [2]. In agreement with the calculations, the character of the eigenmodes changes drastically at the spin-flop transition. The splitting of the observed modes can be well attributed to the resonances from different domains. The domain structure in CuCrO2 can be controlled by annealing of the sample in a magnetic field.

The value of anisotropy of the exchange susceptibility of the spin structure, the constants of anisotropy and the fields of spin reorientation transitions were obtained.

This work is supported by the Russian Foundation for Basic Research, Program of Russian Scientific Schools (Grants No. 12-02-00557-a, No. 10-02-01105-a, No. 11-02-92707-IND-a, and No. 12-02-31220 mol_a) and by Austrian Science Funds (Grants No. I815-N16 and No. W1243).

References

[1] M. Poienar, F. Dumay, C. Martin, V. Hardy, A. Maignan, and G. Andre, Phys. Rev. B **79**, 0144412 (2009).

[2] K. Kimura, H. Nakamura, S. Kimura, M. Hagiwara, and T. Kimura, Phys. Rev. Lett. **103**, 107201 (2009).

^{17}O NMR study of the triangular lattice antiferromagnet $CuCrO_2$

A. Smolnikov[1], V. Ogloblichev[1,2,3], Y. Furukawa[2], A. Sadykov[1], Yu. Piskunov[1], A. Gerashenko[1], S. Verkhovskii[1], A. Yakubovsky[3], S. Barilo[4]

[1]Insutitute of Metal Physics, Ural Division of Russian Academy of Sciences, Ekaterinburg 620990, Russia

[2]Ames Laboratory and Department of Physics and Astronomy, Iowa State University, Ames, IA 50011, USA

[3]Russian Research Centre, "Kurchatov Institute", Moscow 123182, Russia

[4]Institute of Solid State and Semiconductor Physics, Minsk 220072, Belarus

e-mail: smolnikov@imp.uran.ru

Physical properties of the system $CuCrO_2$ with triangular antiferromagnetic lattice have been intensively studied. The competing exchange interactions in $CuCrO_2$ below $T = 24.4$ K lead to the helical magnetic structure with ferroelectric properties [1].

The ^{17}O NMR spectra were measured by a field sweep at frequency $\nu_{res} = 41$ MHz and constant magnetic fields H = 117.4 kOe directed along the *ab*,*c*-axes of single crystal and powder sample $CuCrO_2$ for the temperature range $T = (1.5 – 300)$ K.

In a paramagnetic phase the spectrum consists of single quadrupole split line of ^{17}O NMR (fig.1). The components of electric field gradient (EFG) tensor and of magnetic shifts tensor, $K_{ab,c}$, were obtained. ^{17}O NMR line shift is negative. The temperature dependences of $K_{ab}(H||ab)$, $K_c(H||c)$ are well described by a Curie-Weiss law in the paramagnetic phase and resemble the magnetic susceptibility, $\chi_{ab,c}$, behavior. From the analysis of the $K_{ab,c} - \chi_{ab,c}$ diagram have been certain hyperfine field for oxygen sites: $H_{hf;ab} = H_{hf;c} = 5.2$ kOe/μ_B. The orbital contributions to the line shift ^{17}O are small: $K_{orb;ab} \approx -0.04\%$ and $K_{orb;c} \approx +0.03\%$. The main EFG axis OZ is lying at the *c*-axes. Quadrupole frequency is $\nu_Q = 200(10)$ kHz, asymmetry parameter is $\eta \approx 0$.

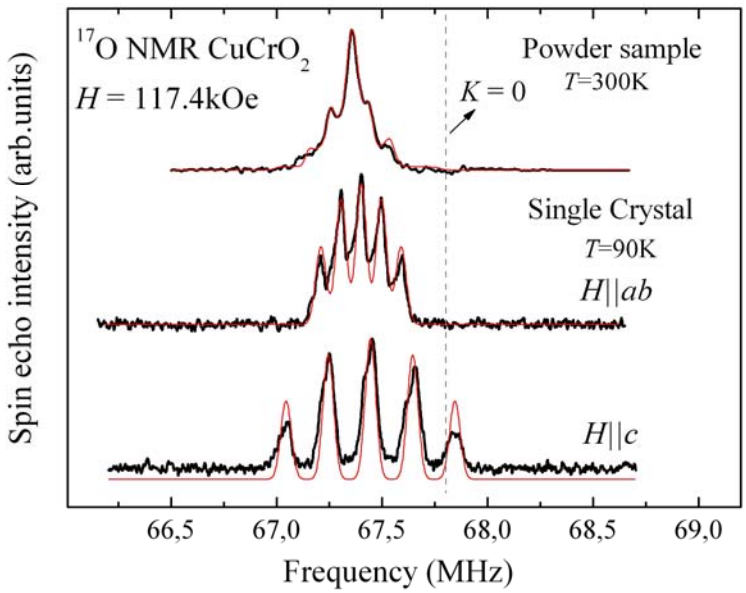

Fig.1. ^{17}O NMR spectra of a single crystal in two orientations H||*ab*, H||c at $T = 90$K and powder sample at $T = 300$ K of $CuCrO_2$ and fit of them.

The single NMR line sharply broadens below T_N = 24(4) K and with further decreasing T the NMR spectrum consisting of two peaks with nonzero spectral intensity between them. Such form of line is characteristic for incommensurate phases [2, 3, 4]. In a magnetic field H = 71 kOe at a temperature T = 1.5 K the distance between peaks, Δ, in orientation $H \| ab$ twice is more than in $H \| c$: Δ_{ab} (T = 1.5 K) = 11kOe and Δ_c (T =1.5 K) ≈ 6 kOe.

This work was supported in part by the Russian Foundation for Basic Research (No 12-02-31814), the Grant-in-Aid for Scientific Research of Ural Branch of RAS (No 12-Y-2-1025). Work at the Ames Laboratory was supported in part by the U.S. Department of Energy, Office of Basic Energy Sciences, Division of Materials Sciences and Engineering.

References

[1] K. Kimura, H. Nakamura, K. Ohgushi, and T. Kimura, Phys. Rev. B 78 140401 (2008)

[2] R. Blinc, Phys. Rep. 79, 331-398 (1981)

[3] Sadykov, A. F., Gerashchenko, A. P. et al. JETP 115, 666-672 (2012)

[4] Ogloblichev, V.V., Kumagai, K. et al. Phys. Rev. B 81, 144404 (2010)

BaV_3O_8: a possible Majumdar-Ghosh system with S = ½

A.V. Tkachev[1,2], A.A. Gippius[1,2], T. Chakrabarty[3], A.V. Mahajan[3], N. Buttgen[4], W. Kraetschmer[4]

[1]Faculty of Physics, Moscow State University, 119991, Moscow, Russia

[2]A.V. Shubnikov Institute of Crystallography, 119333, Moscow, Russia

[3]Department of Physics, IIT Bombay, 400076, Powai, Mumbai, India

[4]Institute of Physics, University of Augsburg, D-86135, Augsburg, Germany

e-mail: av.tkachev@physics.msu.ru

BaV_3O_8 contains magnetic V^{4+} ($S = 1/2$) ions and also nonmagnetic V^{5+} ($S = 0$) ions. The V^{4+} ions are arranged in a coupled Majumdar-Ghosh chainlike network. A Curie-Weiss fit of the magnetic susceptibility $\chi(T)$ data in the temperature region of 80 – 300 K yields a Curie constant $C = 0.39$ cm^{3}K/mole V^{4+} and an antiferromagnetic Weiss temperature $\theta = -26$ K. The χ(T) curve shows a broad maximum at $T \approx 25$ K indicative of short-range order (SRO) and an anomaly corresponding to long-range order (LRO) at $T_N \sim 6$ K. The value of the "frustration parameter" ($f = |\theta/T_N| \sim 5$) suggests that the system is moderately frustrated [1]. Above the LRO temperature, the experimental magnetic susceptibility data match well with the coupled Majumdar-Ghosh (or $J_{nn} - J_{nnn}$ Heisenberg) chain model [2] with the ratio of the nnn (next-nearest neighbor) to nn (nearest neighbor) magnetic coupling $\alpha = 2$ and $J_{nnn}/k_B = 40$K. In a mean-field approach when considering the interchain interactions, we obtain the total interchain coupling to be about 16K. The LRO anomaly at T_N is also observed in the specific heat $C_P(T)$ data and is not sensitive to an applied magnetic field up to 90 kOe.

A ^{51}V NMR signal corresponding to the nonmagnetic vanadium was observed. Unfortunately we were unable to detect the NMR signal associated with the magnetic V^{4+} nuclei probably due to a strong on-site local moment, which naturally couples strongly with its own nucleus. The fluctuations of this moment are very effective in causing a fast relaxation of the nuclear magnetization. This makes the detection of NMR signal difficult like in Cs_2CuCl_4 [3].

Anomalies at 6K were observed in the variation with temperature of the ^{51}V NMR linewidth (fig.1) and the spin-lattice relaxation rate $1/T_1$ (fig.2) indicating that they are sensitive to the LRO onset and fluctuations at the magnetic V^{4+} sites. The FWHM increases slightly with decreasing temperature down to about 6 K and increases drastically below that. It is shown in fig.1 that FWHM in LRO phase ($T = 1.85$ K) decreases with H although it tends to the value of about 1.1 kOe in zero field, which is 2–3 times more than the FWHM above T_N. Thus the externally applied magnetic field H is not the only source of such a broadening, however, the ^{51}V NMR shift does not change much with temperature, which indicates that the V^{5+} ions are very weakly coupled with the electrons of the magnetic vanadium (V^{4+}) ions.

The resulting recovery of the longitudinal ^{51}V nuclear magnetization could be fitted well with a double exponential (consisting of a short and a long component) at all temperatures. It's worth noting that the formula applicable for the recovery of the longitudinal magnetization for an $I = 7/2$ nucleus when the central line is saturated [4] did not fit our data, so two components should be attributed to two inequivalent V^{5+} sites (fig.3). One of them [V^{5+}(2)] is near the center of a triangular plaquette and appears coupled to three V^{4+} ions. The other vanadium [V^{5+}(1)] seems coupled to two V^{4+} ions via oxygen. The V^{5+}(2), which is hyperfine coupled to three V^{4+} might be expected to have a shorter T_1 compared to that for V^{5+}(1). On the fig.2 the faster rate $1/T_1$ is represented.

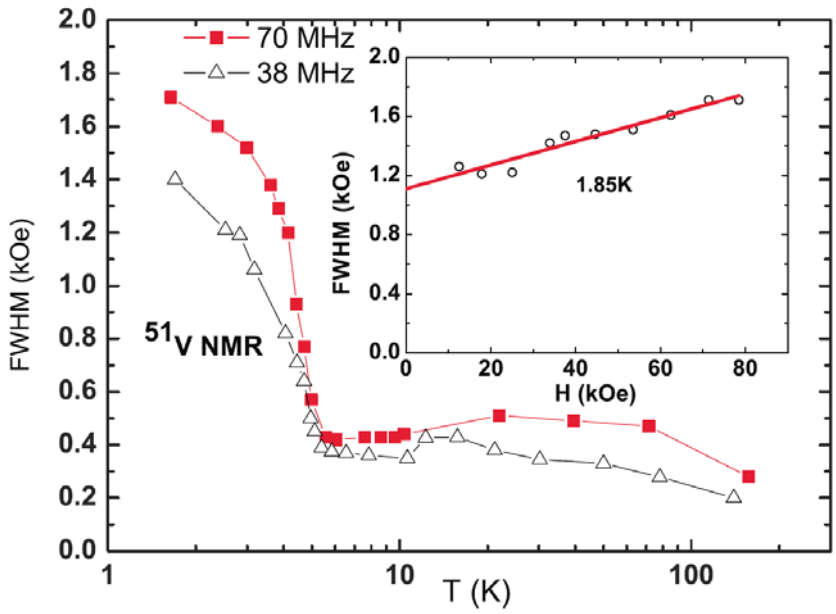

Fig.1. Temperature dependence of FWHM measured at fixed frequencies of 38 MHz (black open triangles) and 70 MHz (red closed squares) for BaV_3O_8. The pulse separation is 50 μs between the pulses of the spin-echo sequence irradiating ^{51}V nuclei. The inset shows the small variation in FWHM with the change in magnetic field measured at 1.85 K. The red line is a linear fit indicating the slight decrease in FWHM with decrease in magnetic field.

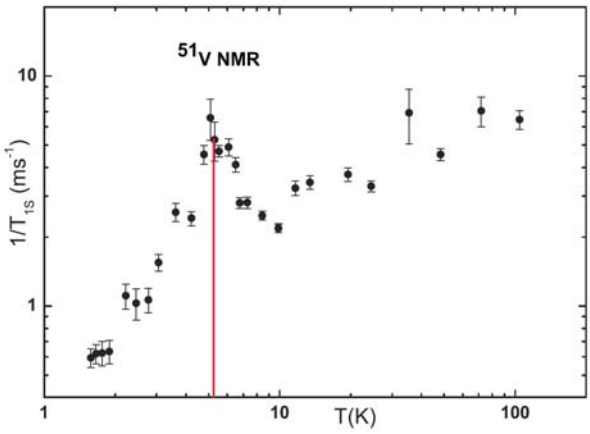

Fig.2. The temperature dependence of the spinlattice relaxation rate ($1/T_1$) corresponding to the faster component. The red vertical line marks T_N.

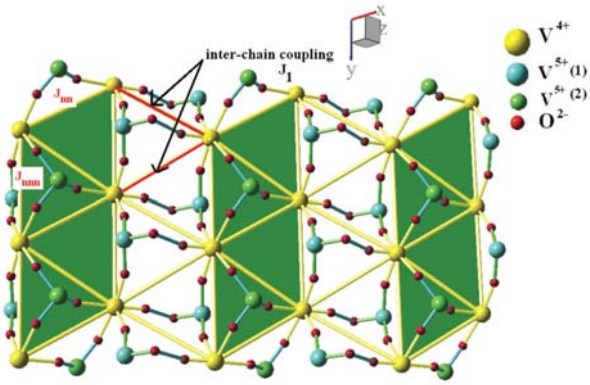

Fig.3. Schematic diagram of the coupled-MG chain network formed by the V^{4+} ions. Possible interaction paths between the V^{4+} ions are shown in the figure.

Additionally, we measured the temperature dependence of the transverse decay and obtained the spin-spin relaxation rates $1/T_2$ presented in fig.4. As seen from the raw data at 2.22 K in fig.4 (right inset), the decay has two components shown by the two dashed lines. Consequently, we have fit the data at each temperature to a double exponential function

$$M_t = A_S \exp\left(-\frac{2\tau}{T_{2S}}\right) + A_L \exp\left(-\frac{2\tau}{T_{2L}}\right) + C\,.$$

Here, T_{2S} and T_{2L} denote the shorter and the longer components, respectively, A_S and A_L stand for their relative weights, respectively, and C is a constant. The variation of $1/T_{2S}$ and $1/T_{2L}$ with temperature is shown in fig.4. As seen from fig.4, the short component, $1/T_{2S}$, exhibits a pronounced ~50% decrease in the vicinity of T_N, while the longer one, $1/T_{2L}$, is insensitive to

the magnetic ordering. The relative weight of the faster component (A_S/A_L) decreases monotonically with increasing temperature (as seen in the inset of fig.4) varying from about 10 at 1.5 K to about 0.1 at about 7.5 K. As is evident, at higher temperatures the spin-spin relaxation is dominated by the longer component. There is, therefore, a larger uncertainty in T_{2S} at higher temperatures. We also note that there is no sharp anomaly in the temperature dependence of A_S/A_L near T_N. Finally, it seems natural to think that A_S/A_L represents the relative amount of magnetically ordered regions with respect to non-LRO regions. We suggest that both magnetically ordered and non-long-range-ordered (non-LRO) regions coexist in this compound below the long-range-ordering temperature.

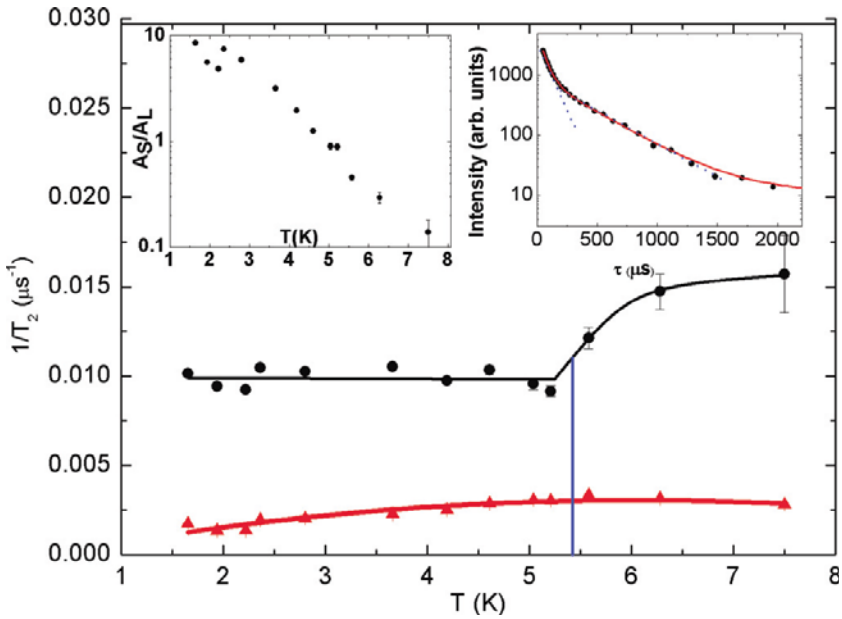

Fig.4. The variation of the ^{51}V spin-spin relaxation rates $1/T_{2S}$ (black circles) and $1/T_{2L}$ (red triangles) with temperature. The solid lines are by-eye lines. The blue vertical line indicates the LRO temperature. The left inset shows the variation of the relative weight of the fast to slow component of T_2 with temperature. The right inset shows the spin-spin relaxation curve at 2.22 K. Here, the black circles correspond to experimental data and the red curve is a double exponential fit. The blue dashed lines correspond to the fast relaxing and slow relaxing components.

In conclusion, complex study of the barium vanadate BaV_3O_8 was performed including both bulk methods and ^{51}V NMR. Forming Majumdar-Ghosh chainlike network V^{4+} ions cause interesting magnetic properties of compound. First of all a LRO at $T_N \sim 6$K was observed by all used methods. Then our NMR experiments revealed certain details of LRO and SRO states. Linewidth analysis provided a possibility to estimate a field at nonmagnetic V^{5+} ions, spin-lattice relaxation distinguishes two different V^{5+} sites, and finally spin-spin relaxation suggests a coexistence of LRO and non-LRO phases in compound.

References

[1] S. Derakhshan, J. E. Greedan, and L. M. D. Cranswick, Phys. Rev. B **77**, 014408 (2008).

[2] C. K. Majumdar and D. K. Ghosh, J. Math. Phys. **10**, 1399 (1969).

[3] M. A. Vachon, W. Kundhikanjana, A. Straub, V. F. Mitrovic, A. P. Reyes, P. Kuhns, R. Coldea, and Z. Tylczynski, New J. Phys. **8**, 222 (2006).

[4] A. Narath, Phys. Rev. **162**, 320 (1967).

Dynamic and decay of NMR quantum coherences in quasi-one-dimensional systems

S.G. Vasil'ev[1], S.I. Doronin[1], A.A. Samoilenko[2], B.A. Shumm[1], E.B. Fel'dman[1]

[1]Institute of Problems of Chemical Physics of RAS, 142432, Academician Semeonov Av. 1, Chernogolovka, Moscow Region, RUSSIA

[2]Institute of Chemical Physics of RAS, 119991, Kosygina St. 4, Moscow, RUSSIA

e-mail: viesssw@mail.ru

Multiple quantum (MQ) NMR spectroscopy [1] is a powerful tool to study spin distributions in different systems and investigate the size of spin clusters when the growth of MQ clusters occurs during the irradiation of the spin system on the preparation period of the MQ NMR experiment [1]. Unique possibilities of MQ NMR to study dynamics of many-spin clusters have been recently used [2] for the measurement of the decoherence rate for highly correlated spin states.

A consistent quantum-mechanical theory of MQ NMR dynamics has been created only for one- dimensional systems [3-5]. In particular, the one-dimension spin chain with nearest neighbor double quantum Hamiltonian is exactly solvable and it has been shown that, starting with a thermodynamic equilibrium state, only the zero and double quantum coherences are produced [3-5]. The experimental investigations of MQ NMR dynamics of one-dimensional systems were started by J.P.Yesinovski [6,7] and continued in [8,9].

We use the system of ^{19}F nuclear spins in a single crystal of natural fluorapatite $Ca_5F(PO_4)_3$. In the fluorapatite crystal, six parallel chains lie along the crystal c-axis with a short intra-nuclear spacing within a single chain and a longer inter-chain separation. The crystal c-axis was aligned along the external magnetic field so that couplings between spins of different chains can be neglected and the system can be considered as a set of isolated one-dimensional spin chains.

The experiments have been performed at room temperature with a Bruker Avance III spectrometer ($B_0 = 9{,}4$ T, 376,6 MHz at ^{19}F) equipped with a 1000 W amplifier and a specially designed high-power probe with a 2 mm o.d. and 5 mm long solenoid coil. The minimum attainable $\pi/2$ pulse duration is about 0,3 μs.

The experimental scheme is shown in fig.1. A phase incremented even-order selective MQ pulse sequence [1] was used in our experiments. During the preparation period the spin system is irradiated with m cycles of multiple pulse sequences consisting of rf pulses and delays to excite even-order MQ coherences. To separate coherences of different orders time-proportional phase incrementation (TPPI) method [1] is used, under which the phases of the preparation pulses are incremented for each successive value of the evolution period t_1 to introduce an artificial offset term into the evolution period. The system is then evolve freely during time t_1 under the influence of the secular dipolar interaction in the rotating reference frame [11]. The spectral width of MQ spectrum is given by $1/\Delta t_1$. Because MQ coherences can not be observed directly they have to be transferred into single-quantum coherences in the mixing (reconversion) period. Time reversal is accomplished here by a 90º phase shift of each pulse in the preparation period regardless the phase shift introduced by TPPI. The detection pulse has to be applied to transfer the magnetization into the transverse plane and the signal is sampled during time t_2 (see fig.1) with the width of single-quantum spectrum. A 2D spectrum is then obtained by Fourier transforming the measured signal with respect to t_1 and t_2.

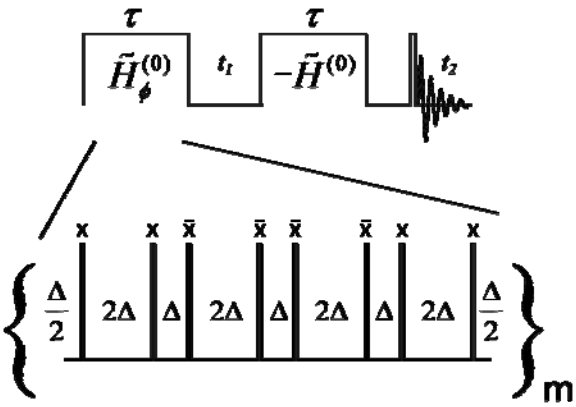

Fig.1. Pulse sequence for exciting MQ coherences in static solids [1].

The $\pi/2$ pulse length was 0,8 μs and the minimum basic cycle time was 21,6 μs. A time of the preparation period was incremented by varying the interpulse delay in the basic cycle from 1 to 2,5 μs and the number of cycles was increased from 1 to 30. The dependence of the intensities of MQ NMR coherences of the zeroth and second orders on a time of the preparation period is represented in fig.2.

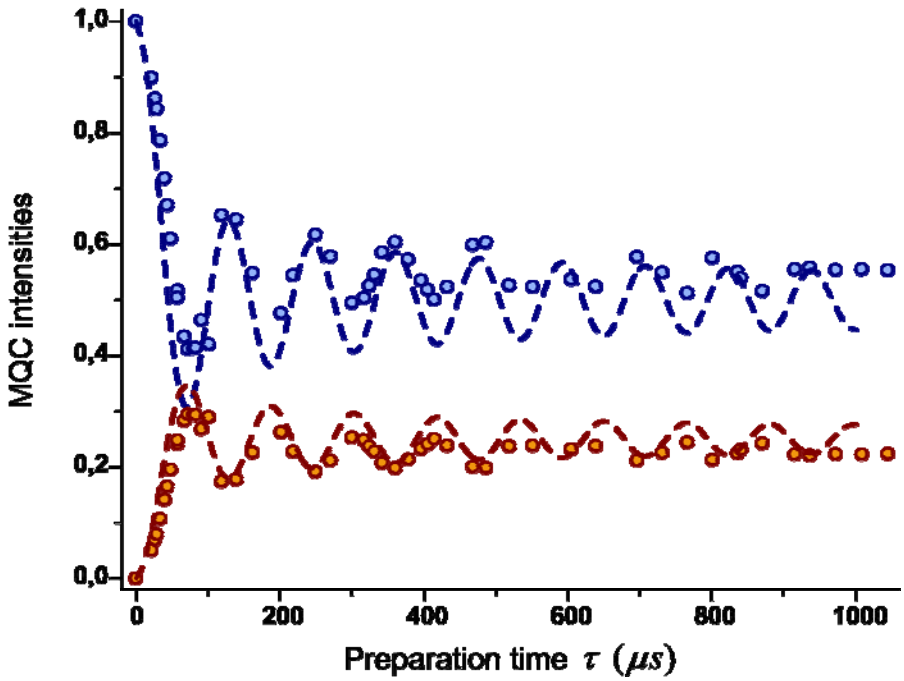

Fig.2. Normalized intensities of zeroth (blue) and second (red) orders ^{19}F multiple-quantum coherences as a function of preparation time. Dashed lines represent theoretical predictions (see Eq.1) for zeroth (blue) and second (red) orders coherences.

The developed theory [3-5] of one-dimensional MQ NMR dynamics is based on the exact diagonalization of the non-secular two-spin/two-quantum Hamiltonian which describes MQ NMR experiments [1]. Such diagonalization is possible because this Hamiltonian is a XY-Hamiltonian [11]. It is evident [3] that dipolar interactions of the nearest neighbors in eight times larger than the interactions of the next nearest neighbors. Thus we can use the approximation of the nearest neighbor intreractions. Then it is possible to obtain the exact expressions for the intensities of MQ NMR coherences of the zeroth ($G_0(\tau)$) and second ($G_{\pm 2}(\tau)$) orders for an isolated one-dimensional chain [3-5]:

$$G_0(\tau) = \frac{1}{2} + \frac{1}{2} J_0(8b\tau)$$
$$G_{\pm 2}(\tau) = \frac{1}{4} - \frac{1}{4} J_0(8b\tau) \quad , \qquad (1)$$

where $J_0(8b\tau)$ is the Bessel function of the first kind of order 0 and b is the dipole-dipole coupling constant. The theoretical predictions are in a good agreement with the experimental data.

We study the dipolar relaxation of the MQ NMR coherences of the zeroth and second orders on the evolution period of the MQ NMR experiment. We compare the experimental decay times of the MQ NMR coherences at different times of the preparation period with the theoretical ones. The theoretical decay times are obtained using the second moments of the line shapes of the MQ NMR coherences. The experimental data are in a satisfactory agreement with the theoretical ones.

Thus, MQ NMR spectroscopy allows us to investigate processes of decoherence in systems of highly correlated spins.

The authors thank Prof. V.I. Volkov for stimulating discussions. The work was supported by the Russian Foundation for Basic Research (grant 13-03-00017).

References

[1] J. Baum, M. Munowitz, A. N. Garroway, A. Pines, J. Chem. Phys. **83**, 2015 (1985).

[2] H. C. Kroyanski, D. Suter, Phys. Rev. Lett. **93**, 090501 (1996).

[3] E. B. Fel'dman, S. Lacelle, Chem. Phys. Lett. **253**, 27 (1996).

[4] E. B. Fel'dman, S. Lacelle, J. Chem. Phys. **107**, 7067 (1997).

[5] S. I. Doronin, I. I. Maximov, E. B. Fel'dman, JETP **91**, 597 (2000).

[6] G. Cho, J.P.Yesinowski, Chem. Phys. Lett. **205**, 1, (1993).

[7] G. Cho, J.P.Yesinowski, J. Phys. Chem. **100**, 15716 (1996).

[8] P. Cappellaro, C. Ramanathan, D. G. Cory, Phys. Rev. A **76**, 032317 (2007).

[9] E. Rufeil-Fiori, C. M. Sánchez, F. Y. Oliva, H. M. Pastawski and P. R. Levstein, Phys.Rev.A **79**, 032324 (2009).

[10] M. Goldman. Spin temperature and nuclear magnetic resonance in solids. Oxford. Clarendon Press. 1970.

[11] D. C. Mattis, The Many-Body Problem: An Encyclopedia of Exactly Solved Models in One Dimension. World Scientific, Singapore, 1993.

Hydration shells of functional groups of organic molecules studied by NMR-relaxation and quantum chemical calculations

A.V. Donets[1], S.O. Rabdano[1,2]

[1]St. Petersburg State University, Faculty of Physics, 198504, Ulianovskaya street, 3, Saint-Petersburg, Russia

[2]St. Petersburg State University, Center for Magnetic Resonance, 198504, Universitetskiy pr., 26, Saint-Petersburg, Russia

e-mail: sevastyan@rabdano.ru

Mutual influence of hydrophobic and hydrophilic interactions in aqueous solutions attracts great interest due to their important role in different phenomena such as assembly of proteins into functional complexes or substance transfer in cells. In this work we studied the hydration shells of hydrophobic and hydrophilic functional groups of amino acids and carboxylic acids by NMR relaxation of water's nuclei and HF/DFT calculations. We have successfully determined temperature and concentration changes of the microstructures and mobility of water molecules in the hydration shells of methylene, amino and carboxylic groups.

Investigated systems are aqueous solutions (D_2O) of malonic acid, glycine and β-alanine. The solvent structure in the solutions with organic molecules can be divided into several substructures: hydration shells of carboxylic, amino, methylene groups and pure solvent. The total relaxation rate of the solvent nuclei is equal to the sum of contributions of each substructure [1]. Investigation of concentration dependences of the spin-lattice relaxation rates of solvent nuclei in the solutions with different organic molecules allows us to determine the mobility of the water molecules near particular fragments of organic molecule. The temperature dependences of NMR relaxation rates help us to understand the temperature variation of the microstructure near hydrophobic and hydrophilic parts of molecules.

The water molecules near the hydrophobic functional groups of organic molecules are characterized by less mobility than in bulk phase. The relaxation rate of the water deuterons near the hydrophobic methylene groups is higher than in bulk water approximately by factor 1.7. This relation shows the decreased mobility of water near hydrophobic fragments and remains at all temperatures from 0 to 75˚C. On the other hand the mobility of the water deuterons near the hydrophilic amino group is higher than in bulk.

References

[1] V. I. Chizhik // Molecular physics, v. 90, № 4, p. 653, (1997).

ENDOR studies of a Cu(II)-bis(oxamato) complex

R.B. Zaripov[1], E.L. Vavilova[1], V.K. Voronkova[1], K.M. Salikhov[1], A. Aliabadi[2], A. Petr[2], V. Kataev[2], B. Büchner[2], M.A. Abdulmalic[3], T. Rüffer[3]

[1]Zavoisky Physical-Technical Institute of the RAS, Kazan, Russia

[2]Institute of Solid State Research IFW Dresden, D-01171 Dresden, Germany

[3]Technical University of Chemnitz, D-09107 Chemnitz, Germany

e-mail: zaripov.ruslan@gmail.com

The mononuclear Cu(II)-bis(oxamato) complexes have been already demonstrated to be useful precursors for the synthesis of multimetallic complexes with a large structural variability (see, e.g., [1]). It is well known that CW and pulse EPR techniques can give valuable information about magnetic properties of paramagnetic systems. It has been already shown that such EPR studies allow to extract information about the spin population distribution of mononuclear copper(II) bis(oxamato) complexes via the analysis of the hyperfine interaction (HFI) tensor [2].

In this work we report on the investigation of a mononuclear copper(II) bis(oxamato) complex (single crystal and liquid solution) where four nitrogen ligands coordinate the central metal ion:

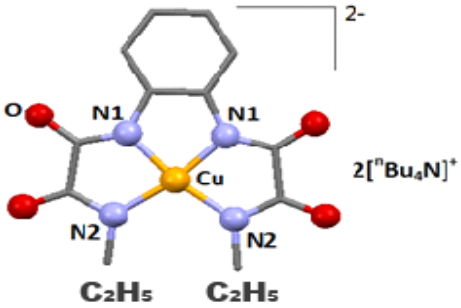

By continuous wave EPR we have got information about the g-factor and the copper hyperfine coupling constant. However, by simulation of the CW EPR spectra it was possible to obtain only the average nitrogen (N^{14}) hyperfine coupling constants. In contrast, in pulse ENDOR spectra we were able to clearly resolve lines from all four nitrogen atoms. We find that the HFI parameters of the N1 pair of nitrogen atoms (as well as of the N2 pair) are rather close to each other. We attribute this to a similar surrounding for the pairs N1 and N2, respectively.

This work has been supported by a collaborative German-Russian research project of the Deutsche Forschungsgemeinschaft (DFG grant BU 887/13-2) and of the Russian Foundation for Basic Research (RFBR grant 12-02-91339-NNIO_a), and by the DFG through FOR 1154 “Towards Molecular Spintronics”.

References

[1] A. C. Dias, M. Knobel, H. O. Stumpf, *J. Magn. Magn. Mater*, **2001**, 226,1961

[2] B. Bräuer, F. Weigend, M. Fittipaldi, D. Gatteschi, E. J. Reijerse, A. Guerri, S. Ciattini, G. Salvan and T. Rüffer, *Inorg. Chem.*, **2008**, 47, 6633.

Monitoring of the paramagnetic reduced forms of the complex Cr(III)(bpy)$_3$

K.V. Holin[1,2], N.A. Tukmakova[3]

[1]A.E. Arbuzov Institute of Organic and Physical Chemistry, Kazan Scientific Center of Russian Academy of Sciences, 420088, Arbuzov str. 8, Kazan, Russian Federation

[2]Kazan National Research Technological University, 420015, K. Marx str. 68, Kazan, Russian Federation

[3]Kazan (Volga region) Federal University, Kremlevskaya str. 18, 420008, Kazan, Russian Federation

e-mail: kholin06@mail.ru, NadejdaTukmakova@yandex.ru.

Transition metal complexes with pyridine ligands continue to attract attention of researchers because of their rich photo-and electrochemical properties. In particular, they are widely used as active components in the photo-and redox-active polynuclear and supramolecular structures with the prospects of application in molecular photonic and electronic devices, molecular magnetics. Basically photo-and redox-activity of polypyridine complexes is caused by presence of unfilled pyridine-localized π-orbitals that can accept electrons during a reduction, or by the possibility of charge transfer between a metal and the ligand. The nature of the metal in the complex often significantly affects on redox potentials of the ligand and on the stability of its reduced (or oxidized) forms. On the other hand, the nature of the ligand has also an impact on the behavior of the metal. A very important research problem of electron transport in such complex but at the same time interesting systems is establishing the localization of the charge after each act of electron transfer, and checking the stability of the complex.

The electron transfer in the series of complexes $[Cr(bpy)_3]^n(ClO_4^-)_n$ (n = 3+, 2+, 1+) (1-3), $[Cr(bpy)_3]^0$ (4), $[Cr(bpy)_3]^{1-}(X^+)$ (5) has been investigated by cyclic voltammetry (CV), electron spin resonance (ESR), cyclic voltammetry detected by electron spin resonance (DESR CV), time-resolved ESR-cyclic voltammetry (TR ESR-CV) methods. Two last methods have been offered and realized for the first time. It has been registered an ESR spectrum of the intermediate 5 in a low-spin state, which has been a result of a number of heterogeneous electron transfer to the initial complex 1**,** and its formation at the fourth peak of reduction has been demonstrated. The comproportionation of the intermediate 5 with the initial complex 1 occuring in the volume of solution has been shown using DESR CV method. Three-electrode helical El-ESR cell, hardware-software complex of El-ESR, new DESR CV and TR ESR-CV methods have been described.

It has for the first time been registered the ESR spectrum of the intermediate $[Cr\,(bpy)_3]^{1-}$ in a low-spin state, which has been a result of a number of heterogeneous electron transfer to the initial complex $[Cr\,(bpy)_3]^{3+}$**,** and its formation at the fourth peak of reduction has been demonstrated.

New DESR CV and TR CV-ESR methods have been given the unique information about the electrochemical and subsequent chemical processes and allow identifying voltammetric waves because of exceptional specificity of ESR signals of the paramagnetic compounds. These tools are very close to the classical methods of voltammetry and that is allowing to use well-known methodological and theoretical developments.

NMR of adsorbed polarity fluid in the zeolite

T.M. Salikhov, A.V.Savinkov

Kazan (Volga Region) Federal University, 420008, Kremlevskaya 18, Kazan, Russia

e-mail: slkhov@gmail.com

Introduction

Currently interest to pores medium has been increasing last years because in these systems a lot of processes such as catalysis, adsorption gases and fluids, cleaning sewage water, desalination water etc proceeds.

There are a lot of experimental and theoretical data that show the difference between properties of bulk fluids and fluids in the pores. Depending on the behavior of the liquid filling the porous medium we can judge the nature of the interaction of the liquid with the pore walls, and hence the properties of the porous medium.

One of the representatives of the porous media are zeolites - a large group of similar composition and properties of minerals, water and sodium aluminum silicates of calcium from the subclass framework silicates, glass or pearl luster, known for its ability to give and re-absorb water, depending on temperature and humidity. Another important feature is the ability of zeolite ion exchange — they are able to selectively absorb and re-emit a variety of substances, as well as to exchange cations.

The particular interest is the use of zeolites as the adsorbent. This requires information on the adsorption properties of zeolites [1].

One of the methods for the study of zeolites is the Nuclear Magnetic Resonance (NMR). NMR method provides information about the structure of the porous media.

The aim of this work is study the dependence of NMR relaxation times on the polarity of the adsorbed liquid zeolite ZSM-5 type.

Materials and methods

The sample was selected type zeolite ZSM-5 with a Si/Al = 326. Zeolite ZSM-5 is a powder composed of microcrystals of the same shape. The size of crystals 170×27×27 mkm. These crystals are penetrated by straight channels that intersect with zigzag channels (fig.1). The size of straight channels 5,4×5,6 Å, and zigzag channels 5,4×5,1 Å. The intersection of the channels have a size about 8 Å.

As adsorbent two fluids were used: $C_{10}H_{22}$ (decan) with size 4,1×4,5 Å, and length 15,5 Å и $C_4H_{10}O_3$ (diethylene glycol).

The zeolite samples were annealed at the temperature of 500 ^{o}C, to remove liquid. Further, the zeolite was filled by the studying liquid. The liquid content in the samples was determined by weighing. The concentration W (masses. %) of the samples was changed by pumping.

All measurements were carried out on NMR relaxometry Hromatek20M with resonance frequency 20 MHz (^{1}H) and the dead time 10mks. The transverse magnetic relaxation of liquid molecules analyzed by free induction decay (FID), and the longitudinal magnetic relaxation by a sequence «inversion - recovery». All measurements were carried out at the temperature 40°C.

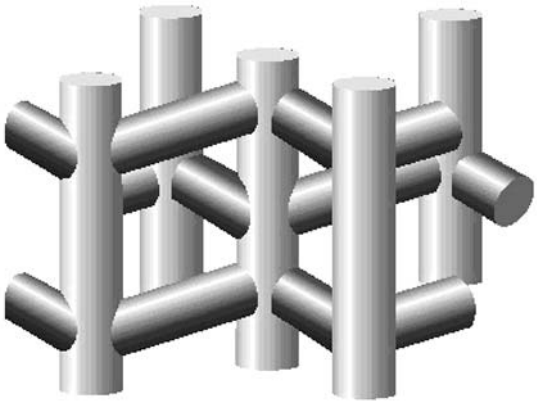

Fig.1. Schematic representation of the zeolite channels

Results and discussion

At the fig.2 (left) the example of the decay of the transverse magnetization (left) and the recovery of the longitudinal magnetization (right) for the ^{1}H nuclei of the system decan/zeolite (15.6% decan). FID for the studying liquid is consisting of fast and slowly

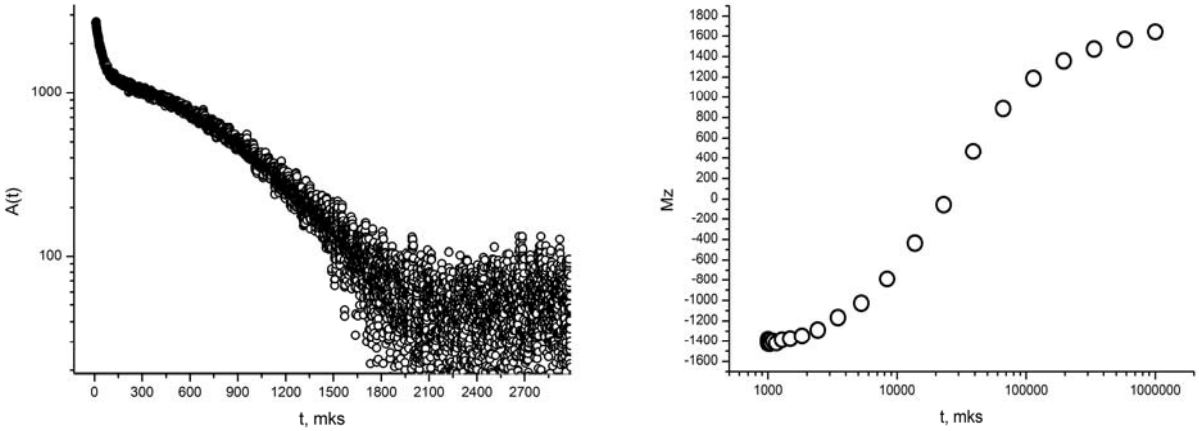

Fig.2. Example of the decay of the transverse magnetization (left) and the recovery of the longitudinal magnetization (right) for the ^{1}H nuclei of the system decan/zeolite (15.6% decan)

relaxing components. Rapidly relaxing component of the FID was refer to the molecules of the liquid in the micropores, and relaxes slowly was refer to the molecules located in the space between the zeolite crystals. This is due to the fact that the molecules inside the zeolite pore space, the anisotropy of the molecular mobility leads to incomplete averaging dipole-dipole interactions and broadening spectral lines (shortening relaxation time).

All measured FID can be represented as:

$$A(t) = P_b \exp\left(-\frac{t}{T_{2b}}\right) + P_a \exp\left(-\frac{t}{T_{2a}}\right)^2, \quad (1)$$

where T_{2b} — relaxation time of short component, T_{2a} — relaxation time of long component, P_b and P_a — the population of the corresponding components. Recovery of the magnetization M_z described by the equation:

$$M_z = P_a\left[1-2\exp\left(-\frac{t}{T_{1a}}\right)\right]+P_b\left[1-2\exp\left(-\frac{t}{T_{1b}}\right)\right] \quad (2)$$

At fig.3 the relaxation time change is shows at w=8-10%. Such changes the relaxation times indicate that in this area increases as the rotational and translational mobility of adsorbed molecules, which leads to increased time T_{2b} and reduction time T_{1b}. Probably, the observed change in the longitudinal and transverse relaxation caused by the rearrangement of the crystal lattice of the zeolite, the monoclinic to orthorhombic, similar to that observed in [2] for the molecules of p - chlorotoluene at w ~ 10%, the Fourier method - Raman spectroscopy.

The adsorption of polar molecules diethylene glycol does not lead to the rearrangement the crystal lattice of the zeolite fig.4.

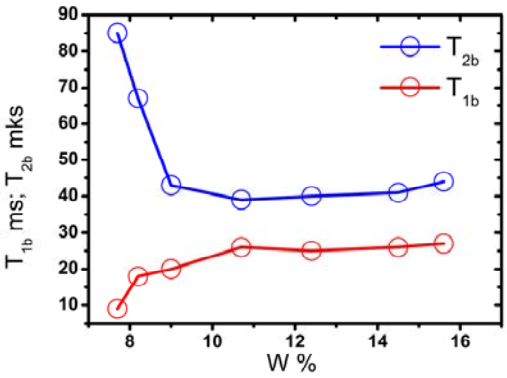

Fig.3. Concentration dependences on transverse (blue) and longitudinal (red) relaxation for the system decan/zeolite.

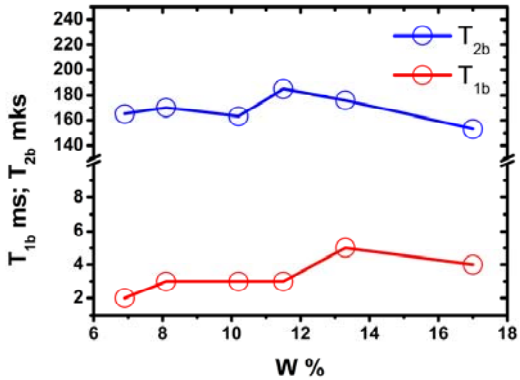

Fig.4. Concentration dependences on transverse (blue) and longitudinal (red) relaxation for the system deg/zeolite

References

[1] Pimenov, G The study of the influence of the nature of the adsorbed molecules on the phase transitions in silicalite type ZSM-5 by NMR and X-ray analysis /G.G.Pimenov, V.D.Skirda, O.A.Opanasuk, V.U.Maksimenko, B.P.Morozov.-Kazan:KSU,2004.

[2] Huang, Y. A Fourier Transform-Raman Investigation of the Host−Guest Interactions of *p*-Chlorotoluene, Toluene, and Chlorobenzene Sorbed on Completely Siliceous ZSM-5/ Huang Y., Havenga E.A. // Chem.Mater.-2001-Vol.13 –p.738

Detection of liquids using low-field magnetic resonance imaging and spectroscopy

N.A. Krylatykh, Ya.V. Fattakhov, A.R. Fakhrutdinov, V.N Anashkin, V.A Shagalov, A.B. Konov, R.Sh. Khabipov

Zavoisky Physical-Technical Institute of the Kazan Scientific Center of the Russian Academy of Sciences, 420029, Sibirsky tract, Kazan, Russia.

e-mail: natalya.p4lka@gmail.com

The problem of security in crowded places is a topical problem to date. The main issue when solving this problem is to detect the dangerous objects in good time and to take every conceivable precaution. However, liquid explosive compounds, which can be prepared in advance or directly before using from corresponding reagents, have been used nowadays as well. Therefore the elaboration of the methods of the operative determination of the type of the liquid is a current problem.

The method of nuclear magnetic resonance is widely used for studying the liquid and solid compounds [1]. The attractiveness of low magnetic fields for solving this problem is in the low cost of the devices themselves and of their operation, and the relatively low energy inputs for the maintenance of the magnetic field.

In this work, it was shown that it is possible to elaborate the methodology of the differentiation of liquid compounds by the nuclear magnetic resonance in low magnetic fields. The most reliable determination of the type of the unknown liquid is possible, when its three parameters are measured: longitudinal and transverse relaxation times, and the self-diffusion coefficient. These parameters can be measured directly in low and ultra-low magnetic fields. On the basis of the above study, it is possible to state that the methodology of the detection of liquid explosive and hazardous compounds using NMR in low and ultra-low fields can be elaborated and successfully introduced for providing security in crowded places.

References

[1] B.Z. Rameev, G.V. Mozzhukhin, R.R. Khusnutdinov, B. Aktas, A.B. Konov, D.D. Gabidullin, N.A. Krylatyh, Y.V. Fattakhov, and K.M. Salikhov, Novel approaches in nuclear magnetic/quadrupole resonance techniques for explosives detection, Proc. SPIE 8357, 83570Z (2012); http://dx.doi.org/10.1117/12.923625. Online Publication Date: May 10, 201

Peculiarities of spin crossover magnetic behavior of dendrimeric iron(III) complex

V.E. Vorobeva, N.E. Domracheva

Zavoisky Kazan Physical-Technical Institute, Russian Academy of Science, Sibirsky Tract 10/7, 420029 Kazan, Russia

e-mail: vvalerika@gmail.com

The motivation of this work is to make a hybrid material that would combine the properties of dendrimer with the unusual magnetic transition metal properties such as spin crossover (SCO) behavior. Their unique magnetic behavior is very useful for various applications such as display devices, optical switches, and magneto-optical storage systems.[1−3] Iron centers in SCO complexes can adopt two different spin states that are transferred from low-spin (LS) to high-spin (HS) states upon external perturbations [2] like heat, light, pressure, and magnetic fields or by chemical alteration (ligand substitution, nature of anion, and crystal solvent).

The synthesis of the bis-chelate Fe^{3+} complex based on 3,5-di(4- cyclohexylbenzoyloxy)benzoyl-4-oxysalicyliden-N′-ethyl-N-ethylenediamine with a chlorine counterion and its characterization by elemental analysis, infrared (IR), NMR, and preliminarity EPR spectroscopy date, the MALDI-ToF-MS method, and DSC calorimetry are described in ref [4]. The elemental analysis and mass-spectrometry results permit one to construct a schematic model of the complex, which is given in fig.1.

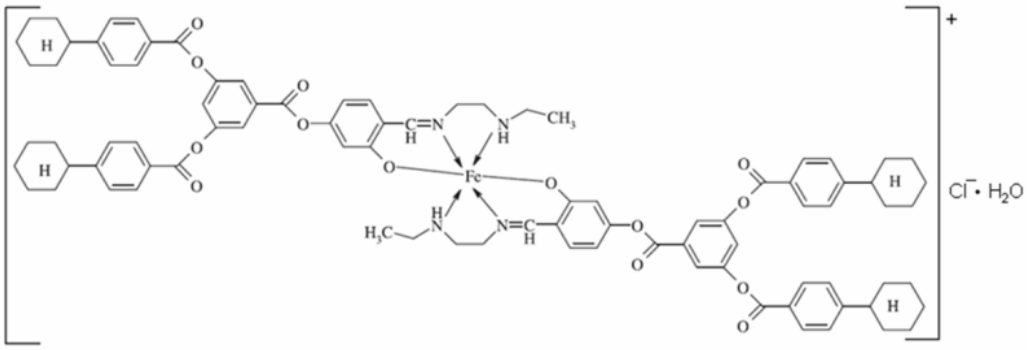

Fig.1. Schematic model of the compound.

EPR is a powerful technique for observing spin transition and studying spin dynamics in Fe^{3+} complexes.[5−11] This method allows not only a confirmation of the existence of LS and HS fractions in the compound but also an investigation of their evolution with temperature. EPR spectra demonstrate the presence in the system of three types of iron(III) centers: two types of HS ions (I-type — $D = 4313$ G, $E = 1437$ G, $g_{eff} = 4.26$, with strong low-symmetry crystal field; II-type — $110\ G < D < 420\ G$, $E = 0$, $2.1 < g < 2.35$ with weak distorted octahedral crystal field) and one of LS ($g_x = g_y = 2.21$, $g_z = 1.935$).

The temperature dependence of the EPR lines integrated intensity (I) is one of the sources of information about the spin transition process (I is proportional to the static paramagnetic susceptibility). The magnetic behavior of the compound reflected by the temperature dependencies of I product of the whole EPR spectrum is shown in fig.2. One can see that the temperature dependence of I has complicated, three-step behavior: it reaches the first maximum at 7 K and then drops to a minimal value at about 50 K, reaches the second

maximum at about 125 K and then drops to a minimal value at about 200 K, and further begins to grow (fig.2).

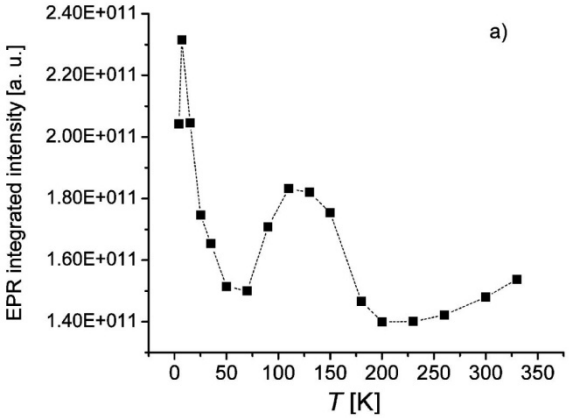

Fig.2. The temperature dependence of the EPR lines integrated intensity of the whole EPR spectrum.

All temperature dependencies in fig.2 are fully reversible. According to the obtained data, we can denote $I(T)$ dependence by three intervals: I (4.2 − 50 K), II (50 − 200 K), and III (200 − 330 K) characterized by different behavior. Let us try to understand the origin of the observed anomaly in our compound. For this purpose, the temperature dependencies of the EPR lines integrated intensity were examined for each type of Fe^{3+} centers separately. The analysis of the EPR signals for each type of Fe^{3+} centers was based on the procedure of fitting of the model spectrum to the observed experimental one. To fit the EPR spectra we used the standard EasySpin-EPR spectrum simulation program. The EPR integrated intensities (I) for all three types of iron(III) centers demonstrate a maximum at $T_N = 7$ K in the temperature interval 4.2 − 50 K. The appearance of a maximum on the curves shows that the LS and HS iron centers are coupled by antiferromagnetic exchange interactions. This fact is confirmed by the Mössbauer spectroscopy. And X-ray diffraction data obtained for a similar iron complex without dendrimeric periphery clearly demonstrate the appearance of intermolecular magnetic interactions between iron ions through the ammine hydrogens, water molecule and chlorine counterion [12].Thus, we can assume that in our complex LS − LS, LS − HS, and HS − HS centers are coupled together, where the Cl^- counterion and H_2O molecule play the role of bridging units.

The analysis of the EPR signal of the LS centers shows that the $g_{x,y}$ and g_z values are independent of temperature. The experimental values of g-factor were used to determine the ground state for LS Fe^{3+} centers in complex. The g-values have been analyzed within the single-electron approximation for the lower orbital triplet according to the approach described in refs [13−15]. The iron complex has the largest coefficient, which indicates that the ground-state Kramer's doublet is characterized by the state where the unpaired electron resides in the d_{xy} orbital, and thus $(d_{xz},d_{yz})^4(d_{xy})^1$ is the ground state for LS Fe^{3+} centers.

The temperature dependence of I for HS centers of the I-type shows that the number of these centers monotonously decreases after 7 K. It means that such HS centers do not take part in the spin transition.

The most interesting features display HS Fe^{3+} centers of the II-type (octahedral centers with weak axial distortion). Their temperature dependence of I_{HS} reproduces the peculiarities of I for the whole EPR spectrum. The behavior of the D parameter, g-factor, and the width of the individual lines of these HS centers are shown in fig.3b, fig.3c, and fig.3d, respectively. In order to understand the observed peculiarities and to establish the temperature range where

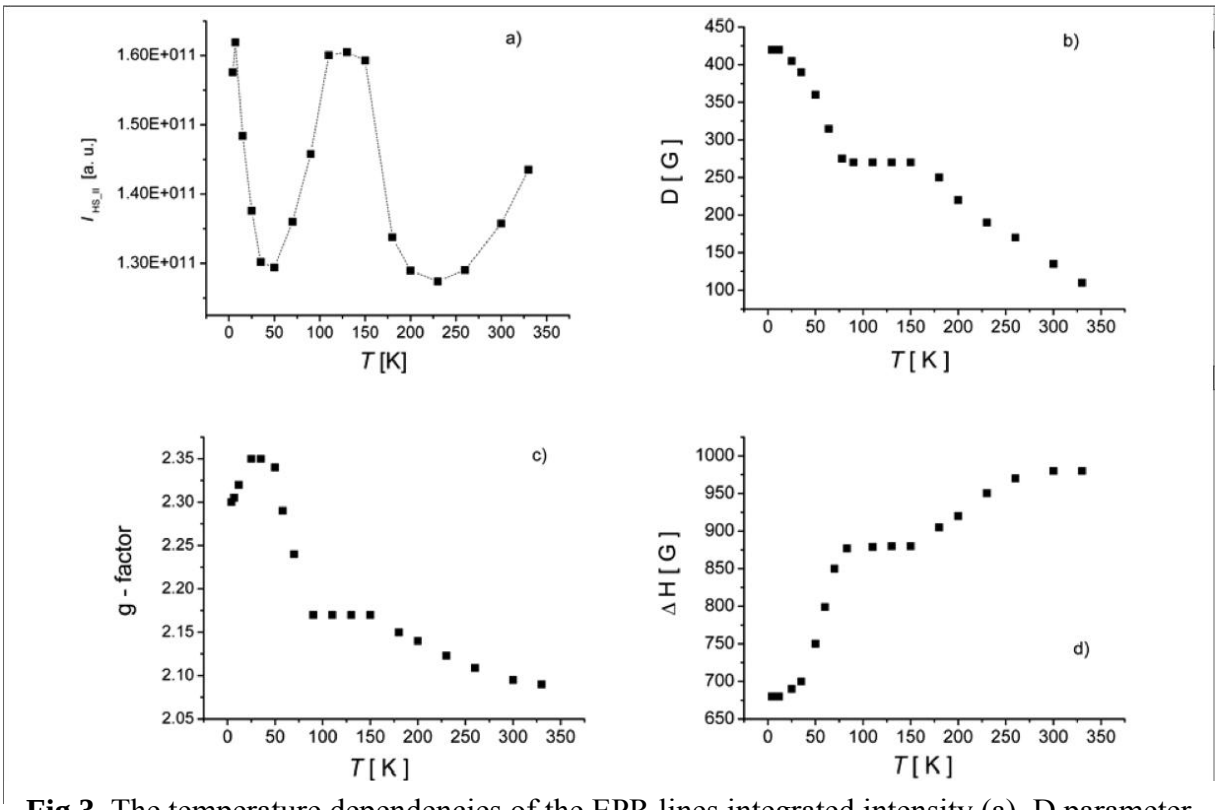

Fig.3. The temperature dependencies of the EPR lines integrated intensity (a), D parameter (b), *g*-factor (c), and the width of the individual lines of the II-type HS iron(III) centers (d).

LS ↔ HS pin transition takes place, we calculate the change in the number of HS molecules of the II-type (HS fraction) with respect to LS molecules (LS fraction) with an increase in temperature. As seen in fig.4a, this ratio n_{HS}/n_{LS} begins to increase sharply after 150 K up to 330 K and such behavior testifies to the spin equilibrium process between $^2T_{2g}$ and $^6A_{1g}$ states

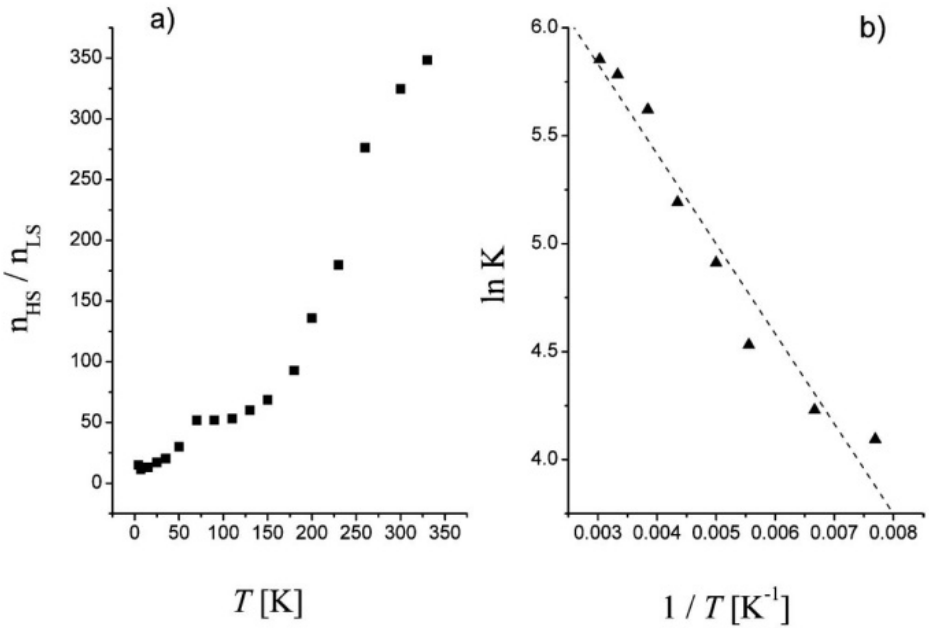

Fig.4. (a) HS/LS vs *T* profile for a gradual SCO behavior. (b) ln *K* vs 1/*T* for complex.

(gradual change in the spin state). The enthalpy and entropy changes accompanying the spin transition are evaluated by using eq (1):

$$\ln K = \ln\left(\frac{n_{HS}}{n_{LS}}\right) = -\frac{\Delta H}{RT} + \frac{\Delta S}{R} \quad (1)$$

where K is the equilibrium constant and R is the gas constant.

The thermodynamic parameters – the enthalpy (ΔH) and entropy (ΔS) of the spin equilibrium process, ΔH = 3.46 kJ/mol and ΔS = 58.88 JK^{-1}/mol — were calculated from the straight line given by plotting $\ln K$ versus $1/T$ (fig.4b). They values estimated are close to those found for other iron(III) spin-crossover complexes.[16,17] The enthalpy changes accompanying the spin transition are 6 times as large as the values expected for the magnetic contribution of the ^{6}A ↔ ^{2}T process $\left(R\ln 3 = 9.1 JK^{-1}/mol\right)$. This fact shows that the lattice vibrations of a complex play an important role in the spin transition.[17] All of these investigations permit one to affirm that a most sharp changing in the spin transition profile takes place from 200 to 330 K. This result agrees well with the Mössbauer.

So, we may conclude, that the antiferromagnetic exchange interactions prevail in the first (I, 4.2 − 50 K) temperature interval, while the spin equilibrium process dominates in the third (III, 200 − 330 K) one. The question arises: what physical phenomenon is responsible for the anomaly behavior of the EPR integrated intensity (I) in the second (II, 50 – 200 K) temperature interval? We think that the anomaly behavior of the EPR integrated intensity (I) in the second (II, 50 − 200 K) temperature interval is caused by the magnetoelectric effect. The observed anomaly arose due to action of the internal electric field (existing in the mesophase) on magnetic properties via the magnetoelectric effect. Analogous behavior of the EPR lines integrated intensity observed in the liquid-crystalline state of the iron(III) complex[18].

The additional arguments for the existence of the internal electric field in our complex are the $g(T)$ and $D(T)$ dependencies of HS Fe(III) centers of the II-type. It is well known [20] that the electric field's effect results in the shift of the g-factor, as well as in that of the D-tensor. fig.3b shows that, when the system transfers from HS to LS state with temperature decrease, the D parameter gradually grows. Such change of D parameter indicates the changing of the electric polarization of iron ion. A similar behavior is registered also for g-factor (fig.3c). Thus, simultaneously with the spin equilibrium process, the changing of electric polarization of iron(III) ion takes place in our compound.

One year ago, a new theoretical approach developed by Bersuker is appeared [21]. In his theoretical approach, the local vibronic coupling between the ground and excited states of opposite parity, the pseudo-Jahn−Teller effect (PJTE), may lead to spontaneous displacements forming local dipole moments; their cooperative interaction results in ferroelectric phase transitions of order−disorder type. This (PJTE) theory of ferroelectricity formulates the necessary conditions of simultaneous coexisting ferroelectric and magnetic properties. In combination with the HS − LS crossover effect, this leads to a novel phenomenon, called by him the magnetic − ferroelectric crossover (MFCO). According to Bersuker analysis, d^5 LS and HS Fe^{3+} ions satisfy the necessary conditions of potential multiferroics. Thus, the change of the spin state for the d^5 configuration can change also the ferroelectric state and the SCO is simultaneously a MFCO.

Conclusion

We have presented a new multifunctional material a dendrimeric Fe^{3+} spin crossover complex exhibiting a magnetic ordering, magnetoelectric effect, and thermally driven spin transition in one and the same material. We suppose that our compound is the first example of

magnetic−ferroelectric (multiferroics) crossover (MFCO) material. This coexistence of strongly correlated magnetic, ferroelectric, and spin-crossover phenomena opens a variety of new possibilities to manipulate the properties of the system with exciting novel functionalities for electronics and spintronics.

References

[1] Gutlich, P.; et all Crossover in Transition Metal Compounds (Topics in Current Chemistry), 1st ed.; Springer-Verlag: Berlin, Heidelberg, New York, 2004; pp 233−235.

[2] Gutlich, P.; et.all, Angew. Chem., Int. Ed. Engl. 1994, 33, 2024−2054.

[3] Linares, J.; et.all Pressure and Temperature Spin Crossover Sensors with Optical Detection. Sensors 2012, 12, 4479−4492.

[4] Gruzdev, M. S.; et.all, Acid. J. Coord. Chem. 2012, 65, 1812−1820.

[5] Conti, A. J.; et.all. Inorg. Chem. 1993, 32, 2670−2680.

[6] Ohshio, H.; et.all stem. Inorg. Chem. 1983, 22, 2684−2689.

[7] Maeda, Y.; et.all. Inorg. Chem. 1984, 23, 2440−2447.

[8] Timken, M. D.; et.all. J. Am. Chem. Soc. 1986, 108, 395−402.

[9] Kennedy, B. J.; et.all Inorg. Chem. 1987, 26, 483−495.

[10] Mohan, M.; et.all. Inorg. Chim. Acta 1988, 141, 185− 192.

[11] Bhadbhade, M. M.; et.all, Polyhedron 1998, 17, 2699−2711.

[12] Inorg. Chim. Acta 1978, 27, 123-128.

[13] Domracheva, N.; et.all. Eur. J. Inorg. Chem. 2011, 8, 1219−1229.

[14] DeSimone, R. E. J. Am. Chem. Soc. 1973, 95, 6238−6244.

[15] Bohan, T. L. J. Magn. Reson. 1977, 26, 109−118.

[16] Conti, A. J.; et.all. Inorg. Chem. 1993, 32, 2681−2693.

[17] Ewald, A.; et.all. Proc. R. Soc. London, Ser. A 1964, 280, 235−257.

[18] Domracheva, N. E.; et.all, J. Magn. Magn. Mater. 2004, 269, 385−392.

[19] Domracheva, N.; et.all. Ferroelectrics 1996, 185, 81−86.

[20] Mims, W. B. The Linear Electric Field Effect in Paramagnetic Resonance; Clarendon Press: Oxford, U.K., 1976.

[21] Bersuker, I. B. Phys. Rev. Lett. 2012, 108, 137202.

Spin glass in the kagome compound $YBaCo_3AlO_7$

M.F. Iakovleva[1,2], E.L. Vavilova[1], H.-J. Grafe[3], M. Valldor[4]

[1]Zavoisky Physical-Technical Institute, Pionerskaya str., Kazan, Russia

[2]Kazan (Volga region) Federal University, Kremlevskaya str., Kazan, Russia

[3]IFW Dresden, Dresden, Germany

[4]Institute of Physics II, University of Cologne, Cologne 50937, Germany

e-mail: ymf.physics@gmail.com

The quantum kagome lattice is a fundamental but experimentally elusive frustrated magnet. Neutron spectroscopy now reveals the ground state and elementary excitations of a kagome lattice in which the quantum spins form an exotic pinwheel valence-bond state, spin liquids etc. [1].

$YBaCo_4O_7$ is a type of mixed valence metal oxide compound with magnetic kagome substructure. Kagome structures contain strong geometrical frustration, which is a source for exotic magnetic states of antiferromagnetically coupled spins generating spin liquids [2]. There are possibilities for magnetic coupling between the kagome layers. In order to divide the kagome planes it was requested to use of aluminum ions. Aluminum could enter the site between the kagome layers, thereby cutting the magnetic interactions between the kagome planes. Another reason for choosing Al^{3+} is its nonmagnetic nature and its relatively small size. We have attempted to study the ground state of local methods, including NMR.

We have measured NMR in a single crystal $YBaCo_3AlO_7$ at different temperatures. The Al NMR spectra were taken at a fixed frequencies of $f = 85{,}42$ MHz and $f = 33{,}28$ MHz (at $H = 7{,}7$ T and $H = 3$ T respectively) by sweeping the magnetic field. We used a standard Hahn-Echo sequence, and integrated the echo at each field step.

At high temperatures the spectrum has a well-resolved quadrupole structure. With decreasing of temperature, a progressive broadening of the spectral line was observed. Below 10 K the linewidth increase dramatically. Also the temperature dependence of the spin-lattice relaxation rates was measured at both frequencies. The most important result of these experiments was that the dependence of $T_1^{-1}(T)$ has a peak around $10-20$ K which shifts with frequency. These facts indicate the possible presence of spin glass state. The absence of well resolved structure of NMR line at low temperatures supports the conclusion that only short-range order occurs in the system but not a long-range antiferromagnetic ordering. Spin glasses are systems whose magnetic moments freeze at low temperature into random orientations without long-range order [3]. It is generally accepted that both frustration and disorder are essential ingredients in all spin glasses.

Our conclusions are supported by measurements [2] of the dynamic susceptibility, which also has a maximum of temperature characteristic that depends on the frequency. The X-ray diffraction data shows, that the 2a metal positions are not fully occupied by Al and the corresponding 6c sites are not occupied only by Co. Hence, we have Al/Co mixed crystal, and most probably it is a structural disorder that leads to a large defect of the magnetic subsystem. For that reason in the compound $YBaCo_3AlO_7$ any conventional or frustrated long-range order does not arise, and a spin-glass state is implemented.

References

[1] Christian Rüegg ., Nature Physics 6, 837–838 (2010)

[2] M. Valldor et al., Phys.review B 78, 024408 (2008)

[3] E. Goremychkin et al., Nature Physics 4, (2008)

Optical properties of fluorite crystals CaF_2: Ce^{3+}, Yb^{3+}, Lu^{3+}

N.F. Rakhimov, A. Nizamutdinov, V.V. Semashko, M.A. Marisov, S.A. Shnaidman

Kazan Federal University, 420008, Kremljovskaja str., 18, Kazan, Russian Federation

e-mail: niyaz_06@mail.ru

Introduction

Fluorite crystals CaF_2: Ce^{3+} have promising optical properties for generating tunable laser oscillation in the UV spectral range, but exhibit poor photochemical stability [1, 2].

The aim of this study is to investigate the influence of Yb^{3+} and Lu^{3+} activator ions on optical characteristics and photo dynamical processes in crystals of CaF_2:Ce^{3+}. Spectral characteristics of a series samples of fluorites, activated by Ce^{3+}, Yb^{3+} and Lu^{3+}, were investigated including absorption spectra of color centers, induced by radiation resonant to transitions of ions Ce^{3+}.

Physical premises to control the optical properties

Impurity centers of Ce^{3+} ions in CaF_2 were first investigated by Feofilov, in the series of alkaline earth fluorides with a fluorite structure MeF_2 (Me = Ca, Sr, Ba), which form a homologous series [3-6]. In these crystals the formation of several types of impurity centers is observed with different mechanisms of compensation of the excess positive charge and, therefore, with different local symmetries of the crystal field.

In CaF_2: Ce^{3+} crystals pumped by radiation resonant to 4f-5d transitions of Ce^{3+} ions formation of different types of color centers absorbing at the wavelengths of luminescence of Ce^{3+} ions was observed (fig.1a). The origin of the emergence of dynamical processes is the appearance of free charge carriers in the conduction band and valence band of the crystal released by the two-step photoionization of the impurity center. After thermalization these free charge carriers can be captured by a variety of traps, such as uncompensated charges in the crystal lattice, lattice defects, or recombine at the impurity centers (fig.1b).

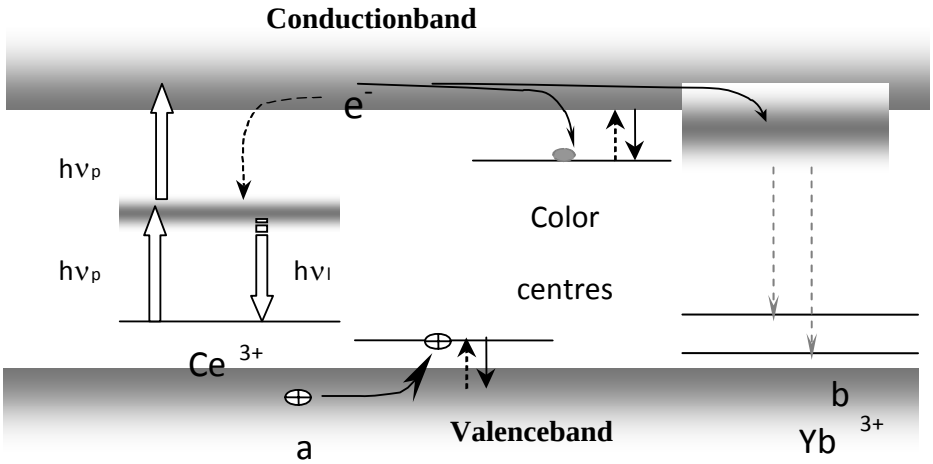

Fig.1. a) the model of solarization of the active medium, activated by Ce^{3+} ions, under UV radiation, and b) accelerating the recombination of free charge carriers through the states of the ion-activator

The objects of study of the presented work are fluoride crystals with the fluorite structure, namely CaF_2: Ce^{3+} (Ce ~ 1%), CaF_2: Ce^{3+} + Yb^{3+} (Ce ~ 0.5%,Yb ~ 1%), CaF_2

(80%) + LuF_3 (20%): Ce^{3+} + Yb^{3+} (Ce ~ 0.5%,Yb ~ 1%), CaF_2 (95%) + LuF_3 (5%): Ce^{3+} + Yb^{3+} (Ce ~ 0.5%,Yb ~ 1%)

Results. The absorption and luminescence

Fig.2a shows the absorption spectra and luminescence of CaF_2: Ce^{3+} crystal. Visible characteristic two-humped spectrum of luminescence of Ce^{3+}, due to the transitions from the excited 5d state to $^2F_{7/2}$ and $^2F_{5/2}$states of 4f configuration.

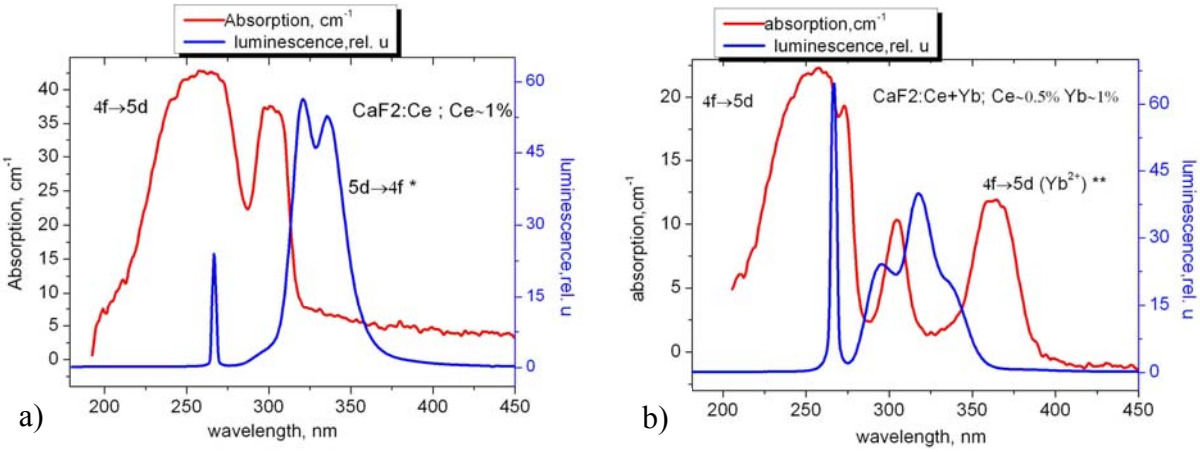

Fig.2. The absorption and luminescence of CaF_2: Ce^{3+} (a) and CaF_2: Ce^{3+} (b), SCe (0.5 at.%), Yb (1 at.%).

In the case of the sample activated by Yb^{3+} (fig.2b) there is an absorption band in the region of 360 nm which is characteristic for Yb^{2+} [6]. Such an impurity center may have formed as a result of dynamic processes, namely the capture of electron from the conduction band by Yb^{3+} ion [1,2]. It is connected with the fact that the crystal was irradiated before the absorption spectra were recorded.

Fig.3 shows the absorption and luminescence spectra of crystals, which are doped by Lu^{3+} in addition to Ce^{3+} and Yb^{3+}. The absorption spectra are not qualitatively different from ones observed for previous samples. Luminescence spectrum reveals not only bands of Ce^{3+} center of tetragonal symmetry but also the band peaked at 380 nm, which can be attributed to the transition of Ce^{3+} impurity center with non-local charge compensation (according to the published data).

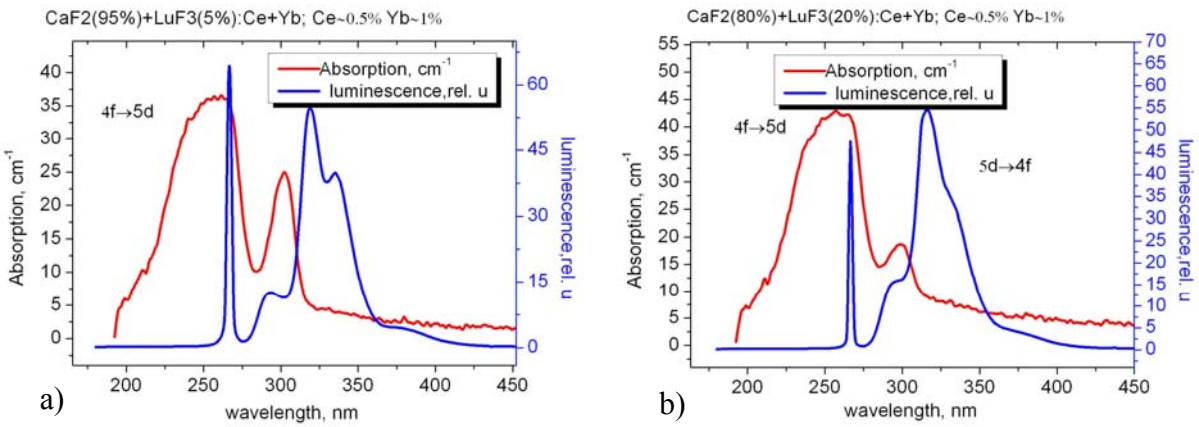

Fig.3. The absorption spectra and luminescence crystal CaF_2: Ce^{3+} (0,5 atm.%), Yb^{3+} (1 at.%), Lu^{3+} (5 at.%) (a) and CaF_2: Ce^{3+} (0,5 at.%) , Yb^{3+} (1 at.%), Lu^{3+} (20 at.%) (b)

Conclusion

We have investigated the effect of doping by Yb^{3+} and Lu^{3+} on the optical characteristics and photo dynamical processes in CaF^2: Ce^{3+} crystals.

As a result of doping by Lu^{3+} ions of CaF_2: Ce^{3+} + Yb^{3+} crystal luminescence spectrum of Ce^{3+} ions reveals new band peakedat 380 nm, which may be interpreted as a transition within Ce^{3+} impurity center with non-local charge compensation.

In this work we have studied mechanisms for controlling the optical characteristics of fluorite crystals activated by rare-earth ions by shifting the balance of dynamical processes. Effective recombination channels providedbyYb^{3+} ions suppress the formation of color centers, but there is an absorption band of Yb^{2+}, which degrades the optical properties of the crystal as the active medium. Additional doping byLu^{3+} ions can suppress the formation of Yb^{2+}.

References

[1] G. J. Pogatshnik, D. S. Hamilton Excited state absorption of Ce^{3+} ions in Ce^{3+}:CaF_2// Phys. Rev. B. 1987. V. 36. № 16. P. 8251–8257.

[2] R. Yu. Abdulsabirov, S. L. Korableva, A. S. Nizamutdinov, M. A. Marisov, A. K. Naumov, V. V. Semashko, Proc. SPIE, 6054, (2006) 172.

[3] Stepanov I. V. O dvuh tipah spektrov ljuminescencii redkih zemel' v iskusstvennyh kristallah fljuorita/ I. V. Stepanov, P. P. Feofilov// Dok. AN SSSR. – 1956. – T. 108. – № 4. – S. 615–618.

[4] Feofilov P. P. Linejchataja ljuminescencija aktivirovannyh kristallov (redkozemel'nye iony v monokristallah MeF2)/ P. P.

[5] Stepanov I. V. O dvuh tipah spektrov ljuminescencii redkih zemel' v iskusstvennyh kristallah fljuorita/ I. V. Stepanov, P. P. Feofilov// Dok. AN SSSR. – 1956. – T. 108. – № 4. – S. 615–618.

[6] Kapljanskij A. A. Spektry dvuhvalentnyh ionov redkih zemel' v kristallah shhelochnozemel'nyh ftoridov/ A. A. Kapljanskij, P. P. Feofilov// Opt.i spek. – 1962. – T.13. – S. 235–241.

Transient responses of the dielectric permittivity of $LiLuF_4$ crystals doped by Ce^{3+} and Yb^{3+} ions

V.V. Pavlov, V.V. Semashko, R.M. Rakhmatullin, S.L. Korableva

Kazan Federal University, 420008, Kremlevskaya 18, Kazan, Russian Federation

e-mail: Vitaly.V.Pavlov@gmail.com

Introduction

Degradation of optical and laser properties of the majority of solid-state active media during operation is associated with photodynamic processes induced by high energy UV pump photons which are in resonance of activator ions 4f-5d transitions [1]. The reason of these processes is excited state absorption of pumping radiation accompanied with ionization of activator ions and photoconductivity effects. Study of characteristics of such intense photodynamic processes in activated crystals is an urgent task, since it allows to determine the necessary conditions for eliminating the harmful influence of photodynamic processes and, eventually, to create effective solid-state active media of UV and VUV spectral ranges.

To determine the timing performances of photodynamic processes we studied the variation of dielectric properties of the fluoride crystals under UV excitation by means of the microwave resonant technique [2]. This work presents investigation of two crystals: $LiLuF_4$ crystal doped by Ce^{3+} (1 mol. %) and $LiLuF_4$ crystal doped by Ce^{3+}, Yb^{3+} (1 mol. %).

Experimental

The microwave resonant technique is the powerful instrument for research of the dielectric permittivity $\varepsilon = \varepsilon_1 - j\varepsilon_2$ of dielectric crystals. This technique is based on the measurements of the cavity resonator parameters variations after the investigated material was put inside. The technical realization of microwave resonant technique is similar to the electron spin resonance technique. The difference is that we do not use the magnetic field and the sample is placed in the antinode of electric field of the cavity. Concept and experimental realization of this technique were previously described in detail [3].

The microwave resonant technique permits to investigate the variation of the real $\delta\varepsilon_1$ and imaginary $\delta\varepsilon_2$ parts of dielectric permeability of the sample under UV radiation, notably the photoconductivity and photodielectric effects. Photoconductivity $\delta\varepsilon_2$ is caused by the appearance of free electrons in the conduction band and photodielectric effect $\delta\varepsilon_1$ is associated with localized electrons at the impurity ions or electron traps.

In this work we used the 8-mm microwave resonant technique. Operating frequency is 35.4 GHz. The resonator´s unloaded quality factor Q_u is 800 and the output frequency band of the microwave detector is 250 MHz. Therefore the time constant of the measuring system is equal to 4 ns.

Excitation of the investigated crystals was carried out by σ-polarization radiation of the third harmonic of Al_2O_3:Ti laser. Excitation wavelength was 240 nm, which corresponds to the 4f-5d transitions of the Ce ions and initiates photoionization of the Ce ions. Pulse duration and pulse-repetition frequency of the exciting radiation were 10 ns and 10 Hz, respectively. Photoconductivity and photodielectric effect were investigated at the room temperature.

Experimental results

Photoconductivity and photodielectric signals for $LiLuF_4:Ce^{3+}$, $LiLuF_4:Ce^{3+},Yb^{3+}$ crystals excited by radiation at 240 nm are shown in fig.1a. The decay time of photoconductivity signal, which characterizes the average life-time of the free charge carriers, in studied crystals appeared to be about 10 ns.

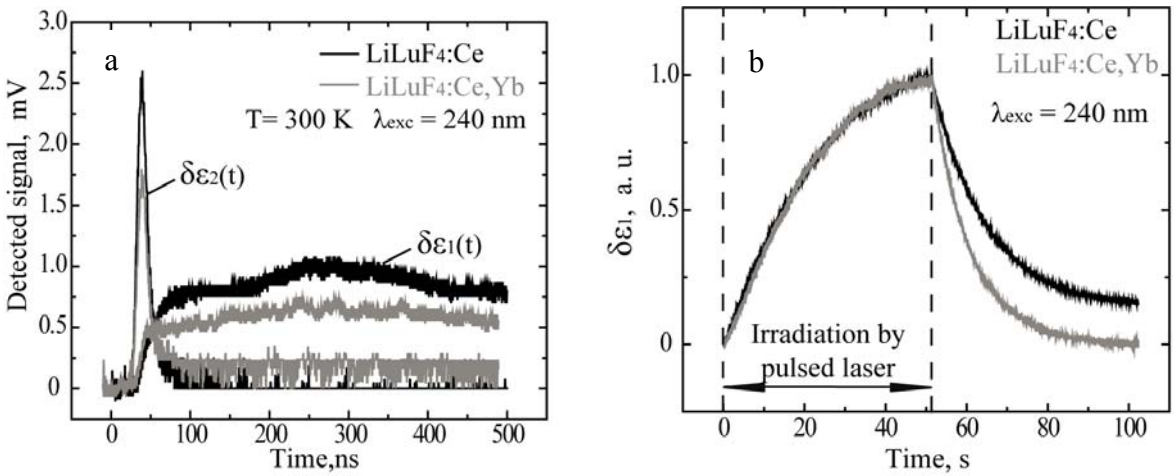

Fig.1. (a) – Time decays of the real and imaginary parts of complex dielectric permittivity for $LiLuF_4:Ce^{3+}$, $LiLuF_4:Ce^{3+},Yb^{3+}$ crystals excited by radiation at 240 nm (T = 300 K); (b) – Saturation of the photodielectric signal of the investigated crystals under irradiation in during 50 second at room temperature (λ_{exc} = 240 nm)

The photodielectric signal is characterized by the decay time of the order of hundred nanoseconds with the build-up time of about 20 ns. Prolonged irradiation of the sample by the pulsed laser radiation leads to saturation of the photodielectric signal. Saturation of the photodielectric signal under irradiation of the samples in during 50 seconds is shown in fig.1b. From saturation of the photodielectric signal we determined that the life-time of long-lived color center for crystals activated only Ce ions is about 14 s and the co-doping of the crystals by Yb ions leads to a decrease of the life-time of long-lived color center by five seconds. This confirms the fact that the additional activation by Yb ions creates a supplementary recombination channel for free carriers. It was previously proposed by the authors in article [4], where they investigated 4f-5d fluorescence decay kinetics of the Ce ions in these crystals.

Summary

We investigated photoconductivity and photodielectric effect in fluoride crystals doped by Ce^{3+} and Yb^{3+} ions using microwave resonant technique. And the average lifetimes of free and color centers bounded charge carriers have been estimated.

References

[1] V.V. Semashko *Phys. Solid State* **47**, 1507 (2005).

[2] M.-F. Joubert , S.A. Kazanskii, Y. Guyot et al., *Opt. Mat.* **24**, 137 (2003).

[3] V.V. Pavlov, V.V. Semashko, R.M. Rakhmatullin et al., JETP Letters **97**, 1 (2013).

[4] A.S. Nizamutdinov, M.A. Marisov, V.V. Semashko et al., Phys. Solid State **47**, 1460 (2005)

Impact of multipole interactions between Tm^{3+} ions on spectral and magnetic properties of $LiTmF_4$ single crystals

I.V. Romanova, B.Z. Malkin, M.S. Tagirov

Kazan Federal University, Kazan, 420008, Kremlevskaya 18, Russian Federation

e-mail: Irina.Choustova@kpfu.ru

Introduction

Double lithium-rare earth fluorides which crystallize in the tetragonal scheelite structure are considered for many years as model objects in physics of rare earth compounds [1]. In particular, studies of spectral, magnetic and magnetoelastic properties of $LiTmF_4$ revealed strong interactions of Tm^{3+} ions with lattice strains [2-4]. The unit cell of $LiTmF_4$ contains two magnetically equivalent Tm^{3+} ions at sites with the S_4 point symmetry. The ground state of Tm^{3+} ions in the tetragonal crystal field is the singlet Γ_2, and the nearest excited crystal field sublevels of the ground $^3H_6$ multiplet are the Γ_{34} doublet and the Γ_1 singlet with energies of 30 and 60 cm^{-1}, respectively. Despite the singlet ground state with the zero magnetic moment, $LiTmF_4$ exhibits a giant forced magnetostriction at liquid helium temperatures [2].

The main goal of the present study was to elucidate the role of magnetoelastic interactions in formation of the magnetization and the energy level structure of the Tm^{3+} ions in $LiTmF_4$ crystals in the external magnetic fields.

The theoretical background

In the presence of an applied magnetic field **B**, we write the Hamiltonian of a single Tm^{3+} ion in the following form:

$$H = H_0 + H_{cf} + \sum_{\alpha\beta} V'_{\alpha\beta} e_{\alpha\beta} + \sum_{\alpha,s} V''_{\alpha}(s) w_{\alpha}(s) + \sum_j [\mu_B(\mathbf{B} + \hat{\mathbf{Q}}\mathbf{M})(\mathbf{l}_j + 2\mathbf{s}_j) - \sum_{pkp'k'} \lambda_{pp'}^{kk'} \langle O_p^k \rangle O_{p'}^{k'}] \quad (1)$$

Here, the first term is the free ion energy, the second term is the crystal field Hamiltonian:

$$H_{cf} = B_2^0 O_2^0 + B_4^0 O_4^0 + B_4^4 O_4^4 + B_4^{-4} O_4^{-4} + B_6^0 O_6^0 + B_6^4 O_6^4 + B_6^{-4} O_6^{-4} \quad (2)$$

determined in the crystallographic system of coordinates by the set of seven crystal field parameters B_p^k (O_p^k are the Stevens operators). The third and fourth terms correspond to linear interactions of rare-earth ions with the homogeneous macro- and microdeformations, respectively, where $\hat{\mathbf{e}}$ is the deformation tensor, and $\mathbf{w}(s)$ is the vector of the s-sublattice displacement. The electronic operators $\hat{\mathbf{V}}'$ and $\mathbf{V}''(s)$ can be presented, similar to the crystal field energy, through the linear combinations of Stevens operators with the parameters which have been calculated earlier in the framework of the exchange charge model (see [1, 4]).

The fifth term in (1) is the electronic Zeeman energy where μ_B is the Bohr magneton, $\mathbf{l}_j$ and $\mathbf{s}_j$ are operators of electronic orbital and spin moments, respectively, and the sum is taken over $4f$ electrons, **M** is the equilibrium magnetization, the tensor $v_0\tilde{Q}$ defines magnetic dipole-dipole interactions between the rare-earth ions (v_0 is the volume of the unit cell). The last term corresponds to the energy of interaction between paramagnetic ions via the phonon field, parameters $\lambda_{pp'}^{kk'}$ were calculated by making use of the characteristics of the lattice dynamics of the $LiTmF_4$ crystal lattice.

The crystal free energy (per unit cell) is:

$$F = \frac{v_0}{2}(\hat{\mathbf{e}}\hat{\mathbf{C}}'\hat{\mathbf{e}} + 2\hat{\mathbf{e}}\hat{\mathbf{b}}\mathbf{w} + \mathbf{w}\hat{\mathbf{a}}\mathbf{w}) + \sum_{pkp'k'} \lambda_{pp'}^{kk'} \langle O_p^k \rangle \langle O_{p'}^{k'} \rangle + v_0 \mathbf{M}\hat{\mathbf{Q}}\mathbf{M} - nk_B T \ln \mathrm{Tr} \exp(-H / k_B T), \quad (3)$$

where k_B is the Boltzman constant, $\hat{\mathbf{a}}$ is the dynamic matrix of the lattice at the Brillouin zone centre, the tensor $\hat{\mathbf{b}}$ determines interaction between macro- and microdeformations, $\hat{\mathbf{C}}' = \hat{\mathbf{C}} - \hat{\mathbf{b}}\hat{\mathbf{a}}^{-1}\hat{\mathbf{b}}$ where $\hat{\mathbf{C}}$ is the tensor of elastic constants, $n = 2$ is the number of rare-earth ions in the unit cell. From the equilibrium conditions:

$$\partial F / \partial < O_p^k >= \partial F / \partial e_{\alpha\beta} = \partial F / \partial w_\alpha(s) = \partial F / \partial M_\alpha = 0 \quad (4)$$

we obtain self-consistent equations for the magnetization vector and the deformation tensor components. This system of equations was solved by making use of the method of consecutive approximations at fixed values of the temperature and the external magnetic field. Calculations were carried out considering the matrix of the Hamiltonian (1) in the total space of the 91 states of the $4f^{12}$ configuration of the Tm^{3+} ion.

The procedure involved the following steps: first, the matrix of the Hamiltonian (1) with $\mathbf{M} = 0$, $\hat{\mathbf{e}} = 0$, $\mathbf{w} = 0$, $< O_p^k >=0$ is diagonalized, and the macro- and micro-deformations ($\hat{\mathbf{e}}(\mathbf{B})$ and $\mathbf{w}(\mathbf{B})$), the magnetization **M,** and the average values of the operators O_p^k are calculated. At the next step, the obtained values of **M**, $\hat{\mathbf{e}}$, **w,** $< O_p^k >$ are substituted into the Hamiltonian (1), and the calculations are repeated. Considering the expansion of the free energy in power series in deformation parameters up to second order, we obtain corrections to the elastic constants depending on the magnetic field and temperature. At the last step, the obtained values of **M**, $\hat{\mathbf{e}}$, **w,** $< O_p^k >$ and $\hat{\mathbf{C}}(\mathbf{B})$ are substituted into the Hamiltonian (1), and the values of **M** are calculated. The results of calculations are presented in fig.1, fig.2 and fig.3.

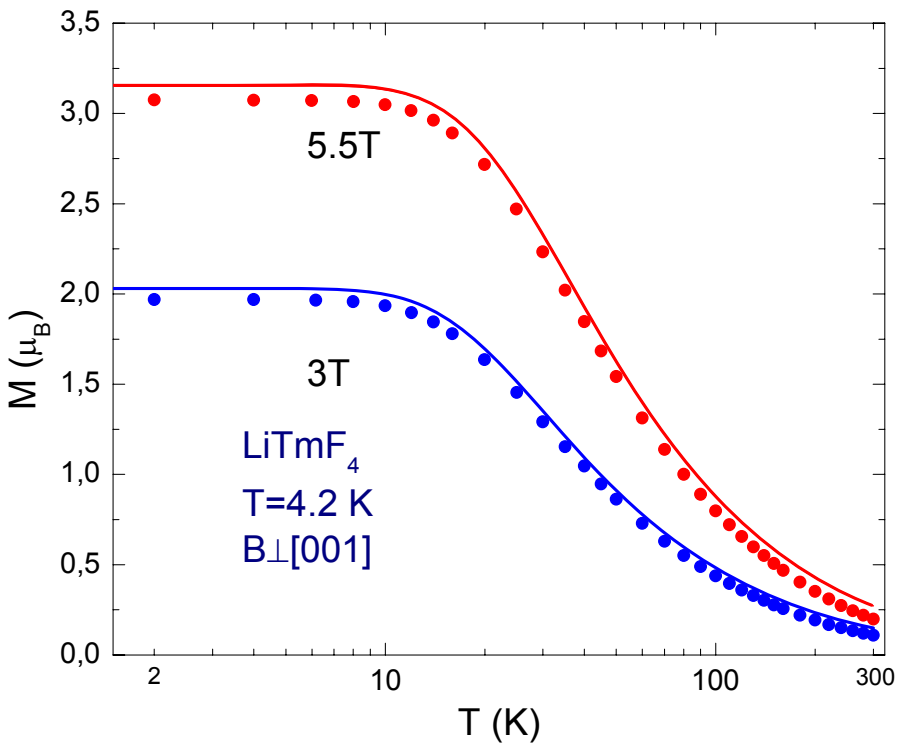

Fig.1. Temperature dependences of magnetization in $LiTmF_4$ in the basis plane.[3] Solid lines are theoretical fits with new crystal field parameters.

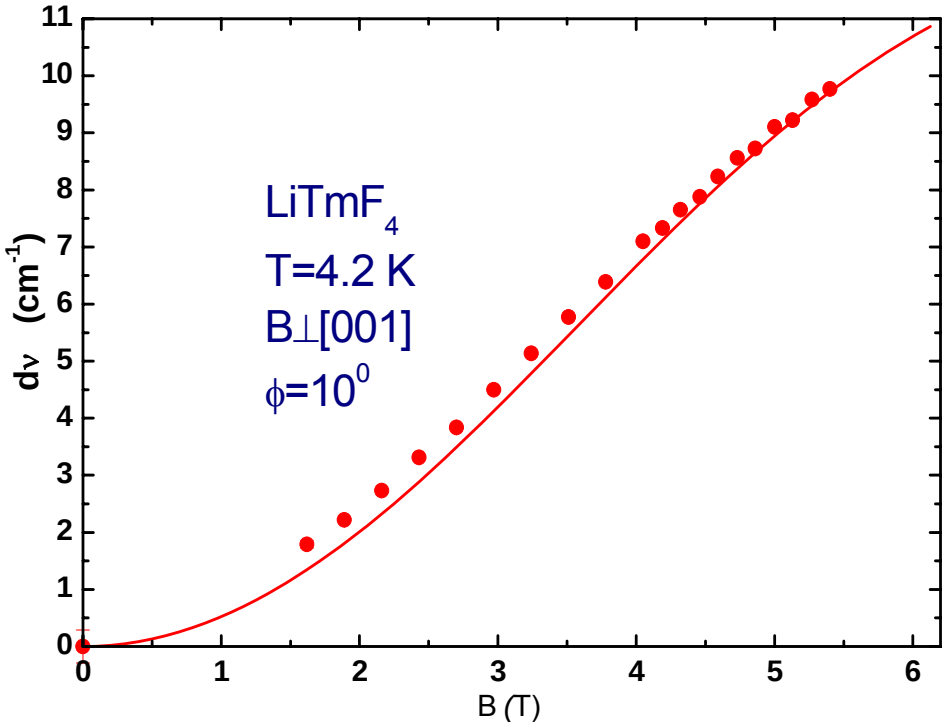

Fig.2. Field dependences of first exited energy level. Solid lines are theoretical fits. Points are experimental data [4].

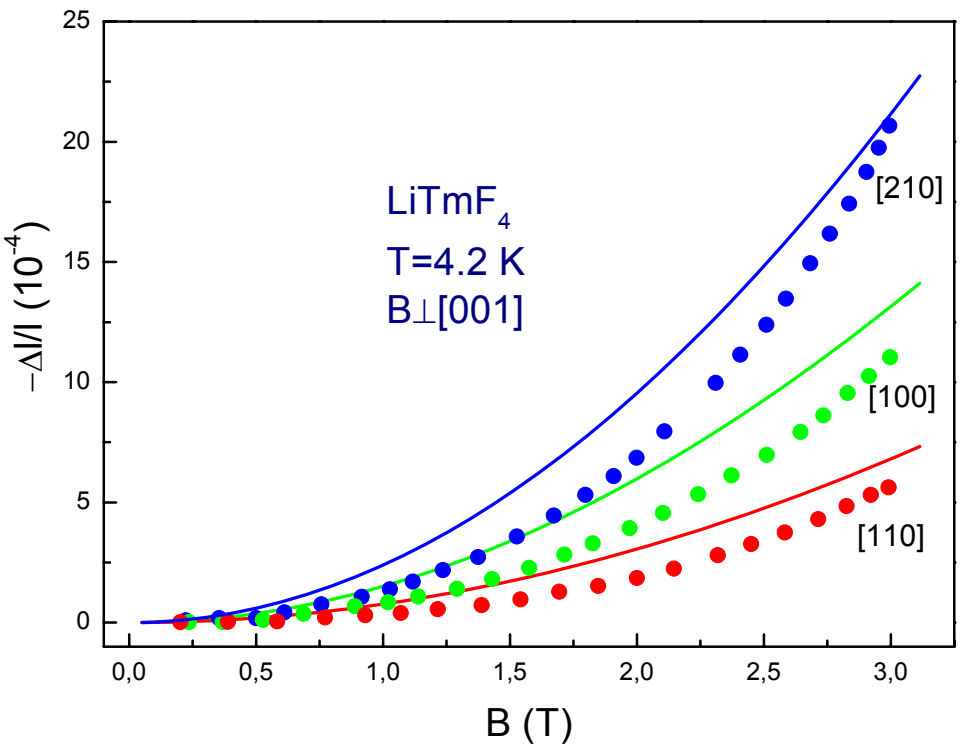

Fig.3. Magnetostriction in $LiTmF_4$ at temperature 4.2 K along three directions of the external magnetic field. Solid lines are theoretical fits. Points are experimental data [1].

Table 1. Crystal field parameters B^k_p (cm^{-1}) for $LiTmF_4$ single-crystals

p k	Tm^{3+}	
	This work	Ref. [3]
2 0	184	184
4 0	-89	-89.6
6 0	-4.06	-4.06
4 4	-529	-727
4 –4	-750	-628.5
6 4	-325	-328
6 –4	-300	-284

Results

From fitting the calculated dependences to the experimental data, corrections to the previously published crystal field parameters were determined (Table 1). Parameters of the multipole interactions were calculated by making use of the characteristics of the lattice dynamics of the $LiTmF_4$ crystal lattice and the electron-phonon coupling constants determined earlier [4]. To interpret temperature and magnetic field dependences of the magnetization and parastriction, field and angular dependences of the first exited energy level, as well as dependences on the magnetic field orientation in the basis *a-b* plane, in variance with the earlier theoretical analysis [2-4], multipole interactions between the Tm^{3+} ions are taken into account in the present work.

At low temperatures, the $LiTmF_4$ single crystals exhibit the giant magnetostriction that can reach the value of 10^{-4} in the magnetic field B ~ 1 T at T=4.2 K. Calculated field dependences of the magnetostriction with the new set of crystal field parameters are in good agreement with experimental data (fig.3).

Conclusion

The temperature, magnetic field and angular dependences of the magnetization, field and angular dependences of the first exited energy level of the Tm^{3+} ions were simulated in the framework of the exchange charge model with taking into account for the electron-phonon interaction and the multipole interactions between the Tm^{3+} ions. Experimental data are well reproduced by simulations based on the microscopic model of the crystal field and magnetoelastic interactions with the new set of the crystal field parameters. It follows from calculations that the electron-phonon interaction in double lithium-rare earth fluorides contribute essentially to the magnetization in external magnetic fields at liquid helium temperatures.

This work was partially supported by RFBR grant №12-02-00372-a.

References

[1] L.K. Aminov et al., Handbook on the Physics and Chemistry of Rare Earths, v. 22, North Holland, Amsterdam, (1996).

[2] V.I. Krotov et al., Sol. St. Phys. 24, 542 (1982).

[3] D. I. Abubakirov et al., J. Phys.: Conference Series 51, 135 (2006)

[4] R.Y. Abdulsabirov et al., J. Lumin. 117, 225 (2006), R.Y. Abdulsabirov et al., SPIE Proc. 4766, 59 (2002).

High-frequency EPR study of crude oils

S.B.Orlinskii, G.V. Mamin, M.A. Volodin

Kazan Federal Unoversity, Federal center of physical and chemical measurements, 420008, Kremlyovskaya St. 18, Kazan, Russian Federation

e-mail: volodinmikhail@yandex.ru

The main scope of the present work is to demonstrate the capabilities of the modern high-frequency (W-band, 94 GHz) EPR spectroscopy for investigations of crude oils.

The list of the investigated samples is presented in Table I. Samples №1 and №2 are present the same oilfield and well, but extracted from a different depth. Sample №4 has been investigated to prove the suggestion about oil leaking from Vereian to Bashkirian horizon.

Table I1. Studied samples

Sample №	Oilfield	Well №	Horizon
1	Akanskoe	2023	Baskirian (bottom)
2	Akanskoe	2023	Baskirian (top)
3	Yamashinskoe	7220	Tournai
4	Akanskoe	27	Vereian

All samples were studied at room temperature both in the continuous wave (cw) and pulsed modes of the commercial Bruker Elexsys-680 spectrometer. The measurements were performed in the microwave W-band (94 GHz). In the CW mode the spectra were obtained utilizing a standard approach with a double modulation of an applied magnetic field B_0 [1, 2].

In fig.1 the CW EPR spectrum of sample №3 is presented which is a typical one for the whole series of samples studied. EPR spectra of the oil originate mainly from the hyperfine structure of vanadyl complex VO^{2+} ($^{51}V^{4+}$, $3d^1$, $S = 1/2$, $I = 7/2$) and from the single line of carbon free radicals (FR), which in agreement with results of [3-5]. Atoms in the vanadyl-porphyrins are arranged practically in a plane defining thus the g-factor and hyperfine A tensor have an axial symmetry [4-6]. The EPR spectrum of the vanadyl-ions consists of the 16 ”lines” representing the 2 × 8 hyperfine patterns for the parallel and the perpendicular complex orientations.

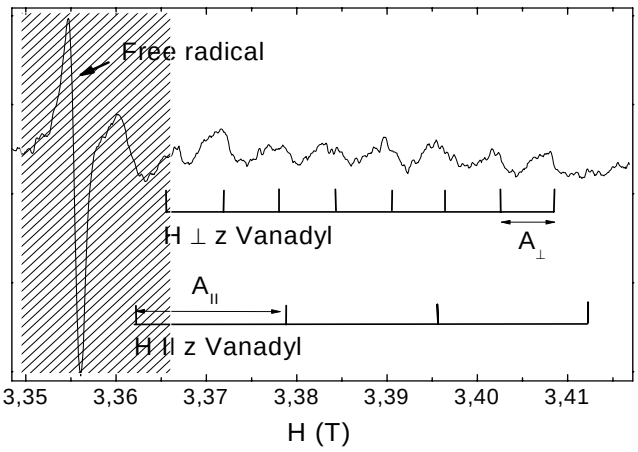

Fig.1. CW EPR spectrum of sample №3.

An important consequence of the microwave frequency increase revealed in the observed CW-spectra in comparison to those measured in the X-band is an almost total spectral resolution between the signals of the vanadyl-ions and the FRs: even a small difference in the g-factor values is enough to avoid the overlap of the two main contributors to the spectra.

For comparison CW EPR spectrums of different oil samples let's consider the relation *K* of FR line intensity to low-field vanadyl line intensity. The shaded area of fig.1 for different oil samples is shown at fig.2 and fig.3.

The maximum of K-parameter had been obtained for sample №3 (fig.2). Samples №1 and №2 extracted from the different depth of the same well have different K-parameter (fig.2 and fig.3). Due to signal/noise ratio difference the concentration of paramagnetic species in

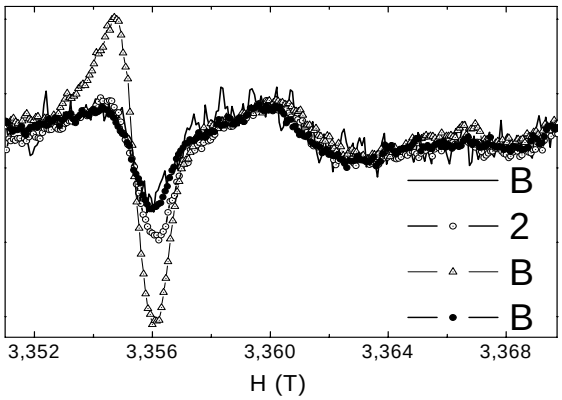

Fig.2. CW spectrum of FR and low-field vanadyl component for all samples.

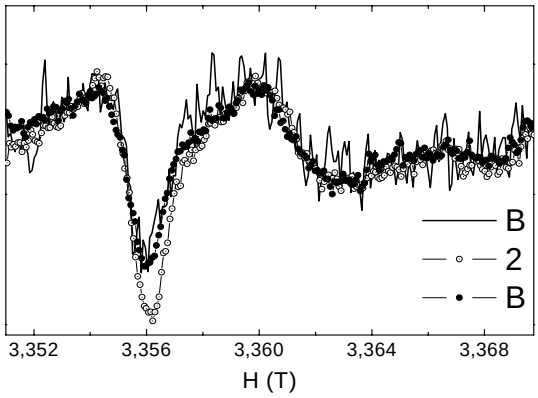

Fig.3. CW spectrum of FR and low-field vanadyl component for samples №1, 2, 4.

sample №2 is significantly higher than in sample №1. The presumable oil leaking from Vereian to the top of Bashkirian horizon can be confirmed by line shape and K-parameter coinciding for samples №2 and №4.

For getting the detailed information about the FR EPR spectra in the pulsed mode were detected via primary electron spin-echo (ESE) amplitude after the two-pulse echo sequence while scanning a magnetic field B_0 (field-swept ESE) [7, 8]. ESE-detected EPR spectrum for oil sample №2 is present at fig.4. ESE-detected spectrums for all samples have the similar structure originating by FR single line only, signals from vanadyl-ions were not obtained. The ESE-signal for sample №1 had not been observed probably due to low paramagnetic species concentration.

Transverse relaxation was studied tracking the primary ESE amplitude while varying τ [7, 8]. For all samples mono-exponential decay of transverse magnetization had been observed (fig.5). Values of transverse relaxation times for all samples are represented in Table II.

Table II. Transverse relaxation times for samples

Sample №	1	2	3	4
T_2, ns	-	185±3	154±2	197±5

The presence of FR ESE-signal in samples of liquid (crude oil) and it's inhomogeneous broadening indicates the location of FR within large molecular clusters of asphaltenes. Otherwise transverse relaxation will be significantly shorter (and unreachable for measuring)

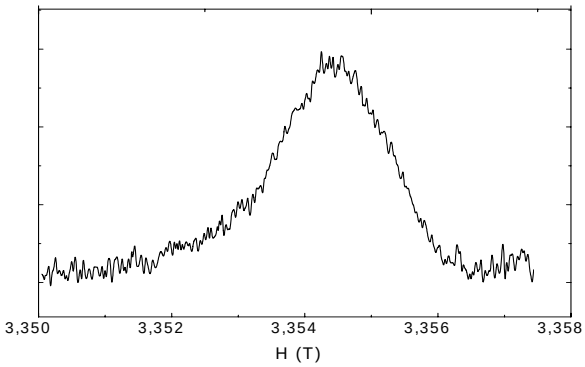

Fig.4. ESE-detected EPR spectrum for sample №2.

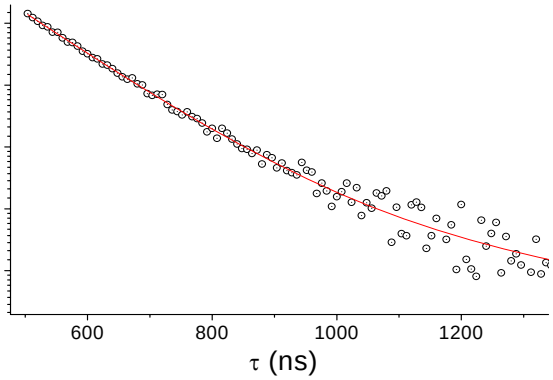

Fig.5. Dependence of the primary ESE amplitude on the delay between the two microwave pulses in the Hahn sequence of the sample №3.

due to averaging by high mobility of paramagnetic species. Slight difference in transverse relaxation time (Table II) between different samples can be explained by differences in viscosity of samples.

Conclusion

The high-frequency W-band EPR allows to resolve spectrally the components of the crude oil EPR spectra originating from the free radicals and the vanadyl-ions. It gives an opportunity to gain a deeper insight to the origin of the paramagnetic centers important both for the fundamental research and industrial applications.

The relation of FR line intensity to low-field vanadyl line intensity (K-parameter) allows distinguishing the oil type and serves as the fingerprint of the hydrocarbon origin.

Using of K-parameter allows to accurately determine the existence of the oil leaking between different horizons of the oilfield.

References

[1] C.P. Poole, Electron Paramagnetic Resonance. Comprehensive Treatise on Experimental Techniques, John Wiley & Sons, 1967.

[2] J.A. Weil, J.R. Bolton, Electron Paramagnetic Resonance: Elementary Theory and Practical Applications, 2nd ed., John Wiley & Sons, Hoboken, New Jersey, 2004.

[3] C.L.B. Guedes, E. Di Mauro, Photochemical Weathering Study of Brazilian Petroleum by EPR Spectroscopy, Marine Chemistry, Vol. 84, №1 (2003), pp.105-112.

[4] L.G. Gilinskaya, Journal of Structural Chemistry 49, 245 (2008).

[5] G.P. Dechaine, M.R. Gray, Energy Fuels 24, 2795 (2010).

[6] M. Espinosa, A. Campero, R. Salcedo, Inorganic Chemistry 40, 4543 (2001).

[7] K.M. Salikhov, A.G. Semenov, Y.D. Tsvetkov, Electron Spin Echo and Its Applications, Nauka, Novosibirsk, 1976.

[8] A. Scweiger, G. Jeshke, Principles of Pulse Electron Paramagnetic Resonance, Oxford University Press, 2001.

Features of the EPR of the ZrO_2-Y_2O_3 system

J.V. Mamedov[1], I.V. Yatsyk[2], I.I. Fazlizhanov[2], T.P. Gavrilova[2], R.M. Eremina[2], N.Yu.Tabachkova[3], F.O. Milovich[3], E.E. Lomonova[4]

[1]Kazan (Volga Region) Federal University, 420008, Kremlyovskaya st., Kazan, Russia

[2]E. K. Zavoisky Physical-Technical Institute RAS, 420029, Sibirsky tract, Kazan, Russia

[3]National University of Science and Technology "MISIS" (MISIS), 119049, Leninskii pr., Moscow, Russia

[4]Prokhorov General Physics Institute, RAS, 119991, Vavilov Str., Moscow, Russia

e-mail: javi-m@yandex.ru

Zirconia (ZrO_2) is a material of great technological potential importance due to its outstanding mechanical and electrical properties, high dielectric constant ($\varepsilon \approx 25$) and wide band gap ($Eg \approx 6$ eV). Among the ZrO_2 applications, are solid fuel cells, gas sensors, high durability coating and other. The gap and the dielectric properties suggested its potential to replace SiO_2 in advanced metal oxide semiconductor devices in gate stack, optical systems and dynamic access memory devices [1-3]. Furthermore, it has a large band-offset in contact with Si and good thermal stability. These attractive properties of zirconia do it interesting to studying.

ZrO_2 presents polymorphism with monoclinic, tetragonal, and cubic phases. The monoclinic phase of ZrO_2 is thermodynamically stable at temperatures below 1170°C. The tetragonal phase structure arises between 1170°C and 2370°C, further above 2370°C the cubic phase is then observed. The temperature in which the tetragonal to cubic transformation occurs can be lowered, by the addition of solutes such as CaO, MgO, Y_2O_3, allowing the achievement of the stabilized cubic phase even at room temperature.

The phase diagram is shown in fig.1. The system (ZrO_2 – Y_2O_3) has a monoclinic phase at 800°C in the range of concentration of impurity from 0 to 2%. In the range from 2 to 7% impurity content the concentration of the tetragonal phase increases. Further in the range from 7 to 14% of impurity the system exists as a mixture of tetragonal phase (93% ZrO_2 + 7% Y_2O_3) and the cubic fluorite structure (86%ZrO_2+14% Y_2O_3). At further increase of concentration impurity the system includes only fluorite phase. From three observed types of crystal structure only the fluorite crystal structure is conductive [4].

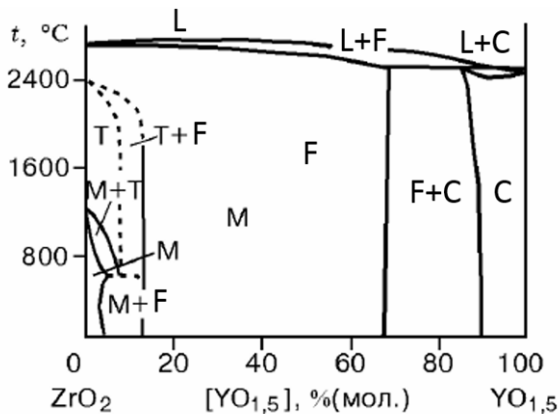

Fig.1. Phase diagram of the ZrO_2 – Y_2O_3 system [4].

Samples, which were studied in this work, were synthesized by directional crystallization of the melt using a direct high-frequency heating. The process includes four steps. This is the starting heating, creating the bulk of the melt, pause for a system to come to a steady state and melt crystallization [5]. The EPR spectra were measured on a Bruker EMX spectrometer equipped with flow type nitrogen cryostats in the temperature range 100 – 300 K at a frequency of 9.4 GHz. The EPR spectrum consists of two intensive lines with $g \sim 4{,}2$ and $g \sim 2$. The position of lines in the magnetic resonance spectrum in ZrO_2 doesn't depend from temperature.

We investigated the angular dependencies of the EPR spectra of the $ZrO_2 + Y_2O_3$ (2,8 mol%) system at room temperature. The intensity of these signals depends on the heat treatment and annealing temperature in an atmosphere of oxygen.

The observed lines of the EPR transitions doesn't connect to ions of metal groups, since they weren't observed in all samples, although they were prepared from the same reactants. The intensity (amplitude) line g ~ 2 and g ~ 4.2 of the samples depended on the temperature *T*, but its position does not depend on angle (fig.2). The evolution of the line shape is observed with increasing temperature.

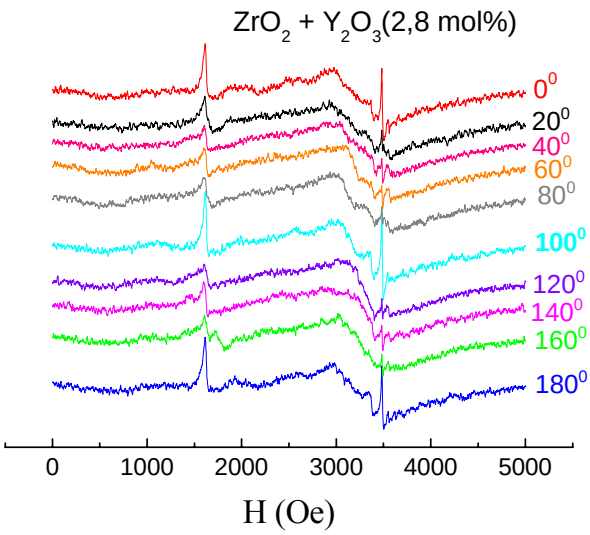

Fig.2. The angular dependence of the EPR spectra of the ZrO_2 + 2,8 mol%Y_2O_3 system

We believe that these EPR signals with g ~ 2 and g ~ 4.2 are due to hole pairs localized on the oxygen ions characterized by the exchange interaction $J\mathbf{S}_1\mathbf{S}_2$, where $S_1 = S_2 = 1/2$ are the spins of the two holes. For the antiferromagnetically coupled hole pair ($J > 0$) the ground state is a singlet and the excited state is a triplet. The EPR spectra can observe when the triplet is thermally populated. Hereafter, lines in spectra refer to the excited triplet state. The presently observed EPR line at $g \sim 2$ is an overlap of the allowed transitions is the electronic quantum number $\pm 1 \leftrightarrow 0$ of the triplet state, occurring at about the same magnetic field value for an isotropic g and negligible zero-field splitting of the triplet levels. The so-called "half-field" signal with $g \sim 4.25$ associated with the "forbidden" transition $\pm 1 \leftrightarrow \mp 1$ is typical of a triplet center [6].

References

[1] G.D. Wilk, R.M. Wallace, and J.M. Anthony, J. Appl. Phys. 89, 5243 (2001)

[2] M. Houssa, V.V. Afanaśev, A. Stesmans, M.M. Heyns, Appl. Phys. Lett. 77, 1885 (2000)

[3] S.J. Wang, C.K. Ong, S.Y. Xu, P. Chen, W.C. Tiju, J.W. Chai, A.C.H. Huan, W.J. Yoo, J.S. Lim, W. Feng, and W.K. Choi, Appl. Phys. Lett. 78, 1604 (2001)

[4] V.M. Zainullina, V.P. Zhukov, V.M. Zhukovskii, N.I. Medvedeva, Journal of Structural Chemistry. 41, 185 (2000)

[5] V.V. Osiko, M.A. Borik, E.E. Lomonova, Technique Springer Handbook of crystal growth. 353, 14 (2010)

[6] S.K. Misra, S.I. Andronenko, R.R. Andronenko, L.P. Mezentseva, Phys.RevB 53, 9442 (1996)

Continuous wave electron paramagnetic resonance of Gd^{3+} in LaF_3 nano- and micro-sized particles

A.M. Gazizulina, S.L. Korableva, R.M. Rahmatullin, A.A. Rodionov, M.S. Tagirov

Kazan (Volga region) Federal University, 420008, Kremlevskaya 18, Kazan, Russia

e-mail: sabitovaalsu@gmail.com

The X-band electron paramagnetic resonance of Gd^{3+} ion doped in the diamagnetic LaF_3 nanoparticles at a room temperature was investigated The four nanosized LaF_3:Gd^{3+} samples 1, 2, 3 and 4 were synthesized using different time of hydrothermal reaction [1, 2]. In typical synthesis, lanthanum oxide is dissolved in nitric acid solution. Then, after filtering, NaF (F:La with 0,5% Gd = 3:1) was added into the above solution under violent stirring. The pH of the suspension was adjusted by ammonia to about 4.0 – 5.0 value. After stirring for 20 min, the suspension was placed in the microwave oven (650 W) for the further hydrothermal reaction. The suspension was heated by microwave irradiation at 70% of the maximum power under refluxing for 0, 20, 40, and 420 min (samples numbers 1, 2, 3 and 4 respectively). The resulting product was collected by centrifugation and washed several times in deionized water. The X-ray experiments showed high crystallinity of synthesized samples. The micron-sized sample was prepared by milling of a single crystal LaF_3:Gd^{3+}.

The X-band EPR of Gd^{3+} ion has been observed for the first time. in LaF_3:Gd^{3+} powders at the room temperature. The EPR spectra (fig.1) were obtained at Bruker ESP-300 spectrometer. The influence of the sample size and hydrothermal reaction duration will be reported.

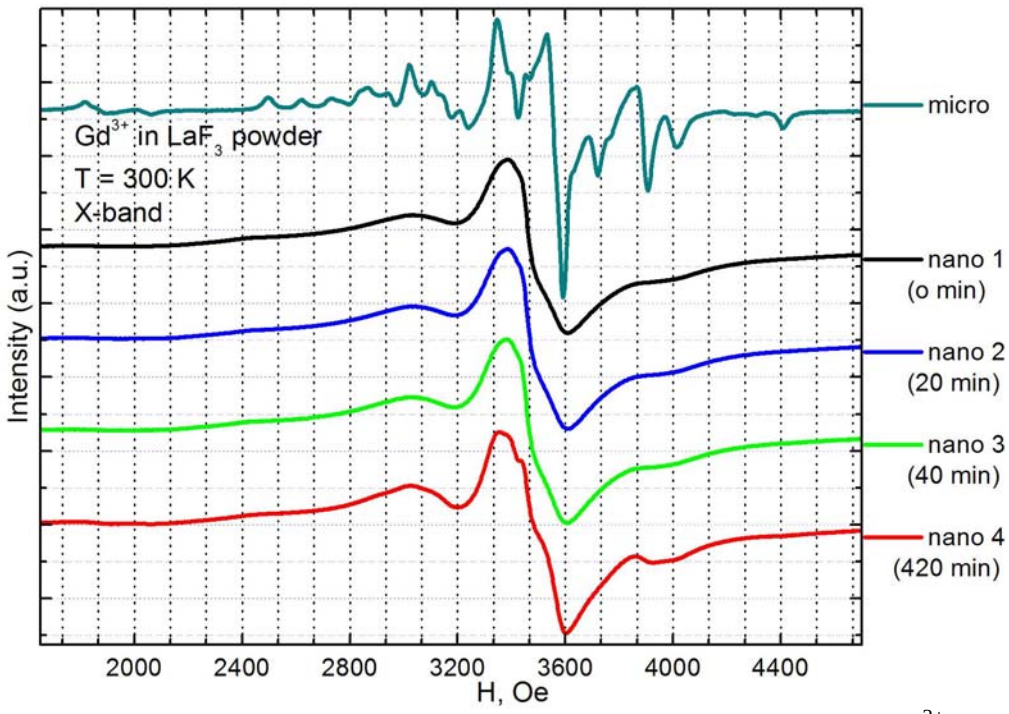

Fig.1. The EPR spectra of nano- and micro- sized powders LaF_3:Gd^{3+}.

The fig.2 shows the EPR spectra of Gd^{3+} ion in micro- (45 micron) and nano- (sample 4, 30 nm) size crystalline LaF_3:Gd^{3+} powders. Spectrum of the sample 4 is similar to the spectrum of micron-sized sample. This can be interpreted as a result of restructuring [3].

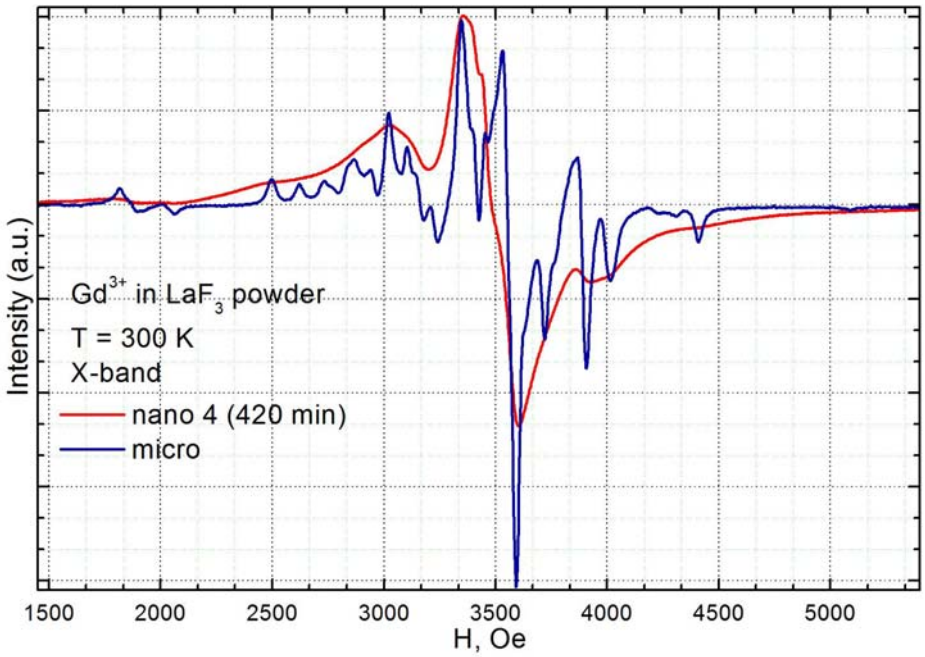

Fig.2. The EPR spectra of nano- (sample 4) and micro- sized powders $LaF_3:Gd^{3+}$.

The first of all, spectrum of the micro-sized sample must be described. This spectrum was described using the Matlab Easyspin module. The experimental and simulated spectra are shown in fig.3. The tuning changed crystal-field parameters were used. The initial parameters of crystal-field were taken from the V.K. Sharma article [4]. These calculations of the spectrum by EasySpin module agree well with an experimental data.

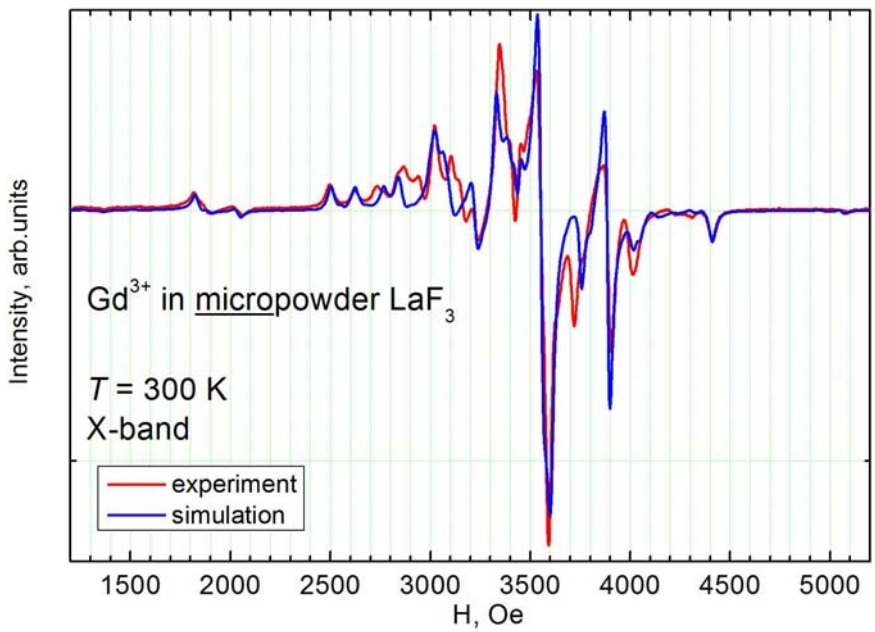

Fig.3. The EPR spectra of micro-sized powder $LaF_3:Gd^{3+}$ and simulation

References

[1] L.Ma et al., JETP Lett., 86, 416 (2007).
[2] E.M. Alakshin et al., J. Low. Temp. Phys., 162, 645 (2011).
[3] E.M. Alakshin et al. JETP Letters, 96, 3, 194 (2012).
[4] V.K. Sharma, The journal of Chemical physics, 54, 2 (1971).

Nitrogen-containing species in the structure of hydroxyapatite nanocrystals: a combined multifrequency EPR/ENDOR and DFT study

T.B. Biktagirov[1], M.R. Gafurov[1], B.V. Yavkin[1], G.V. Mamin[1], S.B. Orlinskii[1], E.S. Klimashina[2], V.I. Putlayev[2]

[1]Institute of Physics, Kazan Federal University, Kazan 420008, Russia

[2]Department of Chemistry, Moscow State University, Moscow 119992, Russia

e-mail: tbiktagirov@gmail.com

Nanosized hydroxyapatite ($Ca_{10}(PO_4)_6(OH)_2$; nano-HAp) is considered to be a promising biomaterial [1]. It is known that the structure of hydroxyapatite is highly labile for the different types of ionic substitutions. These impurities can affect physicochemical properties of nano-HAp and its biocompatibility. Previously we have shown the abilities of high-frequency electron paramagnetic resonance (EPR) spectroscopy for studying paramagnetic impurities both in the synthetic and biogenous HAp [2, 3].

In the present work the combination of X- (10 GHz) and W-band (94 GHz) EPR and electron-nuclear double resonance (ENDOR) pulsed techniques with density functional theory (DFT) based calculations has been employed to investigate the distribution of nitrate impurity in the structure of nano-HAp produced via wet synthesis process.

We have observed the EPR signal of radiation induced paramagnetic center which is supposed to be a stable NO_3^{2-} radical allocated in nano-HAp structure and produced from NO_3^- anionic impurity. X- and W-band field-swept spin-echo spectra and their simulations are presented on fig.1. The concentration of the radical was estimated to be of $4{\cdot}10^{18}$ spins per gram. We assume that the nitrate anions incorporate in the structure of the nano-HAp during the synthesis process from the reagents (by-products).

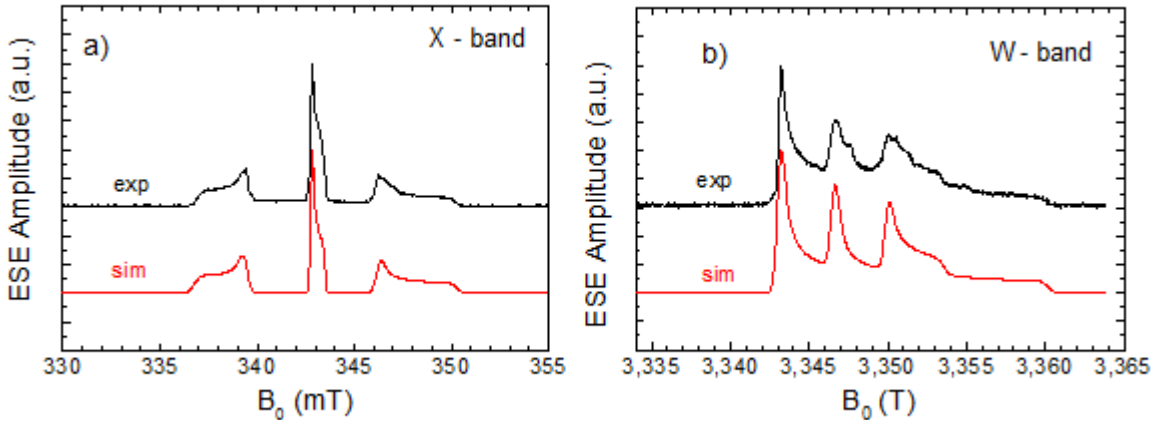

Fig.1. Field swept echo detected EPR spectra (exp) of nano-HAp: (a) X-band (9.6 GHz), T = 300 K; (b) W-band (94.1 GHz), T = 50 K and their corresponding simulations (sim).

To specify the coordination of the obtained paramagnetic centers ENDOR experiments were carried out. Fig.2 presents the Mims-ENDOR spectra in the vicinity of phosphorous (^{31}P) and hydrogen (^{1}H) Larmor frequencies. The interpretation of the ENDOR results suggests two possible crystallographic sites of NO_3^{2-} radical localization, namely the site of OH group and the position of PO_4.

Ab-initio calculations have been carried out within the framework of the plane-wave

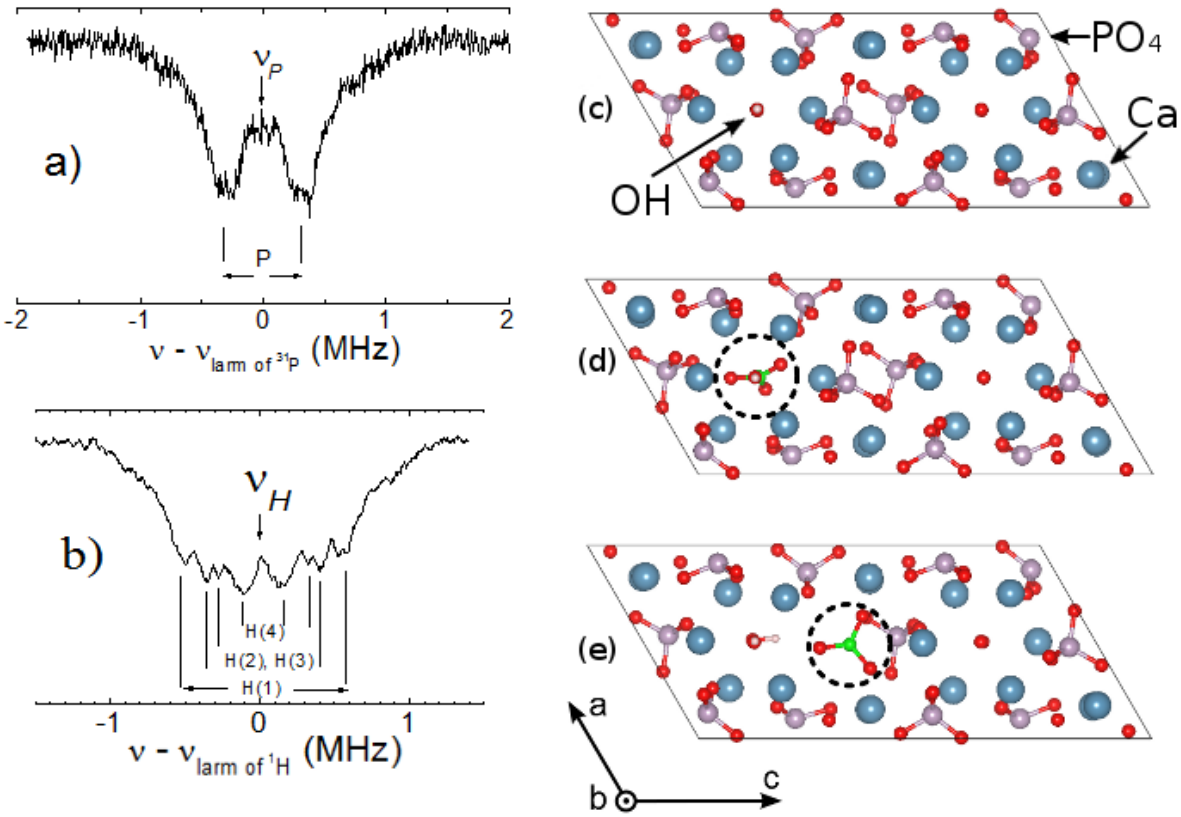

Fig.2. ENDOR spectra of the nano-HAp in the vicinity of (a) phosphorous and (b) hydrogen Larmor frequencies obtained in W-band at T = 300 K and the structures of (c) pure HAp, and HAp with nitrate localized (d) in OH-site and (e) in the position of PO_4. The dashed circles in (d-e) show the positions of the impurity.

pseudopotential DFT using the Quantum ESPRESSO package [4]. Spectroscopic parameters (hyperfine coupling constants and *g*-tensors) of the NO_3^{2-} radical were obtained by using the gauge-including projector augmented wave (GIPAW) approach [5]. Two models of nitrate incorporation were considered (as suggested by ENDOR; cf. fig.2): A-type (OH-site) and B-type (PO_4-site). After the preliminary structural optimization the spectroscopic parameters were calculated. From the excellent correspondence of the calculated hyperfine coupling constants with the experimental ones (Table 1), it can be concluded that the obtained EPR and ENDOR spectra originate from the B-site located radicals only.

Table 1. DFT calculated ^{14}N hyperfine components for the A- and B-types of substitution compared to those derived from experimental EPR spectra (in mT)

	A_{xx}	A_{yy}	A_{zz}
A-type	2.485	2.478	5.183
B-type	3.277	3.273	6.413
experiment	3.35(4)	3.35(4)	6.65(4)

To summarize, we have shown that due to the high sensitivity of the pulsed multifrequency EPR and ENDOR methods we were able to detect the radiation-induced NO_3^{2-} impurity center presented in the structure of nano-HAp in trace concentration. The combination of ENDOR with DFT calculations was found to be helpful for the investigation of the localization of the impurity. All these, finally, could be used for the design of the HAp-

based materials with desired physico-chemical properties.

References

[1] Lafon J.P., Champion E., Bernache-Assollant D.: Eur. Cer. Soc., 28, 139 (2008)

[2] Abdul'yanov V.A., Galiullina L.F., Galyavich A.S., Izotov V.G., Mamin G.V., Orlinskii S.B., Rodionov A.A., Salakhov M.Kh., Silkin N.I., Sitdikova L.M., Khairullin R.N., Chelyshev Yu.A.: JETP Lett., 88, 69 (2008)

[3] Gafurov M.R., Yavkin B.V., Biktagirov T.B., Mamin G.V., Orlinskii S.B., Izotov V.V., Salakhov M.Kh., Klimashina E.S., Putlayev V.I., Abdul'yanov V.A., Ignatjev I.M., Khairullin R.N., Zamochkin A.V., Chelyshev Yu.A.: Magn. Reson. Solids, 15, 13102 (2013)

[4] Giannozzi P.: J Phys Condens Matter, 21, 395502 (2009)

[5] Pickard C.J., Mauri F.: Physical Review B, 63, 245101 (2001)

EPR study of magnetic anomalies in the $La_{2-x}Sr_xCuO_4$ single crystals above the critical temperature

V.O. Sakhin[1], Yu.I. Talanov[2], L.F. Salakhutdinov[2], T. Adachi[3], T. Noji[3], Y. Koike[3]

[1]Kazan Federal University, 420008, Kremlevskaya str. 18, Kazan, Russia
[2]Zavoisky Physical-Technical Institute, 420029, Sibirsky tract, Kazan, Russia
[3]Department of Applied Physics, Tohoku University, Sendai 980-8579, Japan

e-mail: urfinjus67@gmail.com

Since it's discovering in 1986, high-temperature superconductivity remains one of the most intriguing subjects in physics. One of the unsolved problems is unclear scenario of the transition between normal state and superconducting state. The path to solution of this problem lies through understanding the electron and magnetic state of the materials above critical temperature. Recent studies have shown that this state exhibits some properties corresponding to superconducting state. For example, pseudo-gap regime [1], uncorrelated Cooper pairs [2] and giant Nernst effect [3]. There were proposed a few theoretical models to describe this state, but there is no consensus in this question. Superconducting feature can manifest themselves through the magnetic field inhomogeneities in the sample volume and at the superconductor surface. The goals of our study are obtaining and interpretation the experimental data on the magnetic state of the high-*Tc* superconductor LSCO using the ESR technique, and comparison them with theoretical models of electromagnetic state of superconductor above T_C.

The samples we used were three single crystals of $La_{2-x}Sr_xCuO_4$ (LSCO) with different strontium doping concentrations. The crystal with the Sr concentration of $x = 0.16$ is optimally doped and undergoes a superconducting transition at $T_C = 39.4$ K. T_C of the underdoped crystal ($x = 0.077$) is 18 K, and the third sample has Sr concentration near to "1/8 anomaly" doping level ($x = 0.116$, $T_C = 27$ K).

To obtain the information about distribution of magnetic field on the sample surface the EPR method in combination with the surface paramagnetic probe was used, so-called "EPR-decoration" [4]. A thin layer of 2,2-diphenyl-1-picrylhydrazyl (DPPH) was used as a probe. It was deposited onto the crystal surface by the vacuum evaporation technique. The layer thickness was about 150 nm. DPPH was used as a probe because of the very small width of its resonance signal (~1.5 G). We used a crystal of LiF with Li dendrites to obtain reference signal. Also to obtain spatial characteristics of inhomogeneities of magnetic field near the surface of sample we placed paraffin buffer layer between paramagnetic probe and surface of sample.

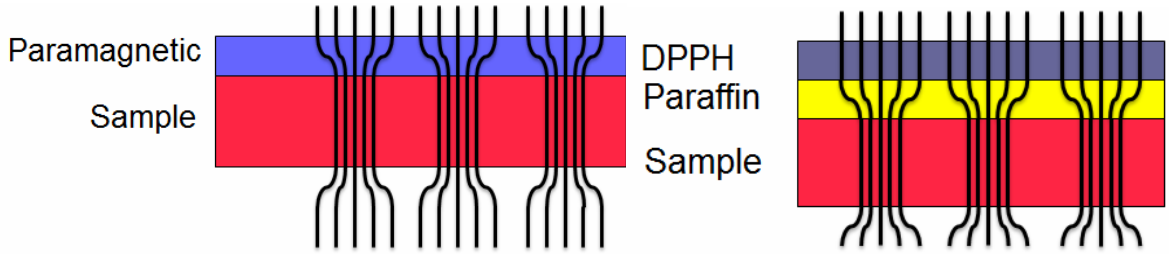

Fig.1. Scheme of sample with paramagnetic probe on its surface (left). Scheme of sample with paramagnetic probe distant from the surface (right).

Change of spectrum with decreasing temperature is shown on fig.2. Spectrum consists of two lines, one is from thin layer of DPPH and another is from Li. While position of the Li signal remains constant, signal of DPPH is shifting and broadening. Before analyzing the shift of DPPH signal, one needs to take into account that there are three contributions to the shift: $\Delta H = H_{g\text{-}g'} + H_d + \Delta H'$. First ($H_{g\text{-}g'}$) is due to difference between g-factors of DPPH and Li, second (H_d) is due to demagnetizing field of thin paramagnetic layer and third contribution is of magnetic anomalies, which is we need to find. To measure first two contributions we deposited DPPH layer on quartz substrate and obtained temperature dependence of shift of DPPH signal, which was approximated by Curie-Weiss law. Here after dependences of signal shift are shown with first two contributions subtracted.

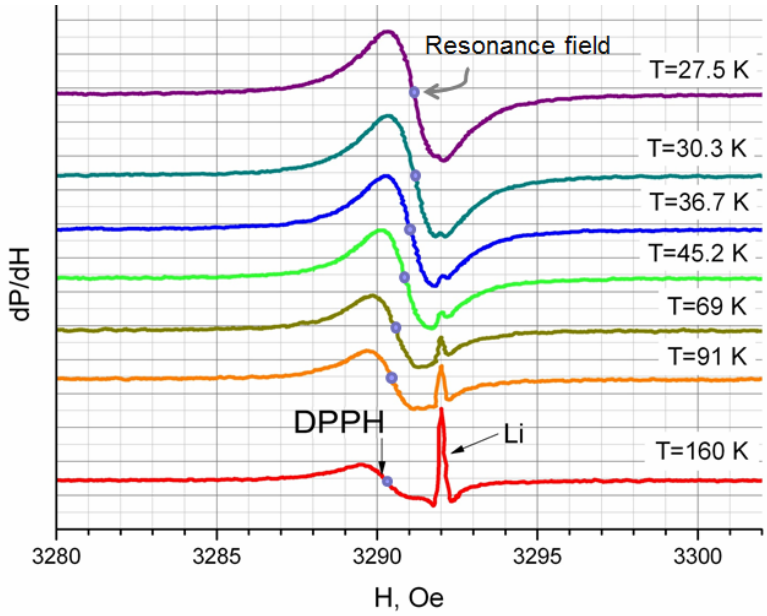

Fig.2. Change of the EPR spectrum of DPPH layer deposited on $La_{1.884}Sr_{0.116}CuO_4$ with varying temperature ($H \parallel c$, Probe thickness: 110 nm)

Temperature dependence of shift of signal of DPPH thin layer deposited on $La_{1.884}Sr_{0.116}CuO_4$ is shown on fig.3. There is absence of shit at the temperatures higher than 100 K, sharp shift to higher fields below T_C, due to formation of Abrikosov vortex lattice, and small shift to lower fields just above T_C. We subtracted side contributions, so this small shift is due to inhomogeneties of magnetic field near the surface of sample that were connected with the magnetic state of superconductor. Because of signal shifts to lower fields we assume that these inhomogeneties are due to paramagnetic inclusions. While distance between probe and surface is increasing, value of shift is decreasing due to decay of this contribution.

But for underdoped sample the temperature dependence of the signal shift of DPPH thin layer above T_C is different (fig.4). Surprisingly, while thickness of probe and distance between sample and probe are increasing, the shift to lower fields is increasing too. It can be explained if there is a two contributions to shift: paramagnetic and diamagnetic, and total shift is determined by relation of these contributions. The distance dependence of the shift indicates that parts of the sample that exhibit paramagnetic behavior and parts that exhibit diamagnetic behavior have different size. So with increasing distance from surface of the sample the contributions decay at different rate. In the case, when probe thickness is minimal, the paramagnetic and diamagnetic contributions almost compensate each other, but as we move away the probe from surface the diamagnetic contribution rapidly decays and the paramagnetic contribution prevails. Mechanism that lies beneath this shift might be stripe order: alternating charge depleted and charge enriched stripes. The charge depleted stripes are

antiferromagnetically ordered and they can exhibit paramagnetic properties under influence of magnetic field due to tilt of sublattices.

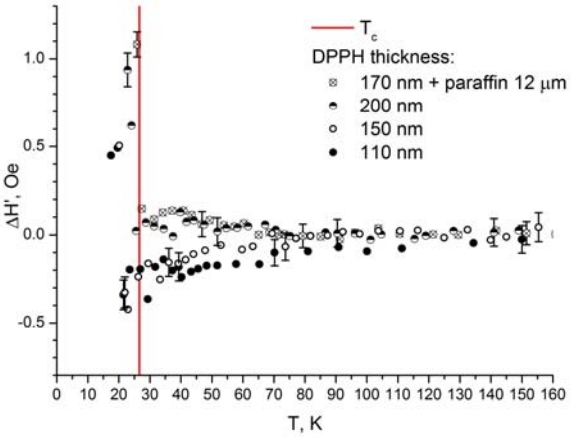

Fig.3. Temperature dependence of the EPR signal shift of DPPH probes with different thicknesses deposited on $La_{1.884}$ $Sr_{0.116}CuO_4$

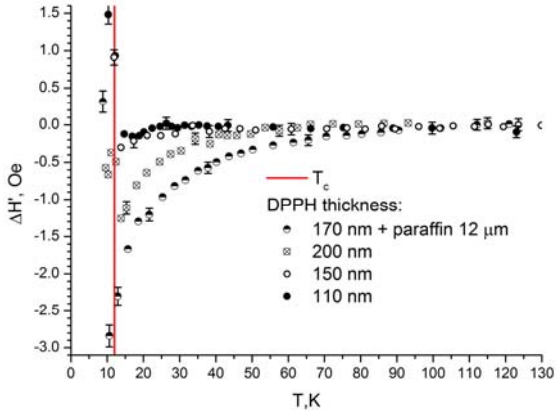

Fig.4. Temperature dependence of the EPR signal shift of DPPH probes with different thicknesses deposited on $La_{1.923}$ $Sr_{0.077}CuO_4$

But stripes are small-scaled, only few nanometers. In contrast to it, the observed magnetic anomalies remain when probe is 12 micron away from surface of sample, so their size should be at least few microns. So the stripe order by itself cannot be explanation of these anomalies. In this temperature range LSCO is in the low-temperature orthorhombic phase (LTO) [5], that leads to the formation of the twinned domain structure. For stripes the domain boundaries are obstacle and stripes pinned on these boundaries. In this case the scale of magnetic anomalies would not be determined by size of stripes, but by size of domains. And size of domains is about tens of microns, that is comparable with size of observed anomalies.

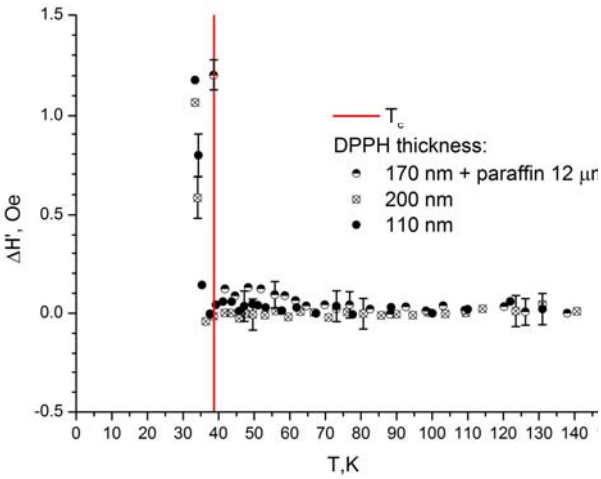

Fig.5. Temperature dependence of the EPR signal shift of DPPH probes with different thicknesses deposited on $La_{1.84}$ $Sr_{0.16}CuO_4$

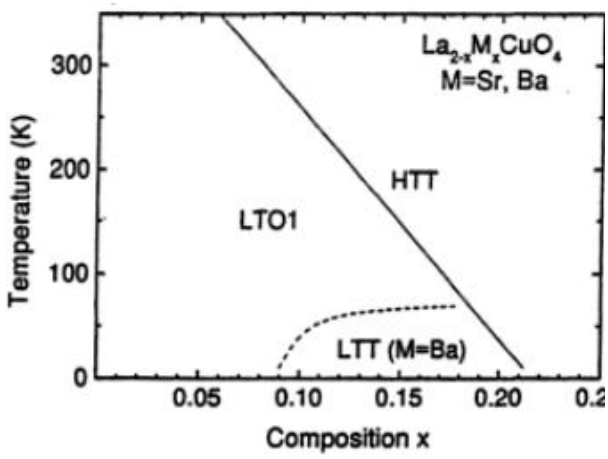

Fig.6. Phase diagram of $La_{2-x}M_xCuO_4$ [5]

For the optimally doped sample contributions almost compensate each other above T_C (fig.5). Overall, in three samples the paramagnetic and diamagnetic contributions behave differently: the largest shift to lower fields is observed in case of underdoped sample, the small shift to lower fields for "1/8 anomaly" sample and the absence of shift in case of optimally doped sample. This can be explained by instability of LTO phase. According to phase diagram shown on fig.6 the temperature of transition between high-temperature tetragonal phase (HTT) and LTO phase is decreasing with increasing Sr concentration. Most

stable LTO phase and, respectively, most stable domain structure corresponds to underdoped sample case. For the optimally doped sample the LTO phase is most unstable and there in no shift of DPPH signal position. And in case of "1/8 anomaly" concentration of Sr the LTO phase is more stable, but it is interrupted by fluctuating low-temperature tetragonal phase (LTT). This phase is stable in similar compound ($La_{2-x}Ba_xCuO_4$) [6] and unstable in LSCO but affects on stability of domain structure.

References

[1] Patrick A. Lee, Naoto Nagaosa, Xiao-Gang Wen, Reviews of modern physics (2006), vol.78, 17-85

[2] Kenjiro K. Gomes, Abhay N. Pasupathy, Aakash Pushp, Shimpei Ono, Yoichi Ando and Ali Yazdani, Nature B(2007) Vol. 47 569-572.

[3] Y. Wang, L. Li, N. Ong, Phys. Rev. B.73, 024510 (2006).

[4] B. Rakvin, M. Pozek, A. Dulcic, Solid State Commun (1989) Vol.72 no.2 199-204

[5] Arnold R. Moodenbaugh Superconductivity and structure in $La_{2-x}M_xCuO_4$, M=Ba,Sr and (Nd,Sr), Studies of High Temperature Superconductors (2000), V.33, 157-181

[6] M. Hucker, M. v. Zimmermann, G. D. Gu, Z. J. Xu, J.S. Wen, G. Xu, H. J. Kang, A. Zheludev and J. Tranquada, Physical Review B **83**, 104506 (2011)

Glycerol penetration profile in phospholipid bilayers measured by ESEEM of spin-labeled lipids

K.B. Konov[1], N.P. Isaev[2], S.A. Dzuba[2,3]

[1]Zavoisky Physical–Technical Institute, Russian Academy of Sciences, Kazan, Russia

[2]Voevodsky Institute of Chemical Kinetics and Combustion, Russian Academy of Sciences, Novosibirsk, Russia

[3]Novosibirsk State University, Novosibirsk, Russia

e-mail: kostyakonov@gmail.com

Introduction

In this work electron spin echo envelope modulation (ESEEM) technique was used to study the penetration of deuterium water (D_2O) and deuterium-substituted water glycerol mixture $H_2O/C_3D_5(OH)_3$ (1:1 v/v) into dipalmitoyl phosphatidylcholine (DPPC) bilayer membranes. ESSEM technique provides penetration profile of glycerol across the lipid membrane and gives quantitative assessment of the glycerol concentration in different location across the membrane. For comparison, penetration profile of deuterated water across the lipid membrane was studied.

The permeation of small molecules across biological membranes is important for cell regulation. The transport of water and cryoprotective chemicals, such as sugars and glycerol, across cell membranes is of fundamental importance for cryopreservation. Glycerol can protect biological membranes under extreme conditions, such as freezing and desiccation. Cryoprotective action of glycerol related to stabilization of the native structures of biomacromolecules, regulation of microviscosity, prevention of intercellular ice formation.

To investigate the properties of membranes at the molecular level, electron paramagnetic resonance employing spin-labeling techniques can be used. ESEEM allows direct examination of the accessibilities of deuterium-substituted molecules to spin labels. Spin labels (stable nitroxide radicals) was attached to sn-2 chain of DPPC. Hydrogen atoms in glycerol were substituted by deuterium atoms. The ESEEM technique is based on the anisotropic interactions between the unpaired electron of a spin label and deuterium nuclei. The interaction can be distinguished for distances less than 0.5 nm, which can be considered as a spatial resolution of the method. Thus, the ESEEM amplitude observed for a spin label attached at different positions along the lipid chain can serve as indicators for the penetration depth of the deuterium-substituted molecules. The deuterium was used for two reasons. First, using deuterium provides much strong ESEEM signal. Second, deuterium and hydrogen ESEEM signals have different frequencies, so deuterium atoms in glycerol penetrating membrane can be easily distinguished from hydrogen atoms in the lipid chains.

Experimental

Phosphatidylcholines spin-labelled at the sn-2 chain,1-acyl-2-(n-doxyl)stearoyl-sn-glycero-3-phosphocholine(n-PCSL, n = 5, 7, 10, 12, 14 and 16), 2-oleoyl-1-palmitoyl-sn-glycero-3-phospho(tempo)choline (denoted as 0-PCSL, the spin label was attached to the polar lipid head), and unlabelled 1,2-dipalmitoyl-sn-glycero-3-phosphocholine (DPPC) were dissolved in chloroform in the molar ratio of 1:100. The solvent was removed and the obtained samples were hydrated for 4h at temperatures above the phase-lipid transition by adding in proportion of 1:4 w/w either D_2O or $H_2O/C_2D_5(OH)_3$ 1:1 v/v mixture.

A Bruker Elexsys E580 X-band FT spectrometer equipped with a split-ring resonator ER 4118 X-MS-3 and CF 935 cryostat was used. A three-pulse stimulated electron spin echo (ESE) $\pi/2 - \tau - \pi/2 - T - \pi/2 - \tau -$ echo was used. The duration of microwave pulses was 16 ns. The temperature was held near 80K.

ESEEM modulations were recorded and base line was corrected. To analyze the ESEEM amplitude, numerical Fourier transformation on modulation traces (Vn(T)) was performed.

$$F_c(f) = \int_{t_1}^{t_2} V_n(t)\exp(-2\pi i f t)dt$$

Results

The fig.1 shows ESEEM oscillations for different spin label positions for samples hydrated in D_2O and $H_2O/C_3D_5(OH)_3$ mixture

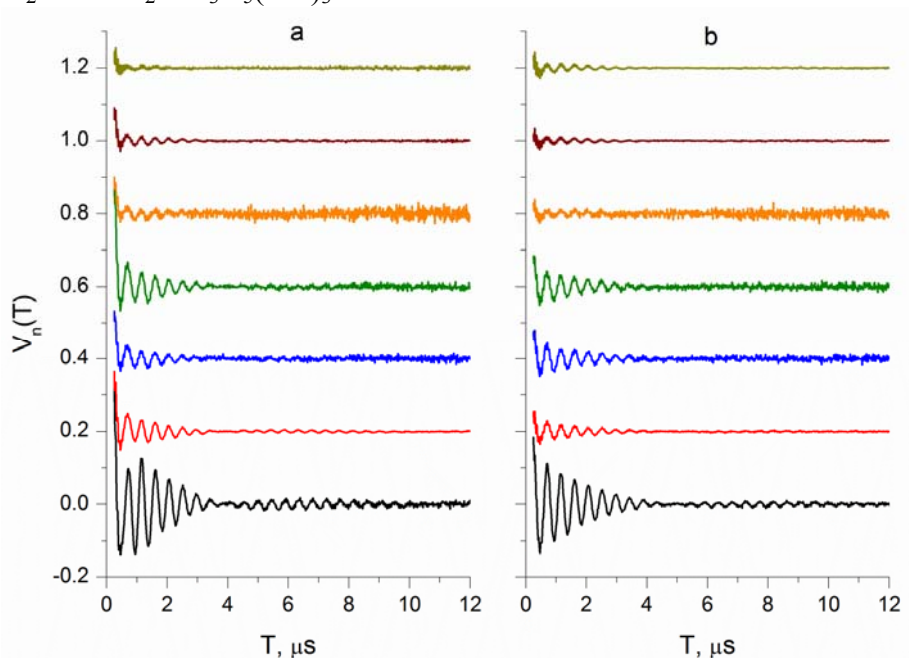

Fig.1. The baseline corrected ESEEM time traces for different n spin label positions, for n-PCSL/DPPC samples hydrated in D_2O (a) and in $H_2O/C_3D_5(OH)_3$ mixture. For convenience, the curves for n > 0 are consequently shifted upwards by a value of 0.2.

The fig.2 shows Fourier spectra of oscillations for different spin label positions for samples hydrated in D_2O and $H_2O/C_3D_5(OH)_3$ mixture. One can see a peaks at 2.2 MHz, these correspond to the resonance frequency of deuterons in the magnetic field of the X-band spectrometer. The peak is split into a doublet, which is assigned to the quadrupole interaction of the nuclear spin of nitrogen.

The peak amplitudes are depicted as a function of *n* in fig.3. The ESEEM amplitude is proportional to the local concentration of deuterium-substituted molecules, so fig.5 reflects the penetration profile of the molecules into membrane. Hydration by pure D_2O results in a very small ESEEM amplitude that is close to the noise level. In contrast, hydration by the $H_2O/C_3D_5(OH)_3$ mixture results in larger amplitude. Data in fig.3 present the averaged results. The error bars show scattering.

For the terminal 16th position the found ESEEM amplitude for the D_2O-hydrated sample is close to the expected zero value. Thus, one may suggest the effect of exclusion of the spin-labelled lipids from the bilayer.

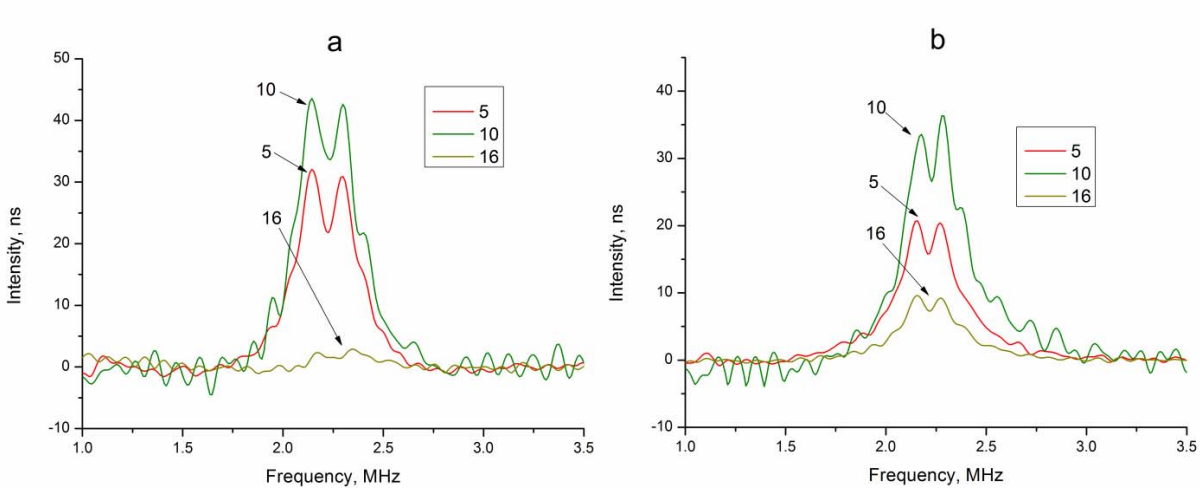

Fig.2. The amplitude Fourier spectra for the selected time traces in fig. 1 for D_2O (a) and for $H_2O/C_3D_5(OH)_3$ mixture (b).

Also data in fig.3 indicate on a local maximum at the 10th label position. This local maximum can be explained by considering results known from another techniques (NMR, molecular dynamics), which indicate that in DPPC lipid disorder increases after the 10th carbon position.

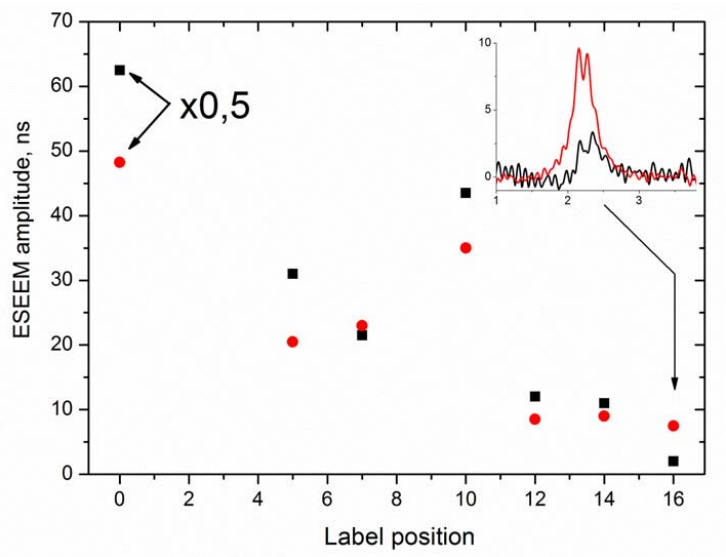

Fig.3. The ESEEM amplitudes for the case of hydration by D_2O (squares) and the case of hydration by $H_2O/C_3D_5(OH)_3$ mixture (circles), as a function of the label position n. The insert shows the amplitude Fourier transformation for the 16th label positions, for these both cases.

The obtained data in fig.3 for $H_2O/C_3D_5(OH)_3$ mixture correspond approximately to 3% v/v of the glycerol concentration in the middle of DPPC bilayer. Thus our data support a model in which small neutral solutes penetrate the membrane by partitioning into the hydrophobic phase of the bilayer.

References

[1] R.B. Gennis, Biomembranes (Springer, New York,1989).

[2] W.D. Stein and W.R. Lieb, Transport and Diffusion Across Cell Membranes (Academic, New York, 1986).

[3] A. Schweiger and G. Jeschke, Principles of Pulsed ElectronParamagnetic Resonance (Oxford University Press, Oxford,2001).

[4] K.B. Konov, N.P.Isaev and S.A. Dzuba, Molecular Physics, 2013

Attempt to detect charge density waves in $YBa_2Cu_3O_{6.5}$ using copper NQR

A.A. Gabitov, A.V. Dooglav

Kazan Federal University, 420008, Kremlevskaya 18, Kazan, Russia.

e-mail: arthurgabitov@gmail.com

Recently, charge density waves (CDW) and the evidence of charge ordering in $YBa_2Cu_3O_y$ (YBCO) and (Y:Nd)$Ba_2Cu_3O_y$ high-temperature superconductors were detected. The existence of ground states with competing order is central to many theories of HTS. A widely discussed example is “stripe order”. These two phenomena develop in a region inside the celebrated pseudogap phase. It is important to establish whether the tendency towards stripes is a generic property of the cuprates and whether the spin and charge correlations are always related. The aim of our research was the attempt to detect the charge ordering in $YBa_2Cu_3O_{6.5}$ by NQR of copper.

In fig.1 the ^{65}Cu copper NQR spectrum of the ^{65}Cu-enriched $YBa_2Cu_3O_{6.5}$ sample is presented. To identify the lines of copper NQR in different positions we used the results of works [1, 2], in which copper NQR spectra in superconducting $YBa_2Cu_3O_{6+x}$ with different content x of oxygen were presented.

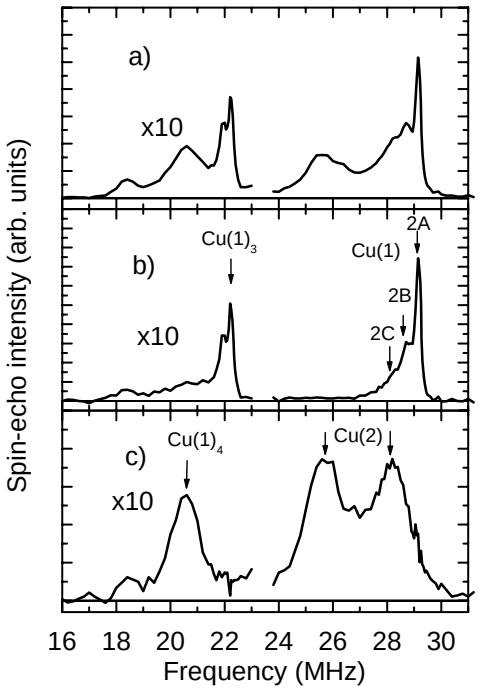

Fig.1. Copper NQR spectra for the ^{65}Cu-enriched $YBa_2Cu_3O_{6.5}$. (a) Nonsaturated spectrum taken with the 1 sec repetition time. (b) was obtained as the difference of spectrum (a) and of a scaled spectrum taken with short repetition time (20 ms). (c) was obtained as the difference of the spectrum with short repetition time (20 ms) and a scaled spectrum (a).

Measurements of copper NQR spectrum of the ^{65}Cu-enriched $YBa_2Cu_3O_{6.5}$ sample at the temperature 4.2K showed that the lines of planar copper Cu(2) are inhomogeneously broadened. This broadening is related to imperfect oxygen ordering in $Cu(1)O_{0.5}$ chains. Because of this the change of frequency or the width of NQR lines due to the emergence of CDW in the CuO_2 plane can’t be detected: according to the results of [3] the effect might be

small. During our experiments it was decided to trace the temperature dependence of the width of the narrowest and intensive NQR lines of chain copper Cu(1)2A, which are also, though to a lesser extent than the line of NQR plane copper, should “feel” the emergence of a CDW.

In fig.2 the ^{65}Cu copper NQR spectra of the ^{65}Cu-enriched $YBa_2Cu_3O_{6.5}$ sample measured at the 4.2K and 77 K are presented. The measurements were carried out in the frequency range 27.7 – 29.7 MHz. It is seen that the width of NQR line of Cu(1) is reduced at 77 K. According to [3], in the temperature range 4.2 – 77 K CDW do not arise. Reducing the width of the line in this temperature range, apparently, is related to the averaging influence of thermal movement on the inhomogeneity of the electric field gradient at the $Cu(1)_{2A}$ nuclei location.

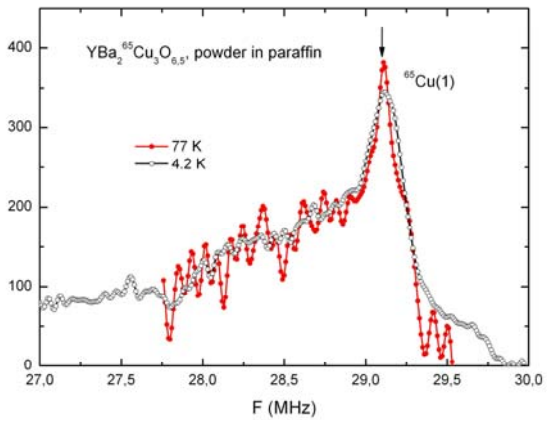

Fig.2. Part of NQR spectrum of the ^{65}Cu-enriched $YBa_2Cu_3O_{6.5}$ sample at 4.2 K and 77 K. With temperature increase from 4.2 K up to 77 K the width of NQR line of twofold-coordinated copper from an empty chain $Cu(1)_{2A}$ is reduced.

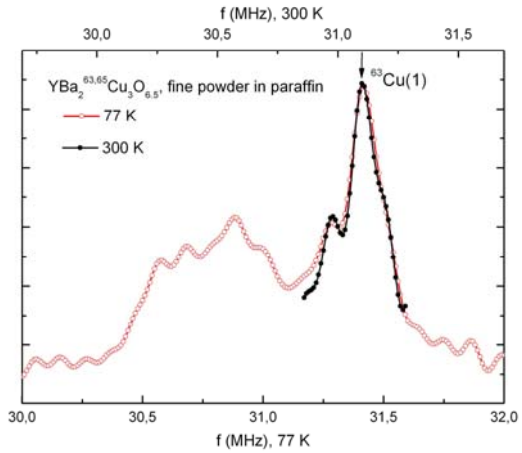

Fig.3. Part of NQR spectrum of the sample $YBa_2Cu_3O_{6.5}$ with natural content of copper isotopes at 77 K and 300 K. With temperature increase from 77 K up to 300 K the width of NQR lines of two-coordinated copper from an empty chain does not change.

Comparison of NQR spectra of chain copper at 77 K and 300 K was made in the sample $YBa_2Cu_3O_{6.5}$ with natural content of copper isotopes. NQR lines in this specific sample were unprecedently narrow. These spectra are presented on fig.3. As can be seen, even in this sample the line at 300 K is not narrower than at 77 K. So, it turned out impossible to detect the CDW regime onset using copper NQR in $YBa_2Cu_3O_{6.5}$ compound.

References

[1] Heinmaa I., et. al. Appl. Magn. Res., 3, 689 (1992).

[2] Yasuoka H., et. al. Phase transitions., 15, 183 (1989).

[3] Wu T., et. al. Nature (London)., 477, 191 (2011).

ODMR study of NV centers in HPHT diamond

B. Yavkin[1], E. Goovaerts[2], S. Orlinskii[1], I. Vlasov[3]

[1]Kazan Federal University, Kremlyovskaya Street 18, 420008 Kazan, Russia

[2]ECM, University of Antwerp, Universiteitsplein 1, 2610 Antwerp, Belgium

[3]General Physics Institute, Vavilov Street 38, 119991 Moscow, Russia

e-mail: boris.yavkin@gmail.com

NV center in diamond is a complex of substitutional nitrogen atom and nearest lattice vacancy. In the bulk diamond this complex is stable in two charge states NV^- and NV^0, with electron spin $S = 1$ and 1/2 correspondingly. Both configurations have quite intense optical transitions in the visible range, with zero-phonon lines at 637 nm and 575 nm, usually pumped with green laser light of 514 – 532 nm wavelength [1].

NV centers, especially NV^-, although have been researched for a few decades, still attract a lot of attention in scientific community for potential realization of qubits and quantum memory storages using these centers [2], for their local magnetometry [3] and thermometry [4] applications, and for their biological applications as optical biomarkers [5].

This interest arouses from the coupled magnetic and optical transitions, which is manifested in spin-dependent fluorescence, producing preferential population of one of the ground spin sublevels [3]. This non-Boltzmann spin population could be detected using EPR, fluorescence measurements or by ODMR.

In this report the results of ODMR experiments are presented. They performed in two microwave ranges (2.8 GHz and 95 GHz), and at two temperatures of 77 K and 300 K. The results of ODMR experiments are compared with each other and with conventional HF EPR measurements, and technical details of ODMR spectrometers realizations are discussed.

References

[1] P.G. Baranov *et al*. Enormously High Concentrations of Fluorescent Nitrogen-Vacancy Centers Fabricated by Sintering of Detonation Nanodiamonds. Small **7**, 11, 1533-1537 (2011).

[2] J. Wrachtrup *et al*. Quantum computation using the 13C nuclear spins near the single NV defect center in diamond. Optics and Spectroscopy, **91**, 3, 429-437 (2001).

[3] G. Balasubramanian *et al*. Nanoscale imaging magnetometry with diamond spins under ambient conditions. Nature **455**, 648-651 (2008).

[4] G. Kusko *et al*. Nanometer scale quantum thermometry in a living cell. arXiv:1304.1068

[5] C.C. Fu *et al*. Characterization and application of single fluorescent nanodiamonds as cellular biomarkers. PNAS, **104**, 3, 727-732 (2007).

Time-resolved and pulse EPR study of photo-induced spin polarization of zinc porphyrin trimer and zinc porphyrin-copper ion dimmer

A.A. Sukhanov[1], K.B. Konov[1], V.K. Voronkova[1], E.A. Mikhalitsyna[2], V.S Tyurin[2]

[1]Zavoisky Physical -Technical Institute RAS, 420029, Sibirsky tract 10/7, Kazan, Russia

[2]A.N. Frumkin Institute of Physical chemistry and Electrochemistry RAS, 199071, Leninsky prospect 31, Moscow, Russia

e-mail: ansukhanov@mail.ru

Porphyrins and their derivatives have a unique ability to bind a wide variety of metals and paramagnetic ligands and to provide a wide range of redox photophysics and photochemistry. Due to this combination of properties the porphyrin complexes are interesting in many fields of research including the conservation of solar energy and electron transfer processes [1]. Special attention is attracted to the formation of nanoscale porphyrin assemblies. The study of photo-induced spin polarization of system containing of porphyrins and their derivatives is aimed at creation of new materials spin and magnetic properties can be controlled by the light [2].

Time-resolved electron paramagnetic resonance (TREPR) is a powerful tool to study the spin- involved processes initiated by the light irradiation. Most of the TREPR experiments were carried out on the diamagnetic molecules which generate the excited singlet states after the laser flash. The following intersystem crossing populates the relatively long-lived triplet states of the molecules the EPR spectra of which are observed in the experiment. The photo-induced processes are non-adiabatic and the spin states are strongly polarized. The spin polarization mechanisms of such systems are well-established.

Recently, the study of the polarization states arising from the interaction of such systems with other paramagnetic centers has become intense. These systems consist of one or more unpaired electrons in the ground state, which affect the photophysical properties of the excited states of the porphyrins.

In this report we present results of the CW, TR and pulse EPR investigations two systems (fig.1 and fig.2).

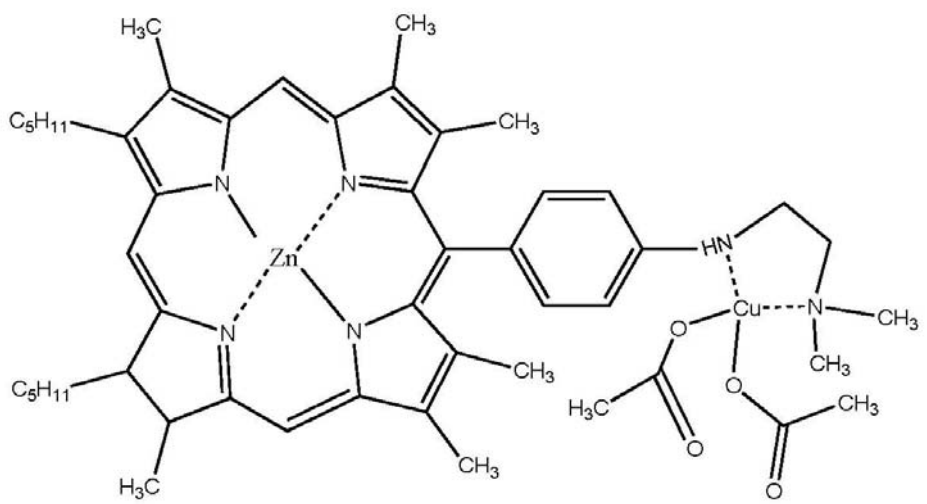

Fig.1. Chemical structure of zinc porphyrin - copper ion dimer (system I).

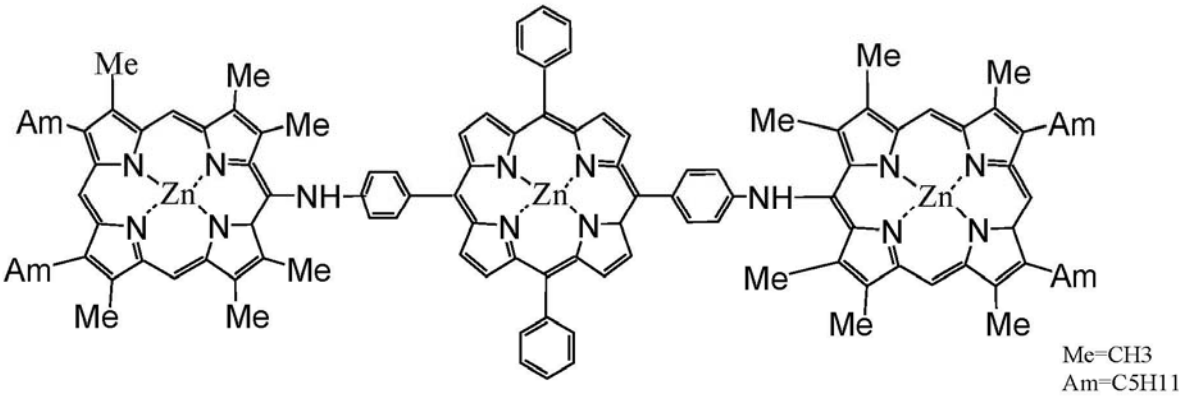

Fig.2. Chemical structure of zinc porphyrin trimer (system II).

The triplet state of the monomeric zinc porphyrin is well studied by TR EPR, and the characteristic values of zero-field splitting parameters of the monomeric zinc porphyrin are known [3, 4]. The shape of the TR EPR spectra of I (fig.3) and II (fig.4) is different from the characteristic shape of the spectrum for monomeric zinc porphyrin. The application of pulsed EPR spectroscopy allows us to obtain additional information about the studied system, which simplifies the analysis of the data.

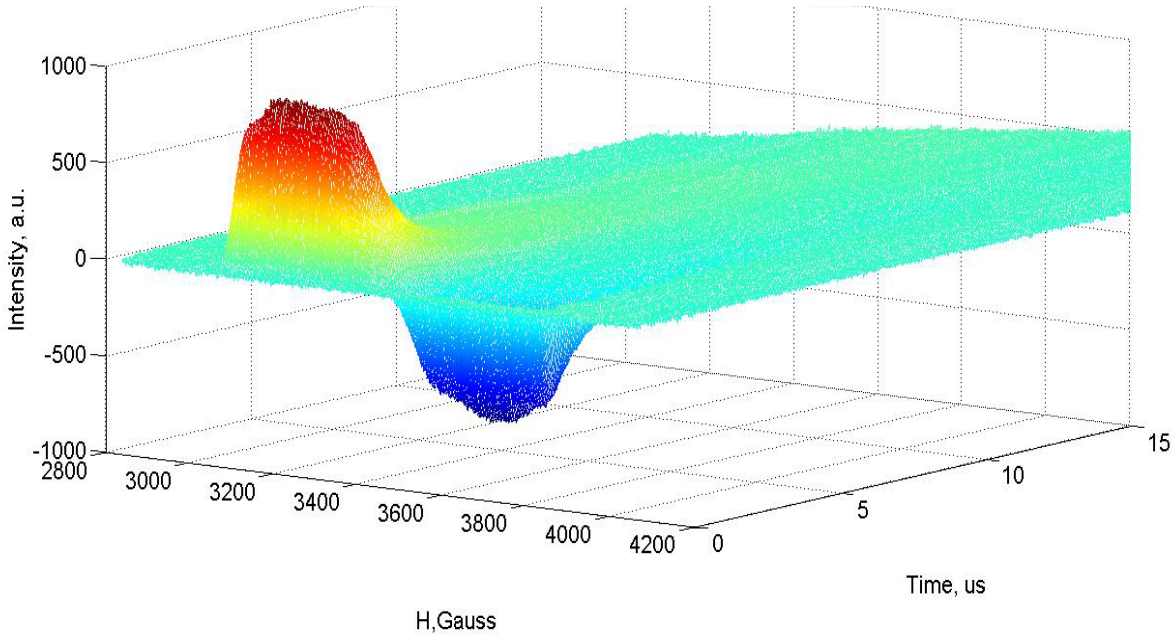

Fig.3. TR EPR spectrum of system I at 40 K in X-band.

For I, it was shown that there is a partially transfer of spin polarization from the triplet state of zinc porphyrin to the doublet state of the copper ion. It was found that the observed spectrum of II is the sum of two spectra from two slightly different zinc porphyrin complexes. Zero-field splitting parameters for each zinc porphyrin included in the system II were determined from the analysis of EPR spectra. Simulation of the EPR spectra was performed using Matlab toolbox 'EasySpin' [5].

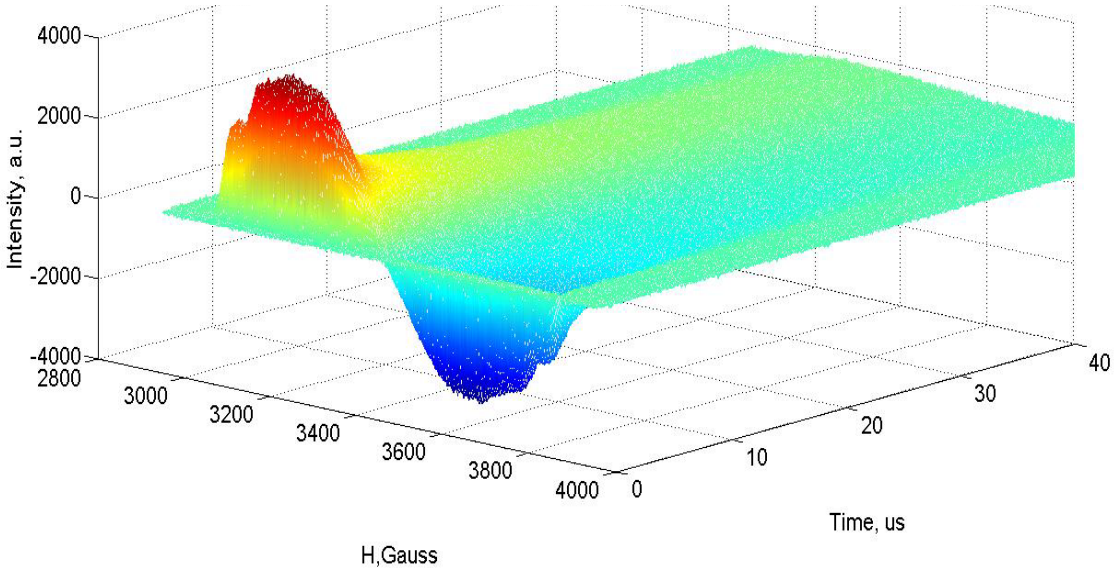

Fig.4. TR EPR spectrum of system II at 30 K in X-band.

This work was supported by the Grant of the President RF (MK-6407.2012.2) and by the Russian Foundation for Basic Research (project no. 12-03-97078-p).

References

[1] J. Porphyrins Phthalocyanines, 2010, 14, 759–792

[2] J. Am. Chem. Soc., 2011, 133, 9364–9369

[3] J. Phys. Chem. B., 2010, 114,14559-14563; Appl. Magn. Reson., 2003, 25, 157-198

[4] J. Chem. Phys., 1975, 62, 169-176; Synthetic Metals, 2001 116, 247-253

[5] J. Magn. Reson., 2006, 178, 42-55.

High-frequency EPR/ENDOR study of charge-compensated Fe^{3+} centers in ZnO single crystals

Yu.S. Kutin, G.V. Mamin, S.B. Orlinskii

Kazan Federal University, 420008, Kremlyovskaya St.18, Kazan, Russia.

e-mail: yuri_kutin@mail.com

Theoretical prediction of a high Curie temperature in ZnO doped with Mn, Fe, and other transition metals has stimulated the investigation of these materials by many research groups. In ZnO crystals containing Fe, EPR experiments reveal the spectrum of the trigonal Fe^{3+}_{Zn} center [1], as well as multiple additional signals assigned to charge-compensated Fe^{3+} [2, 3]. Although the charge-compensated Fe^{3+} centers have been known for decades, conclusions on the chemical nature of these defects are still contradictory. Originally, these centers were treated as Fe^{3+}-Li^{+} complexes with both ions occupying adjacent cationic position [2]. Recently, however, the centers were interpreted as a substitutional Fe^{3+} ion with a vacancy at an adjacent zinc or oxygen site (Fe-V_{Zn} or Fe-V_O) [3]. In order to conclusively determine the chemical nature of these complexes, electron-nuclear double resonance (ENDOR) spectroscopy was used in the present work [4].

Fig.1 (left) shows the EPR spectrum of a hydrothermally grown ZnO crystal for $B \parallel c$. Spectra of the Mn^{2+} (d^5, ^{55}Mn, $I = 5/2$, abundance 100%) and Fe^{3+} (d^5, ^{54,56,58}Fe, $I = 0$, abundance 97.9%) ions at substitutional sites are easily recognized and correspond to known spin Hamiltonian parameters. The remaining fifteen EPR lines are grouped into three fine-structure quintets originating from three types of the charge-compensated Fe^{3+} centers with the electron spin $S = 5/2$. These complexes are labeled C1, C2, and C3; with C1 showing the smallest fine-structure splitting and C3 showing the largest. The hyperfine structure is not resolved in these spectra. Therefore, the chemical nature of the charge compensator cannot be established by EPR.

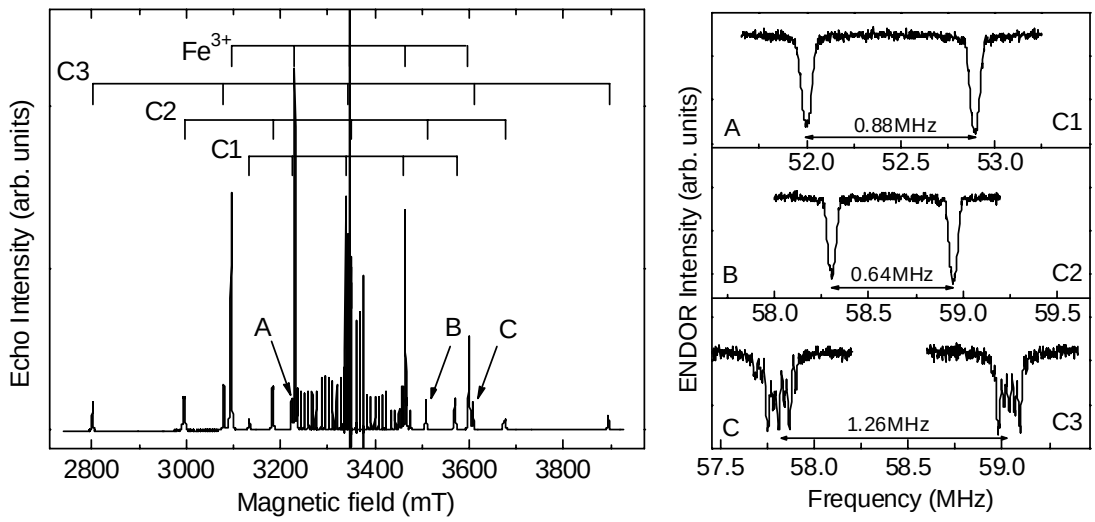

Fig.1. (left) EPR spectrum of a ZnO single crystal for B || *c*. $T = 20$ K, $f \sim 93.9$ GHz. The 30 lines near g ~ 2 originate from Mn^{2+} and the five high-intensity lines correspond to Fe^{3+}. Three fine-structure quintets originating from the charge-compensated Fe^{3+} centers are indicated. (right) ENDOR transitions of the ^{7}Li nuclei recorded in the indicated 1/2 ↔ 3/2 EPR transitions of the three charge-compensated Fe^{3+} centers.

Fig.1 (right) shows ENDOR spectra recorded in the $M_S = 1/2 \leftrightarrow M_S = 3/2$ EPR transitions of the three Fe-related centers (the corresponding EPR lines are indicated by arrows). The ENDOR spectra of C1 and C2 consist of two signals with a fixed spacing of about 0.88 MHz and 0.64 MHz, respectively. For C3 the spacing is about 1.26 MHz, and the ENDOR lines are further split into quadrupole triplets, which implies that the nuclear spin is $I = 3/2$. The appearance of multiple lines can be explained by the fact that the magnetic field deviates slightly from the $B \parallel c$ direction. Therefore, EPR lines from magnetically inequivalent positions do not entirely coincide, and each EPR signal produces its own pair of quadrupole triplets.

The EPR and ENDOR data for $B \parallel c$ were analyzed for the spin system $S = 5/2$, $I = 3/2$ using the following Hamiltonian:

$$\hat{H} = \sum B_k^m O_k^m + g\mu B S_Z - g_N \mu_N B I_Z + A_{ZZ} S_Z I_Z + F\left[I_Z^2 - \frac{1}{3} I\left(I+1\right)\right], \qquad (1)$$

where all terms have their usual meanings. The nuclear Larmor frequency can be written as $f_L = g_N \mu_N B/h$.

Since the hyperfine structure is not resolved in EPR, all four allowed electronic transitions are exited in the Mims ENDOR experiments simultaneously. Thus, all six allowed nuclear transitions should occur in the ENDOR spectrum. For instance, the resulting ENDOR spectrum recorded in the $M_S = 1/2 \leftrightarrow M_S = 3/2$ EPR transition should consist of two triplets at the frequencies $\nu = f_L - 3A/2$ and $\nu = f_L - A/2$, with the quadrupole splitting of $2F$. The triplets are placed symmetrically around the frequency $f_L - A$, and the spacing between the triplets is equal to the hyperfine interaction constant A. The nuclear g-factor can then be determined from the Larmor frequency.

ENDOR spectra recorded in all fifteen EPR lines of the charge-compensated Fe^{3+} centers reveal nuclear transitions corresponding to a nucleus with g-factor $g_N = 2.171$ and spin $I = 3/2$. This unambiguously shows presence of Li as a charge compensator. Therefore, the model involving Zn and O vacancies can be rejected.

Depending on the relative positions of the two impurity ions in the hexagonal lattice of ZnO, three kinds of $Fe^{3+} - Li^{+}$ complexes are formed. As seen in fig.1 (right), the hyperfine and quadrupole interactions strongly depend on the particular arrangement of the complex. The hyperfine interaction constant is positive for C1 and C3, and negative for C2. The quadrupole splitting is only resolved for C3. The electric field gradients at the ^{7}Li nuclei were estimated to be at least 5 times lower than at undistorted Zn sites.

Acknowledgements

The experiments were carried out at the Federal Center of Shared Facilities of Kazan Federal University. The authors would like to thank Prof. Pavel Baranov for providing samples and stimulating discussion.

References

[1] W.M. Walsh, Jr., L.W. Rupp, Jr., Phys. Rev., 126, 952-955 (1962).

[2] W.C. Holton, M. de Wit, T.L. Estle, et al., Phys. Rev. 169, 359 (1968)

[3] D.V. Azamat, M. Fanciulli, Physica B, 401–402, 382 (2007)

[4] Yu.S. Kutin, G.V. Mamin, S.B. Orlinskii, Identification of Fe^{3+}-Li^{+} complexes in ZnO by means of high-frequency EPR/ENDOR spectroscopy, J. Magn. Res., in press, DOI: 10.1016/j.jmr.2013.09.014.

ESR in the laves phase alloy $YbNi_2$

E.M. Gataullin[1], V.A. Ivanshin[1], A.A. Sukhanov[2], D.P. Rojas[3], L. Fernández Barquín[4]

[1]MRS Laboratory, Institute of Physics, Kazan Federal (Volga Region) University, Kremlevskaya str. 18, 420008 Kazan, Russia

[2]Zavoisky Physical-Technical Institute, Sibirsky trakt 10/7, 420029 Kazan, Russia

[3]Departamento de Física e Instalaciones-ETSAM, Universidad Politécnica de Madrid, Av. Juan Herrera, 4, Madrid 28040, Spain

[4]DCITIMAC, Facultad de Ciencias, Universidad de Cantabria, Av. de los Castros s/n, Santander 39005, Spain

e-mail: edikgat@gmail.com

Introduction

The magnetic properties of Yb-based heavy-fermion (HF) metals are sensitive to the degree of hybridization between the 4f electrons (holes) and the conduction 3d electrons through the Kondo effect and the Ruderman–Kittel–Kasuya–Yoshida (RKKY) exchange interaction. Their study have become the focus of considerable interest in recent years, boosted by the use metallic-flux techniques for growing single crystals of high quality [1, 2]. Alternatively the field is also developed by the preparation of new alloys promoting attractive electronic states. Precisely, the recently prepared $YbNi_2$ Laves phase alloy is a good example of enhanced ferromagnetism and HF behavior among Yb compounds [3].

The electron spin resonance (ESR) technique probes directly the local moments of f electrons and their interaction with conduction electrons (CE). The well-defined ESR signals have been found out in some dense Yb-based intermetallic systems, such as mixed-valence compound YbCuAl [4] or quantum critical (QC) materials $YbRh_2Si_2$, $YbIr_2Si_2$, and $YbAlB_4$ [5-7]. Different theoretical predictions [8-11] propose that the narrow anisotropic ESR can be really observed in the undoped HF intermetallics with ferromagnetic (FM) correlations in a broad range of magnetic fields as a result of hybridization between 4f and CE. In this case, the FM fluctuations strongly reduce the width of ESR line and make it observable. In the present work, we report the data of magnetic, thermodynamic, and ESR measurements in the binary $YbNi_2$ studying the role of the crystalline electric field (CEF) excitations on the magnetic behaviour of the alloy.

Experimental Techniques

The specific heat and DC-magnetization were collected with a Quantum Design PPMS multipurpose instrument on the polycrystalline pellets of $YbNi_2$ obtained by arc melting [3]. ESR measurements were performed with a Bruker ESM/plus spectrometer (frequency ~9.45 GHz) coupled to a helium-gas-flux temperature controller system at $4.2 < T < 300$ K in magnetic fields (H) up to 1.4 T.

Results and Discussion

Fig.1 presents the temperature dependence of the specific heat (c) at $H = 0$ and 10 kOe. The lambda-type anomaly is observed at the main contribution stemming from the FM ordering at $T_C = 10.5$ K, as previously reported [3]. One can see also, that the peak associated to the magnetic transition broadens and shifts to higher temperatures when the magnetic field increases, consistent with a FM order [13].

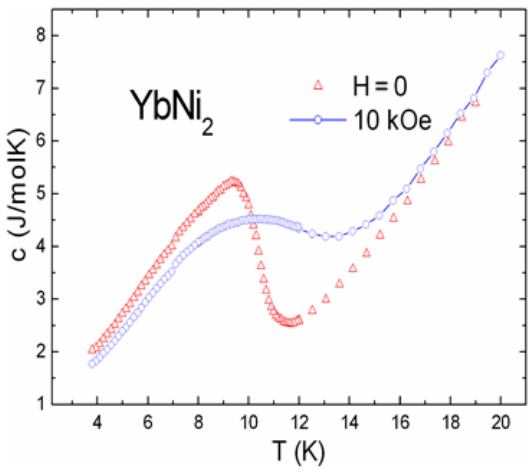

Fig.1. Temperature dependence of specific heat at $H = 0$ and $H = 10$ kOe. The maximum for $H = 0$ broadens and shifts to higher temperatures when increasing the magnetic field.

The magnetic contributions to the specific heat (c_{mag}) and the magnetic entropy (S_{mag}) can be calculated using the procedure described elsewhere [3], and the results for S_{mag} are depicted in fig.2. It is seen that the value expected for the doublet magnetic ground state is reached around the magnetic transition (at $H = 0$). However, at $H = 10$ kOe, the value is only recovered at 18 ÷ 20 K. This last feature is consistent with a FM order. Under magnetic field, the variation in the magnetic entropy $\Delta S_{mag} = \left[S_{mag}(H,T) - S_{mag}(0,T) \right]$ reaches a maximum of 1.02 J/molK near the magnetic transition, as shown in fig.3, a lower value respect to that reported for other strongly correlated materials with a first order FM transition [13].

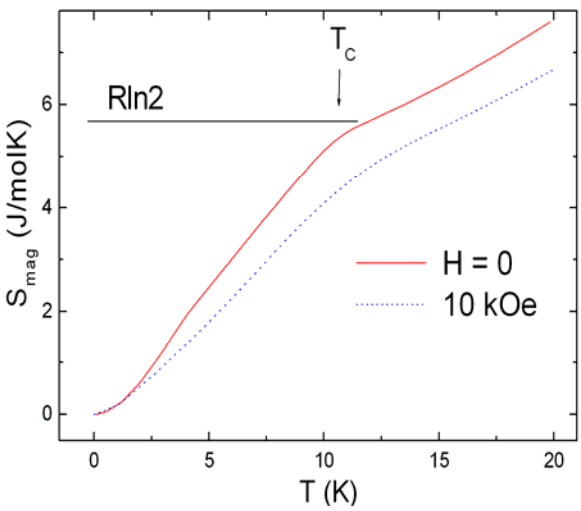

Fig. 2. Temperature dependence of the magnetic contributions to the magnetic entropy, S_{mag}.

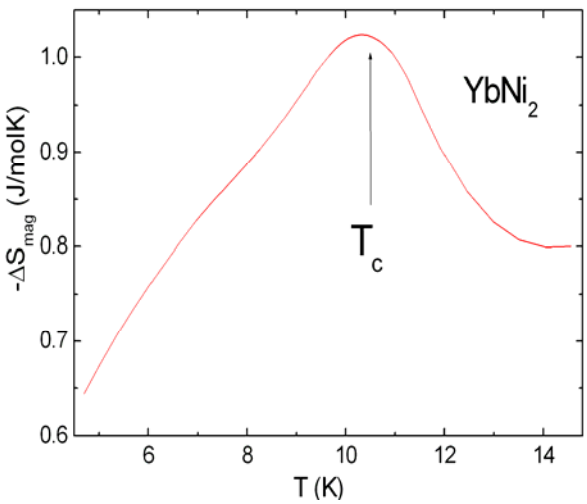

Fig. 3 Magnetic entropy change of $YbNi_2$ as a function of temperature at 10 kOe. A maximum value of the. magnetocaloric effect is obtained near $T_C = 10.5$ K.

Fig.4 shows ESR spectra at selected temperatures. In the vicinity of $T_C = 10.5$ K, the ESR parameters (linewidth and g-factor) show distinct anomalies, which can be associated with a presence of strong magnetic fluctuations at an onset of FM ordering. Below 10 K, the ESR line shape was essentially distorted. The ESR spectra demonstrate a single asymmetrical line of Dysonian shape at $T > 11$ K, typical of conducting materials due to skin effect, similar to another FM HF metals exhibiting ESR [4-7]. The ESR peak-to-peak linewidth ΔH increases exponentially at $T > 15$ K. Above 20 K, the ESR signal is too weak and too broad to be detected.

The temperature dependence of ΔH in $YbNi_2$ (fig.5) in the paramagnetic (PM) phase can be well fitted by the expression [5]

$$\Delta H = A + BT + C \exp\left(-\frac{\Delta}{T} \right), \qquad (1)$$

where the residual ESR linewidth $A \approx 166.27$ Oe, the measured Korringa rate $B \approx 27$ Oe/K which corresponds to a local-moment relaxation toward CE was within the usual order of magnitude of Yb^{3+}, and the fitting parameter $C \approx 56.3$ kOe. The value of activation energy

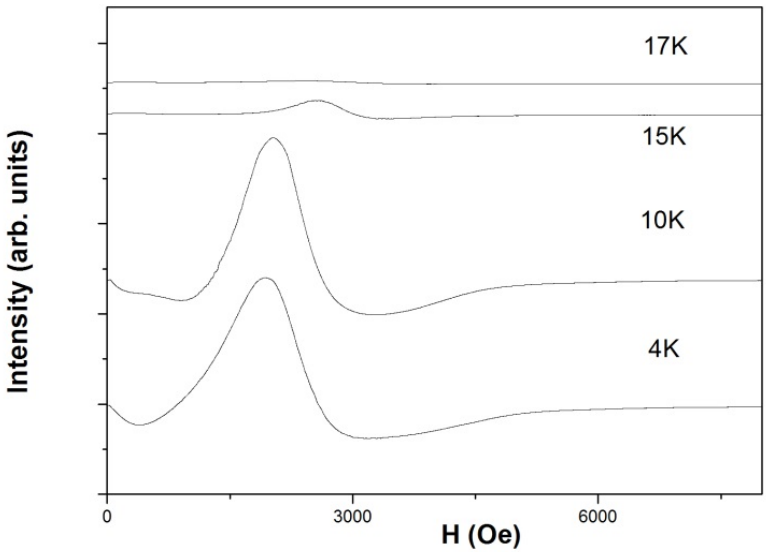

Fig.4. Temperature evolution of the ESR spectra.

$\Delta \approx 75$ K correlates very well with the estimations of the first excited CEF level of the Yb^{3+} ion $\Delta_1 \approx 72$ K [3] or $\Delta_1 \approx 78$ K [14] which have been derived in $YbNi_2$ after thermal and magnetic measurements and Mössbauer studies, correspondingly. The CEF level scheme obtained from these experiments represents Γ_6 ground state doublet, Γ_8 first excited quartet, and Γ_7 further excited doublet. The Γ_6 symmetry of the ground doublet is also confirmed by the mean value of the ESR *g*-factor which is slightly changing between 2.4 and 2.6 in the PM phase as it was predicted by Low and Rubins for the theoretical value $g_{\Gamma 6} = 2.667$ of the Yb^{3+} ion in the cubic CEF [15]. The deviation of the experimental ESR g-factor from the calculated one was attributed to an existence of partially covalent bonding among ytterbium ions.

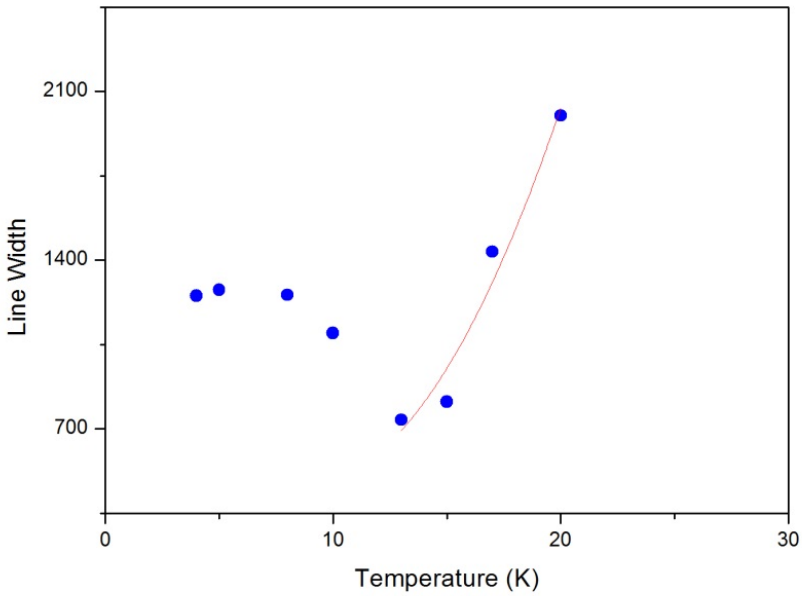

Fig.5. Temperature dependence of the ESR linewidth ΔH. Solid line describes the high-temperature data in PM phase by equation (1) with the fitting parameters given in the main text.

Therefore, the spin dynamics of $YbNi_2$ in PM regime at $T > 11$ K can be related to the Orbach-Aminov spin-lattice relaxation process via first excited state of the Yb^{3+} ion in accordance to the findings in $YbRh_2Si_2$ and $YbIr_2Si_2$ [5, 6]. Moreover, our observations strongly confirm that FM fluctuations or static FM order are a necessary precondition for the observation of pronounced ESR in a variety of dense intermetallic compounds [16, 17].

Conclusions

In summary, we have observed the low temperature ESR signals in the binary alloy $YbNi_2$. Our results are consistent with a HF-FM behavior at $T_C = 10.5$ K. Data of ESR measurements confirmed the ground state of the Yb^{3+} ion as Γ_6 state. Spin-lattice relaxation processes involving the first excited CEF level of Yb^{3+} at $\Delta \approx 75$ K dominate the electron spin dynamics of $YbNi_2$ in the PM phase.

References

[1] C. Klingner, C. Krellner, M. Brando, C. Geibel, and F. Steglich: New J. Phys. 13 (2011) 083024.

[2] M.C. Aronson, M.S. Kim, M.C. Bennett, Y. Janssen, D.A. Sokolov, and L. Wu: J. Low Temp. Phys. 161 (2010) 98.

[3] D. P. Rojas, L. Fernández Barquín, C. Echevarria-Bonet, and J. Rodríguez Fernández: Solid State Commun. 152 (2012) 1834.

[4] C. Tien, J.-T. Yu, and H.-M. Du: Jpn. J. Appl. Phys. 32 (1993) 2658.

[5] J. Sichelschmidt, V.A. Ivanshin, J. Ferstl, C. Geibel, and F. Steglich: Phys. Rev. Lett. 91 (2003) 156401.

[6] J. Sichelschmidt, J. Wykhoff, H.-A. Krug von Nidda, I.I. Fazlishanov, Z. Hossain, C. Krellner, C. Geibel, and F. Steglich: J. Phys.: Cond. Matt. 19 (2007) 016211.

[7] L. M. Holanda, J. M. Vargas, W. Iwamoto, C. Rettori, S. Nakatsuji, K. Kuga, Z. Fisk, S. B. Oseroff, and P. G. Pagliuso: Phys. Rev. Lett. 107 (2011) 026402.

[8] E. Abrahams and P. Wölfle: Ann. Phys. (Berlin) 523 (2011) 591.

[9] D. Huber: Mod. Phys. Lett. B 29 (2012) 1230021.

[10] P. Schlottmann: J. Appl. Phys. 113 (2013) 175E109.

[11] A. Ramires and P. Coleman: arXiv cond-mat/1307.4109v1.

[12] D. P. Rojas, J. Rodríguez Fernández, J. I .Espeso, J.C. Gómez Sal: Physica B 404 (2009) 2938.

[13] D. P. Rojas, J. I. Espeso, J. Rodríguez Fernández and J. C. Gómez Sal: Phys. Rev B 80 (2009) 184413.

[14] I. Nowik and B.D. Dunlap: J. Phys. Chem. Solids 34 (1973) 465.

[15] W. Low and R.S. Rubins: Phys. Rev. 131 (1963) 2527.

[16] C. Krellner, T. Förster, H. Jeevan, C. Geibel, and J. Sichelschmidt Phys. Rev. Lett. 100 (2008) 066401.

[17] H. Jang, G. Friemel, J. Ollivier, A.V. Dukhnenko, N. Yu. Shitsevalova, V. B. Filipov, B. Keimer, and D.S. Inosov: arXiv cond-mat/1308.4491v1.

Application of EPR for controlling wood properties during processing

E.I. Kondratyeva, K.R. Safiullin, I.G. Motygullin

Kazan Federal University, 420008, Kremlevskaya 18, Kazan, Russia

e-mail: katarina.kondratyeva@gmail.com

Vacuum-drying and heat treatment of wood are the most promising methods of treatment of wood. These treatments can significantly improve the properties of the wood such as durability, strength, thermal conductivity, water penetration into the product.

EPR and NMR spectroscopy can determine some of the properties of wood. In this article we consider the preliminary EPR experiments, namely, the effect of moisture content of wood on the properties of the EPR signal of wood samples.

In this work a number of the oak wood samples with various moisture content (MC) were investigated. All samples had a shape of a cylinder with the diameter d = 5 mm and the height h = 45 mm. The samples were kept at the atmosphere of vapors above saturated salt solutions. The moisture content (MC) values for all samples were measured before the experiments by the special Hydro Easy Control device. This device is based on the dielcometric method of measuring of the moisture content of wood. The measured values for all samples are presented in table 1.

Table 1.

Sample	MC, %	Weight, g
1	6.7	0.65
2	9.7	0.68
3	12.5	0.7
4	16.4	0.55

In the present work the samples were studied by the electron paramagnetic resonance (EPR) method. EPR experiments were carried on the Varian E–12 X-band 9.3 GHz spectrometer.

The sample of MgO with Mn^{2+} with a known amount of spins $N = 5 \cdot 10^{14}$ were used as a reference sample. The displacement of the samples in the resonator was well controlled to achieve similar positions throughout the series of experiments.

A typical EPR spectrum in our experiments is shown on fig.1. The observed spectrum consists of seven lines, six of them are narrow equidistant lines that correspond to the Mn^{2+} ion in MgO. The central broad line corresponds to the signal of free radicals in the wood on the g-factor g = 2,002.

The spectra were obtained for all samples with different moisture contents. The amplitudes of the signals were normalized using a reference sample. It appeared that the line widths are close to 6 G and do not depend on the moisture content values. However, a strong moisture content dependence of the amplitude of the signal of free radicals in the wood was observed (fig.2).

Various research groups explored wood properties using EPR methods and it is known that an amplitude of the EPR signal of free radicals in wood and pulp samples strongly depend on the sample properties. Dependence of the signal amplitude of free radicals on a microwave power during the experiment, on a wood processing temperature [1], on a

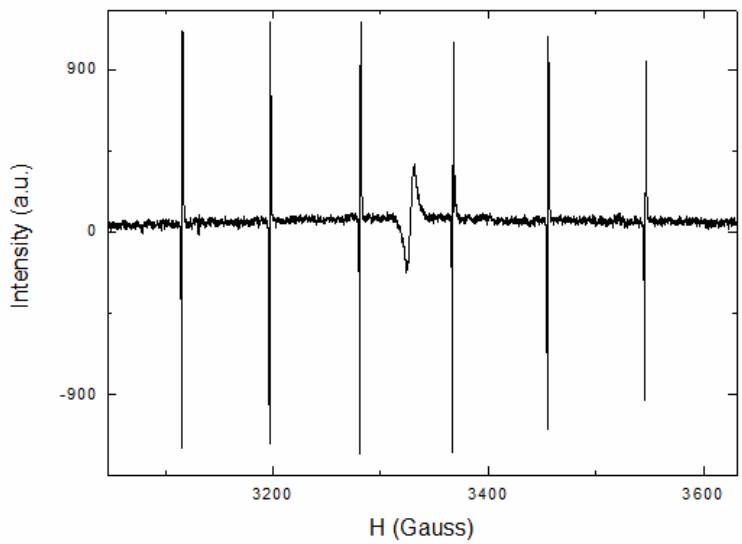

Fig.1. The EPR spectrum of the sample 1 with 6.7% moisture content and the reference sample. Six equidistant narrow lines correspond to Mn^{2+} ion in MgO and the central broad line corresponds to the signal of free radicals in the wood.

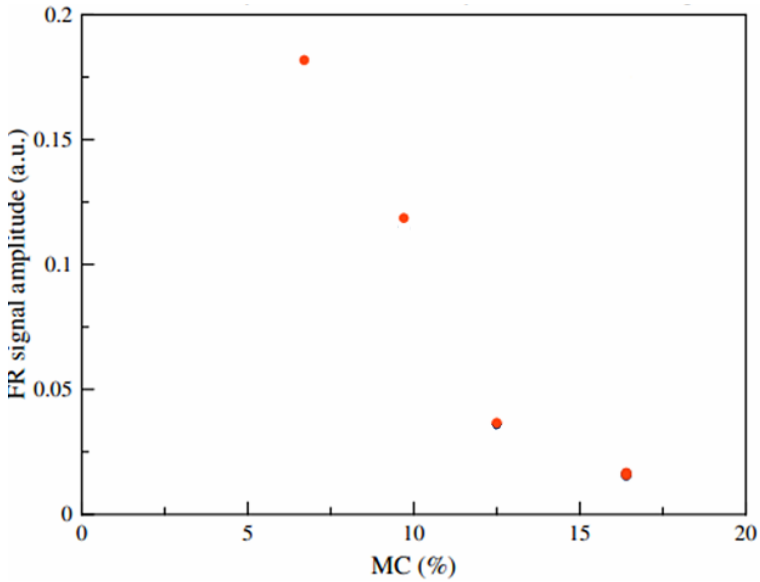

Fig.2. Dependence of free radicals signal amplitude on moisture content of samples.

moisture content of samples were obtained [2, 3]. It was reported in [2] that relative intensity values of the EPR signals in the range of 5-7% is low and rises as the moisture content increases. Completely different dependence was observed in [3]: amplitudes of the EPR signal decay if the moisture content increase. Similar results were obtained in the present work. However the convincing explanation for this phenomenon is not provided.

To access the influence of the water properties on the signal's amplitude of free radicals in wood the following measurements were performed. The measurements were performed on two samples. The first sample was dry, the second one was soaked in ethanol during 4 hours. The signal of free radicals didn't change. The EPR spectrum of the sample 1 with a humidity of 6.7% and the spectrum of a sample 2 saturated with ethanol are shown on the fig.3. The spectra were shifted on the 50 G on each other on the fig.3 and amplitude of signal were normalized.

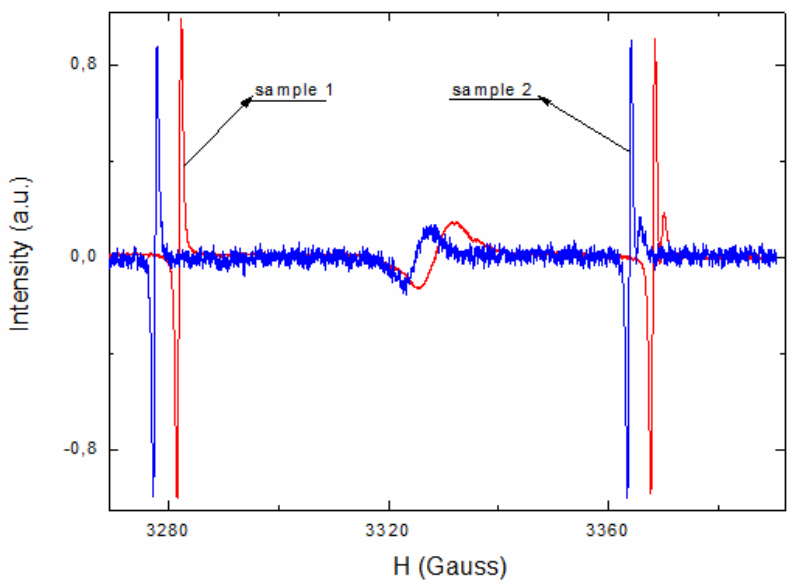

Fig.3. EPR spectrum of the sample 1 with a humidity of 6.7% (sample 1) and the spectrum of a sample 2 saturated with ethanol (sample 2).

Probably, the reducing of signal's amplitude with increasing of humidity associated with features of water molecules. The water molecules are polar and represent an electric dipoles. The molecules of water round the dangling bonds in the wood and, possibly, associated unpaired electrons.

References

[1] Hanne Sivonen et al, Magnetic resonance studies of thermally modified wood, Holzforschung, Vol.56, No.6 (2002)

[2] Nyok-sai Hon, Formation of free radicals in photoirradiated cellulose. II. Effect of moisture, Journal of polymer science: Polymer chemistry edition, Vol. 13, 955-959 (1975)

[3] Miha Humar et al, Influence of wood moisture content on the intensity of free radicals EPR signal, Holz als Roh- und Werkstoff 64: 515-516 (2006)

Long-lived free induction decay signal in $CsMnF_3$ single crystal

T.R. Safin[1], E.M. Alakshin[1], Yu.M. Bunkov[1,2], R.R. Gazizulin[1], A.M. Gazizulina[1], L.I. Isaenko[3], S.A. Zhurkov[3], A.V. Klochkov[1], K.R. Safiullin[1], M.S. Tagirov[1]

[1]Kazan Federal University, Kazan, Russia

[2]Institut Neel, CNRS et Universite Joseph Fourier, Grenoble, France

[3]V.S.Sobolev Institute of geology and mineralogy, Siberian Branch of Russian Academy of Sciences, Novosibirsk, Russia

e-mail: imfador@gmail.com

Introduction

The Bose-Einstein condensation (BEC) corresponds to the formation of a collective quantum state in which macroscopic number of particles is governed by a single wave function. The formation of this state was predicted by Einstein in 1925 [1].

The BEC of magnons was discovered experimentally in superfluid phase of ^{3}He-B [2]. It manifests itself by coherent precession of magnetization. Then 6 different states of superfluid ^{3}He with BEC formation were observed. The review of various experiments on the BEC observation can be found in [3, 4]. In all cases BEC forms by excited non-equilibrium magnons. To excite it the pulse or continuous pumping at nuclear magnetic resonance (NMR) frequency was used.

In [5] it was assumed by Yu.M.Bunkov that the BEC formation is also possible in solid antiferromagnets $CsMnF_3$ and $MnCO_3$ with coupled nuclear-electron precession. The predictions were successfully confirmed. It was found that the coupled nuclear-electron precession shows all properties of coherent spin precession and magnon BEC [6]. The main experimental fact of magnon BEC evidence was independence of the nuclear-electron magnetic resonance (NEMR) signal amplitude on applied RF power [7-9]. These experiments were done by means of continuous wave NMR and “switch-off” NMR. Two regimes of radiofrequency (RF) pumping was found. In the first regime the induction signal is observed after short (about 1 μs) resonant RF pulse. Let us call this pumped state as a normal. In this state spins precess with its local frequency due to the external magnetic field inhomogeneity. In the second regime the induction signal is observed after long (about hundreds of ms and longer) non-resonant RF pulse (so called “switch-off” NMR) and the signal amplitude is well described in framework of magnon BEC.

We report here the experimental investigations of the free induction decay (FID) signal behavior in both pumping regimes in two samples of easy-plain antiferromagnet $CsMnF_3$.

Results and discussion

The experiments were done at the temperature of 1.5 K. The first sample $CsMnF_3$ was grown by S.V.Petrov in the P.L. Kapitza Institute for physical problems RAS in 70th of XX century. The second investigated sample $CsMnF_3$ was grown by L.I. Isaenko and S.A. Zhurkov in the V.S. Sobolev Institute of geology and mineralogy SB RAS in 2012. X-ray investigations show that the second sample was more homogeneous.

The complete details of the experimental setup were published in [10]. We applied RF pulses (homogeneous on the scale of the sample) of different amplitudes and durations with frequencies, which were equal to or higher than the resonant NEMR frequency at given

external magnetic field, and observed FID signal. The typical FID signals in both RF pumping regimes in the first sample are shown in fig.1.

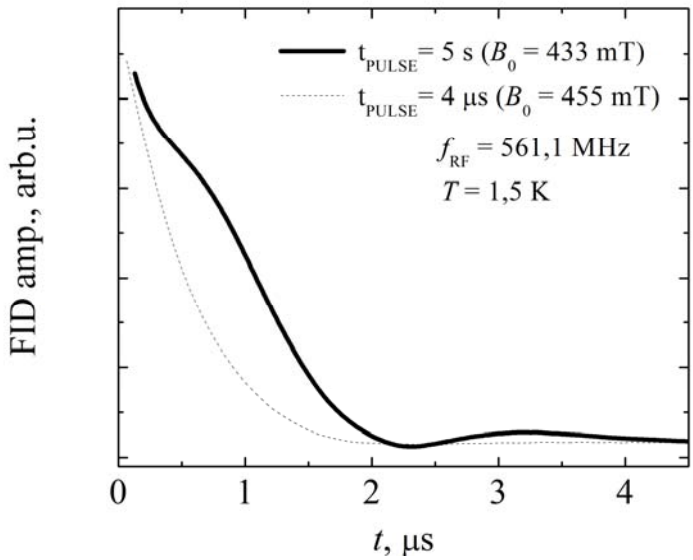

Fig.1. The FID signal $CsMnF_3$ amplitude in the first sample in two RF pumping regimes.

It can be seen that after the 5 s pulse the FID signal duration is about 2 times longer than in normal pumped state. It is khown from the experiments with ^{3}He-A [11] that the lifetime of magnon BEC state is more than order of magnitude longer than the lifetime of usual FID. Not so big difference between two exhibitions in our case of $CsMnF_3$ can probably be explained by low crystal quality. It well known [12] that the relaxation times of $CsMnF_3$ crystals can vary more than order of magnitude. It depends on the impurity type and features of crystal growth. That is why the next step in our investigations was search of new $CsMnF_3$ crystal with better homogeneity and longer relaxation times. The series of new crystals were grown by L.I. Isaenko and S.A. Zhurkov. The typical FID signals in both RF pumping regimes in the second sample are shown in fig.2.

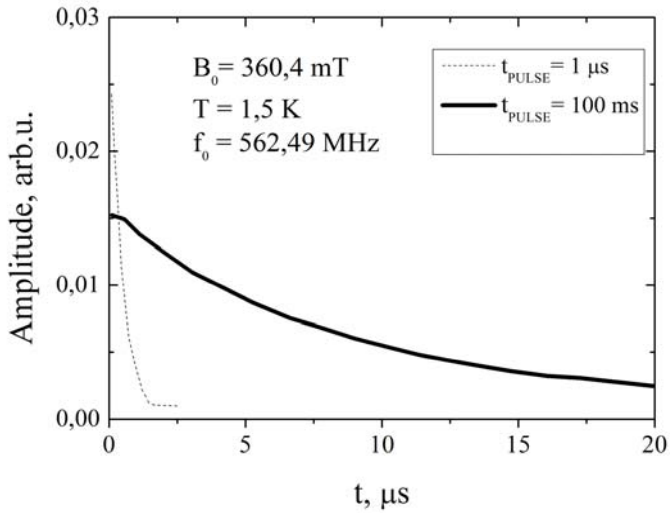

Fig.2. The FID signal $CsMnF_3$ amplitude in the second sample in two RF pumping regimes.

It is seen in the fig.2 that in both cases the FID time is well described by the exponential function. The FID time is about 0.5 μs in normal state and about 9.5 μs in magnon BEC state. The FID signal duration is more than an order of magnitude than in normal pumped state. In the second (more homogeneous) sample the signal duration increases more than order of magnitude at transition from one RF pumping regime to another. These results are in full agreement with observed in superfluid ^{3}He-A in aerogel (fig.3).

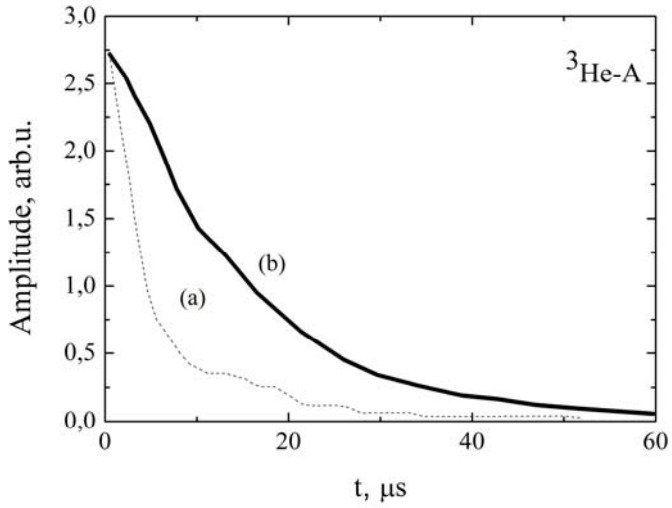

Fig.3. The FID signal amplitude in superfluid ^{3}He-A in aerogel in two RF pumping regimes.
(a) - FID after short RF pulse;
(b) - FID after continues pumping [11].

Conclusions

We have investigated the durarion of the FID signal in two samples of easy-plain antiferromagnet $CsMnF_3$. In addition to our previous investigations of the signal amplitude by means of cw NMR and pulse NMR these results also confirms the formation of magnon BEC in antiferromagnet $CsMnF_3$. In more homogeneous sample in coherent precession state we see the long-lived induction decay signal which duration is longer than in the first low quality sample. So the search of homogeneous samples of good quality is a key task for exact detection all the properties of magnon Bose-Einstein condensation in solid antiferromagnets.

Acknowledgements

This study was partly supported by the Siberian Branch of the Russian Academy of Sciences (Grant N28).

References

[1] S. Giorgini, L.P. Pitaevskii, and S. Stringari, Rev. Mod. Phys., **80**, 1215 (2008).

[2] A.S. Borovik-Romanov, et al., JETP Letters, **40**, 1033 (1984).

[3] Yu.M. Bunkov and G.Volovik, J. Phys: Condens. Matter, **22**, 164210 (2010).

[4] Yu.M. Bunkov, Progress of Low Temperature Physics, **14**, 68, ed. by W.P. Halperin, Elsevier Science B.V., Amsterdam (1995).

[5] Yu.M. Bunkov, Phys. Usp., **180**, 884 (2010).

[6] Yu.M. Bunkov, E.M. Alakshin, R.R. Gazizulin, et al., JETP Letters, **94**, 68 (2011).

[7] Yu.M. Bunkov, E.M. Alakshin, R.R. Gazizulin, et al., J. Phys: Conf. Series, **324**, 012006 (2011).

[8] Yu.M. Bunkov, E.M. Alakshin, R.R. Gazizulin, et al., J. Phys: Conf. Series, **400**, 032001 (2012).

[9] Yu.M. Bunkov, E.M. Alakshin, R.R. Gazizulin, et al., Phys. Rev. Lett., **108**, 177002 (2012).

[10] E.M. Alakshin, Yu.M. Bunkov, R.R. Gazizulin, et al., Appl. Magn. Reson., **44**, 595 (2013).

[11] P. Hunger, Yu.M. Bunkov, E. Collin, et al., J. of Low Temp. Phys., **158**, 129 (2010).

[12] L.B. Welsh, Phys. Rev., **156**, 370 (1967).

The spin kinetics of ^{3}He in contact with nanosized crystalline powders LaF_3

E.M. Alakshin, R.R. Gazizulin, A.V. Klochkov, T.R. Safin, K.R. Safiullin, M.S. Tagirov, M.Y. Zakharov

Kazan Federal University, 420008, Kremlevskaya, 18, Kazan, Russia.

e-mail: mikhailzakharo@yandex.ru

Introduction

Hyperpolarized ^{3}He gas is widely used in neutron accelerators for the polarization of neutron beams [1–4], nuclear magnetic resonance tomography, and diverse fundamental scientific researches [5–10]. Therefore, obtaining the hyperpolarized spin state of ^{3}He nuclei using new methods remains a topical problem to date.

In 1995 the possibility of dynamic ^{3}He nuclear polarization using dielectric Van Vleck paramagnetic was discussed [11]. The channel of energy transfer from the PrF_3 to liquid ^{3}He via magnetic coupling between the nuclear spins was proposed. The "^{141}Pr – ^{3}He" system has been studied in detail [12-16].

The process previously interpreted [13] as a relaxation mechanism of ^{3}He on the surface through the adsorbed layer may be a cross-relaxation effect. To confirm this idea the additional experiments with nano-sized crystalline powders LaF_3 (diamagnetic analogue of PrF_3) have been required. The ^{3}He – LaF_3 system is easier to study because there is no relaxation mechanism through the magnetic field inhomogeneity.

We report here the experimental investigation of ^{3}He relaxation times in system "LaF_3 nanoparticles – ^{3}He". The complete details of the experimental setup were published earlier [17].

Results and discussion

The series of LaF_3 nanosamples were synthesized using different microwave irradiation time, the procedure described in [13]. The X-ray analysis of synthesized samples is shown in fig.1.

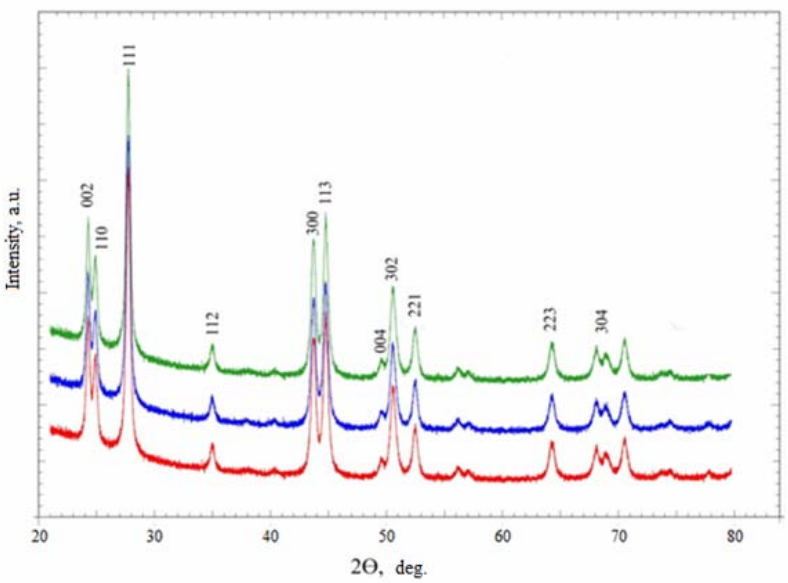

Fig.1. X-ray analysis of LaF_3 nanoparticles

The typical particle of PrF_3 (analogous to LaF_3) nanoparticle obtained by high resolution transition microscopy is presented in fig.2.

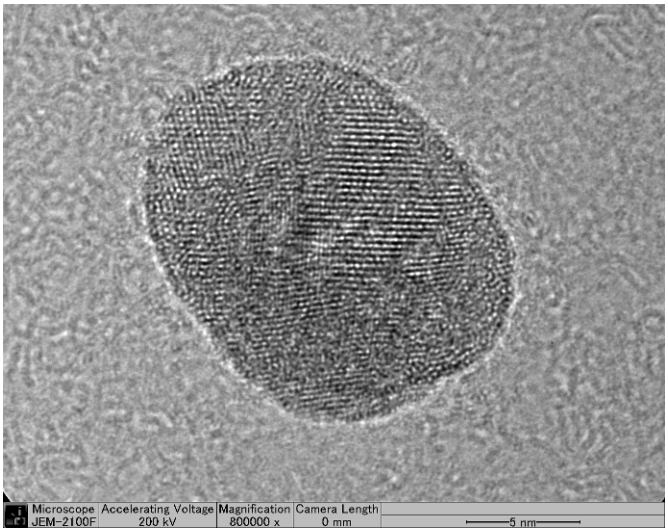

Fig.2. HRTEM of PrF_3 nanoparticles

The frequency dependence of the ^{3}He relaxation times in contact with LaF_3 nanoparticles in different aggregate states of ^{3}He has been investigated. Dependences of the ^{3}He relaxation times T_1 and T_2 on the magnetic field for the three aggregate states are shown on fig.3 and fig.4.

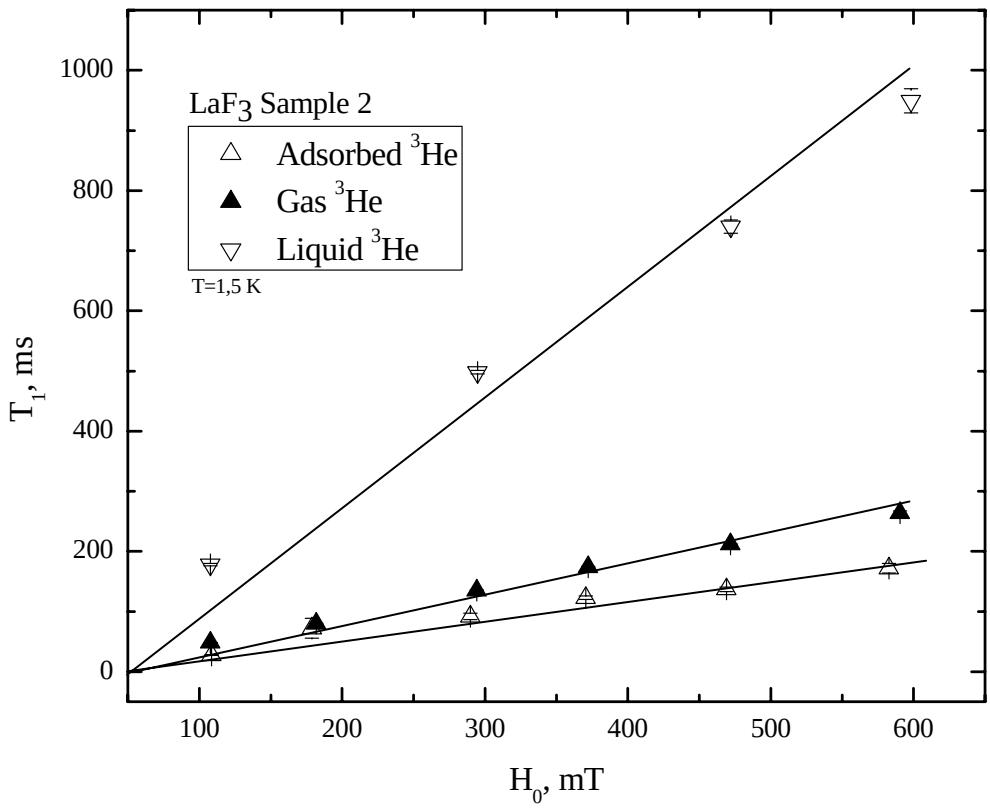

Fig.3. Longitudinal relaxation time of ^{3}He in contact with LaF_3 depends on magnetic field.

It is seen in fig.3 that the longitudinal relaxation time increases proportionally to the magnitude of the external magnetic field and the transverse relaxation time does not depend on the magnetic field (fig.4).

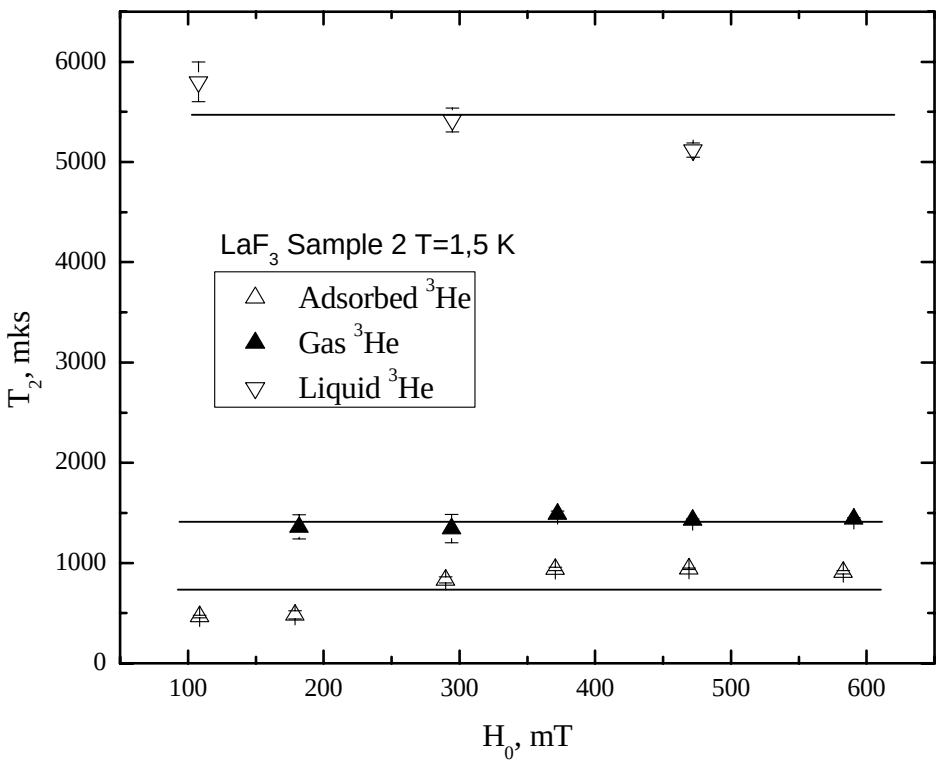

Fig.4. Transverse relaxation time of ^{3}He in contact with LaF_3 depends on magnetic field.

Along with increasing of the amount of ^{3}He in the cell the relaxation times increase significantly, therefore the relaxation occurs through the adsorbed layer. This fact as well as the character of dependence of the relaxation times on the magnetic field is described by Cowan [18].

The T_1 and T_2 of ^{3}He nuclei in the gaseous and liquid phases in the cell depending on the total number of ^{3}He atoms (fig.3, fig.4) show that the magnetic relaxation times are directly proportional to the corresponding relaxation times in the adsorbed layer, and the ratio of the number of ^{3}He spins of all nuclear spin system to the number of ^{3}He spins in layer, i.e.

$$T_1 = T_{1S} \frac{N_0}{N_S}, \tag{1}$$

where T_1, T_{1S} — longitudinal magnetization recovery times, N_0, N_S — number of spins in the whole system and the adsorbed layer, respectively,

$$T_2 = T_{2S} \frac{N_0}{N_S}, \tag{2}$$

where T_2, T_{2S} — times of the transverse magnetization decay, N_0, N_S — number of spins in the entire system and in the adsorbed layer, respectively.

Conclusion

Relaxation of the gaseous and liquid ^{3}He in contact with nanosized crystalline powder LaF_3 takes place by the adsorbed layer through mechanism of Cowan.

Acknowledgments

This work was partly supported by the Russian Foundation for Basic Research (project no. 120297048r_povolzhie_a)

References

[1] T. R. Gentile, E. Babcock, J. A. Borchers, et al., Phys. B: Condens. Matter 356, 96 (2005).

[2] A. K. Petoukhov, K. H. Andersen, D. Jullien, et al., Phys. B: Condens. Matter 385–386, 1146 (2006).

[3] L. J. Chang, R. Mueller, S. Appelt, et al., Phys. B: Condens. Matter 350, E707 (2004).

[4] J. Krimmer, M. Distler, W. Heil, et al., Nucl. Instrum. Methods Phys. Res. 611, 18 (2009).

[5] E. J. van Beek, J. M. Wild, H.U. Kauczor, et al., J. Magn. Reson. Imag. 20, 540 (2004).

[6] W. G. Schreiber, A. E. Morbach, T. Stavngaard, et al., Respir. Physiol. Neurobiol. 25, 23 (2005).

[7] S. Patz, I. Muradian, M. I. Hrovat, et al., Acad. Radiol.15, 713 (2008).

[8] E. Baudin, M. E. Hayden, G. Tastevin, et al., Compt. Rend. Chim. 11, 560 (2008).

[9] R. R. Gazizulin, A. V. Klochkov, V. V. Kuzmin, et al., Appl. Magn. Reson. 38, 271 (2010).

[10] R. R. Gazizulin, A. V. Klochkov, V. V. Kuzmin, et al., Magn. Reson. Solids 11 (2), 33 (2009).

[11] Tagirov, Tayurskii, JETP Letters, 1995, 61: 652–655

[12] E.M. Alakshin, B.M. Gabidullin, A.T. Gubaidullin, et al., arXiv:condmat., V.1104., P.0208. - http://arxiv.org/abs/1104.0208 (2011).

[13] E.M. Alakshin, R.R. Gazizulin, A.V. Egorov, et al., Journal of Low Temperature Physics V.162, N.5/6, P.645 – 652, (2011).

[14] E.M. Alakshin, D.S. Blokhin, A.M. Sabitova, et al., JETP Letters. V.96, N.3, P.194-196 (2012).

[15] E.M. Alakshin, A.S. Aleksandrov, A.V. Egorov, et al., JETP Letters V.4, N.3, P.259-261, (2011).

[16] E.M. Alakshin, R.R. Gazizulin, A.V. Klochkov, et al., JETP Letters. V.97, N.10, P.665-668 (2013).

[17] E.M. Alakshin, R.R. Gazizulin, A.V. Klochkov, et al., Magnetic Resonance in Solids V.15, N.1, 13104, (2013).

[18] P.C. Hammel and R.C. Richardson Phys. Rev. Lett. 51, 1441 (1970).

Index

Y

Z

Table of Contents

TABLE OF CONTENTS